Author Response for "Aqueous SOA formation from photosensitized guaiacol oxidation: Comparison between non-phenolic and phenolic methoxybenzaldehydes as photosensitizers in the absence and presence of ammonium nitrate" by Mabato et al.

We thank the Reviewer for their thorough comments. We have revised the manuscript accordingly, and below are our point-by-point responses (in blue) to the comments (in black) and changes to the manuscript (in red). In those changes that begin with line numbers, the original text is also in blue. In addition, please note that the line numbers in the responses correspond to those in the original manuscript.

Reviewer 1

This study analyzes the characteristic of the DMB and VL as photosensitizers reacting with GUA for aqSOA formation, including kinetic analysis, product distributions and chemical characteristics, as well as optical properties. Meanwhile, the effect of AN for aqSOA formation was analyzed. In general, the paper is well written and conclusions are convincing in terms of rational and rigorous experimental design and analyses. I just have several minor comments on it.

1. In terms of abundance of products, for GUA+DMB, the abundance of products in the presence of AN is less than that in the absence of AN, however, for GUA+VL, the results are the opposite. Please elaborate.

Response: It is very common to compare the relative abundance of products based on peak areas from mass spectrometry (MS) results (e.g., Lee et al., 2014; Romonosky et al., 2017; Wang et al., 2017; Fleming et al., 2018; Song et al., 2018; Klodt et al., 2019; Ning et al., 2019) to show the relative importance of different types of compounds (K. Wang et al., 2021). However, comparisons of relative abundance among different compounds can be subject to uncertainties as ionization efficiencies in soft ionization, such as ESI, may significantly vary between different compounds (Kebarle, 2000; Schmidt et al., 2006; Leito et al., 2008; Perry et al., 2008; Kruve et al., 2014). **In our previous work (Mabato et al., 2022), we introduced the normalized abundance of products ([P], unitless).** The calculation assumes equal ionization efficiencies of different compounds, which is commonly used for estimation of O:C ratios of SOA (e.g., Bateman et al., 2012; Lin et al., 2012; Laskin et al., 2014; De Haan et al., 2019). **This allows us to have a better comparison with the literature results.** It is therefore emphasized that the normalized abundance of products is a semi-quantitative analysis of the detected products under different experimental conditions, instead of absolute concentrations of them.

Moreover, as stated in the footnote of Table 1, the normalized abundance of products was calculated using only the positive ion mode data as the GUA signal from the negative ion mode was weak and thus may present large uncertainties during normalization. Therefore, products that may not give signals or may have weak signals in the positive ion mode were possibly underestimated in the normalized product abundance. The contrasting trends of the normalized abundance of products for GUA+DMB and GUA+VL in the absence and presence of AN may therefore be related to the differences in the ionization efficiencies of the products formed. Nevertheless, the much higher normalized abundance of products for

GUA+DMB vs. GUA+VL is consistent with the other more quantitative measurements in this work (i.e., faster GUA decay and stronger light absorption by reaction products in GUA+DMB vs. in GUA+VL).

Sect. 2.2 has been revised to give more information about the normalized abundance of products as follows:

Section 2.2 Calculation of ~~the~~ normalized abundance of products

Several recent studies have used comparisons of relative abundance of products based on peak areas from mass spectrometry (MS) results (e.g., Lee et al., 2014; Romonosky et al., 2017; Wang et al., 2017; Fleming et al., 2018; Song et al., 2018; Klodt et al., 2019; Ning et al., 2019) to show the relative importance of different types of compounds (K. Wang et al., 2021). However, comparisons of relative abundance among different compounds can be subject to uncertainties as ionization efficiencies in soft ionization, such as ESI, may significantly vary between different compounds (Kebarle, 2000; Schmidt et al., 2006; Leito et al., 2008; Perry et al., 2008; Kruve et al., 2014). ~~The normalized abundance of products ([P], unitless) was introduced in our previous work (Mabato et al., 2022).~~ In our previous work (Mabato et al., 2022), we introduced the normalized abundance of products ([P], unitless) (Eq. 2) as ~~Nevertheless, it is~~ a semi-quantitative analysis that gives an overview of how the signal intensities changed under different experimental conditions but not the quantification of the absolute product concentration. ~~Briefly,~~ The calculation assumes equal ionization efficiencies of different compounds, which is commonly used to estimate O:C ratios of SOA (Bateman et al., 2012; Lin et al., 2012; Laskin et al., 2014; De Haan et al., 2019) ~~was assumed for the calculation~~:

$$[P] = \frac{A_{P,t}}{A_{GUA,t}} \cdot \frac{[GUA]_t}{[GUA]_0} \qquad \text{(Eq. 2)}$$

where $A_{P,t}$ and $A_{GUA,t}$ are the extracted ion chromatogram (EIC) peak areas of the product P and GUA from UHPLC-HESI-Orbitrap-MS analyses at time t, respectively; $[GUA]_t$ and $[GUA]_0$ are the GUA concentrations (µM) determined using UHPLC-PDA at time t and 0, respectively. Note that the normalized abundance of products has intrinsic uncertainties due to the variability in ionization efficiencies for various compounds. Moreover, it should be noted that the normalized abundance of products was calculated using only the positive ion mode data as the GUA signal from the negative ion mode was weak and thus may present large uncertainties during normalization. Therefore, products that may not give signals or may have weak signals in the positive ion mode were possibly underestimated in the normalized product abundance. Nevertheless, it enables the comparison of MS results among different experiments. As demonstrated in our previous work (Mabato et al., 2022) and the current study, a higher normalized abundance of products generally correlates with higher efficiency of oxidation. The reported uncertainties were propagated from the changes in [GUA] measured using UHPLC-PDA and the MS signal intensities.

2. For Fig.4, why choose an absorbance wavelength of 180 min for the study? What is the change of absorbance during the whole reaction process, and is the effect of AN obvious on the change of absorbance?

Response: We apologize for the confusion. In Figure 4, the absorbance enhancement was based on the integrated area of absorbance from 350 to 550 nm, and 180 min refers to the total irradiation time. An irradiation time of 180 min was chosen for this study as it was sufficient to show the differences in the extent of the reaction of GUA among the reaction systems studied. Moreover, the same irradiation time was applied to all experiments as we were trying to evaluate the product distributions after a certain time of photosensitization. For reaction systems with precursors of different reactivities, chemical analysis at a fixed reaction time may be looking at different generations of products of each precursor, as Yu et al. (2014) reported. Measuring the product distribution at a fixed time might have missed the information on what/how many products are formed at the similar amounts of precursors reacted. The situation could be even more complicated if different precursors had major differences in pathways and dominant intermediates. However, comparing the product distributions after a certain time of light exposure, as is the case for this study, is useful to evaluate what products would form after a certain time of photosensitization. This information has been added to the discussion of product distributions as follows:

Lines 194-197: The products detected using UHPLC-HESI-Orbitrap-MS were used to ~~represent~~ characterize the aqSOA formed in this work. The signal-weighted distributions of aqSOA calculated from combined positive (POS) and negative (NEG) ion modes MS results are summarized in Figure 2. The signal-weighted distributions calculated separately from POS and NEG ion modes MS results are available in Figures S2~~1~~ and S3~~2~~. It should be noted that in this work, the product distributions for all experiments were based on the same irradiation time of 180 min. An irradiation time of 180 min was chosen as it was sufficient to show the differences in the extent of reaction of GUA among the reaction systems studied. For reaction systems with precursors of different reactivities, chemical analysis at a fixed reaction time may be looking at different generations of products of each precursor, as Yu et al. (2014) reported. Measuring the product distribution at a fixed time might have missed the information on what/how many products are formed at the similar amounts of precursors reacted. The situation could be even more complicated if different precursors had major differences in pathways and dominant intermediates. However, comparing the product distributions after a certain time of light exposure, as is the case for this study, is useful to evaluate what products would form after a certain time of photosensitization.

For all experiments in this work, we measured the absorbance every 30 min from 0 to 180 min and observed an increase in visible light absorption from 350 to 550 nm. As mentioned in lines 353-358, the effect of AN was not evident on the absorbance enhancement. For GUA+DMB+AN, the N-containing products may have offset the decrease in oligomers to maintain the absorbance enhancement noted from GUA+DMB. For GUA+VL+AN, the decrease in monomers may have counteracted the increased oligomers and the generated N-containing products.

The absorbance enhancement from 0 to 180 min for all reaction systems studied have been added to Figure 4(a). Based on suggestions from Reviewer 4, the original Figure 4 (now Figure 4b) has also been replaced with the change in the rate of sunlight absorption (ΔR_{abs}) from 350-550 nm at 180 min during typical clear and haze days in Beijing, China. Moreover, the absorption spectra after 180 min of irradiation for each solution have been added to the supplement (Figure S7) based on suggestions from Reviewer 4.
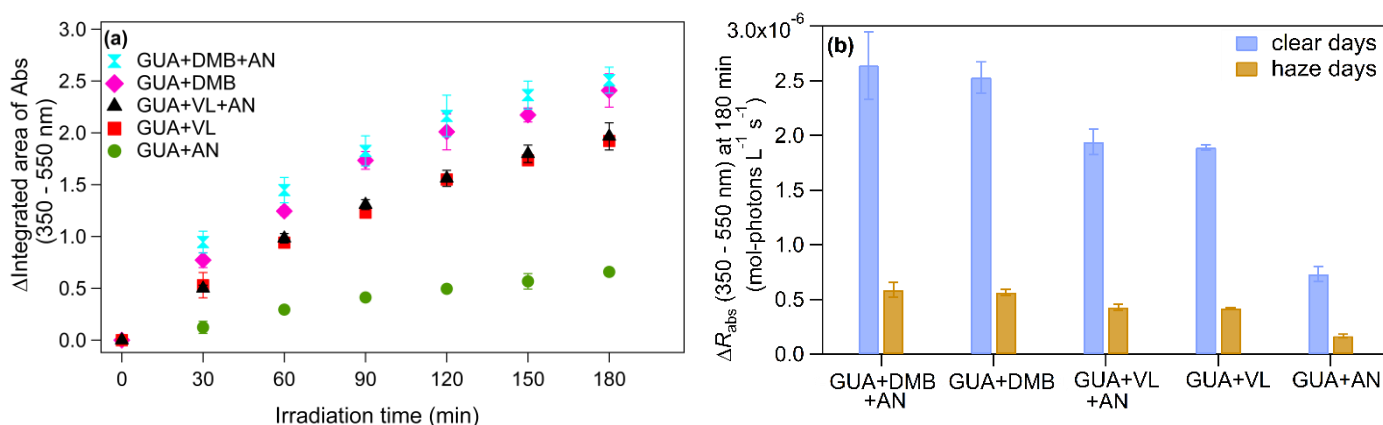
Figure 4. (a) Increase in light absorption throughout 180 min of irradiation for all reaction systems studied and (b) Change in the rate of sunlight absorption (ΔR_{abs}) from 350-550 nm at 180 min during typical clear and haze days in Beijing, China for aqSOA from GUA+DMB+AN, GUA+DMB, GUA+VL+AN, GUA+VL, and GUA+AN. ~~Increase in visible light absorption for aqSOA from GUA+DMB, GUA+VL, GUA+DMB+AN, and GUA+VL+AN.~~ Error bars represent one standard deviation of triplicate experiments.
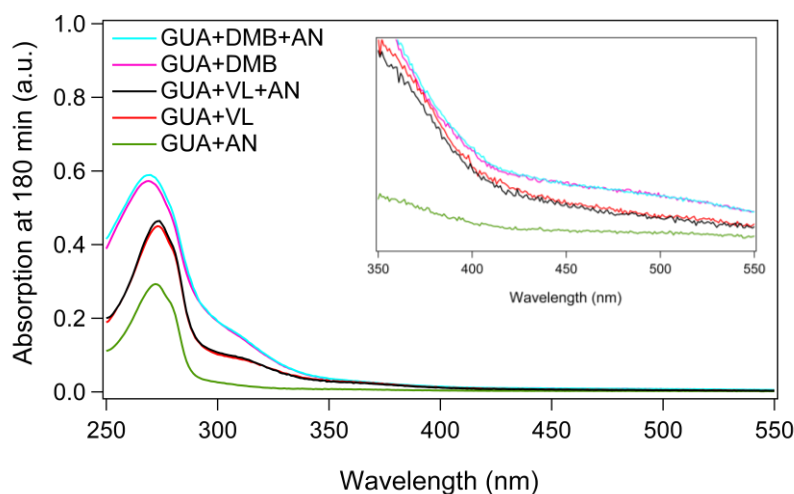

Figure S7. UV-Vis absorption spectra of GUA+DMB+AN, GUA+DMB, GUA+VL+AN, GUA+VL, and GUA+AN after 180 min of irradiation. The inset is the expanded view from 350 to 550 nm.

The corresponding revisions in the text are as follows:

Lines 253-260: The increase in light absorption throughout 180 min of irradiation and the change in the rate of sunlight absorption (ΔR_{abs}) (Jiang et al., 2021) from 350 to 550 nm at 180 min during typical clear and haze days in Beijing, China for all the reaction systems studied are provided in Figure 4. Figure S7 shows the absorption spectra after 180 min of irradiation for each reaction system studied. In this work, the absorbance enhancement of GUA+DMB and GUA+VL (Fig. 4a) could be due to ~~correlates with~~ oligomers and

functionalized monomers, which are the highest contributors to the product signals. Identifying the chromophores responsible for the absorbance enhancement may be beneficial in understanding the impact of aqSOA on the Earth's radiative balance and determining the reactions that affect light absorption by aqSOA (Mabato et al., 2022). However, the detected products did not exhibit distinct peaks in the UHPLC-PDA chromatograms, likely due to the concentration of the chromophores being below the detection limit of PDA. Nevertheless, the higher absorbance enhancement and ΔR_{abs} for GUA+DMB than GUA+VL was ~~most likely associated with~~ probably due to the higher contribution and normalized abundance (by ~6 times) of oligomers in the former.

Line 353: The presence of AN also did not appreciably affect the absorbance enhancement and ΔR_{abs} for both GUA+DMB+AN and GUA+VL+AN (Fig. 4).

3. (a) Why the entire reaction time of this study was 180 minutes, and (b) did the precursors get reacted completely?

Response: (a) As mentioned in our response to question #2, an irradiation time of 180 min was chosen for this work as it was sufficient to show the differences in the extent of reaction of GUA among the reaction systems studied. Moreover, the same irradiation time was applied to all experiments as we were trying to evaluate the product distributions after a certain time of photosensitization. To clarify this in the text, the discussion of product distributions has been amended, as shown in the response to question #2.

(b) No, GUA and the photosensitizers were not fully consumed within the 180 min irradiation. The estimated fraction of GUA and the photosensitizers that remained after irradiation were as follows:

Reaction conditions	Estimated fraction of GUA and the photosensitizers that remained after 180 min of irradiation
GUA+AN	84% GUA
GUA+DMB	39% GUA and 89% DMB
GUA+DMB+AN	40% GUA and 89% DMB
GUA+VL	79% GUA and 46% VL
GUA+VL+AN	78% GUA and 47% VL

References for responses to Reviewer 1:

Bateman, A. P., Laskin, J., Laskin, A., and Nizkorodov, S. A.: Applications of high-resolution electrospray ionization mass spectrometry to measurements of average oxygen to carbon ratios in secondary organic aerosols, Environ. Sci. Technol., 46, 8315–8324, https://doi.org/10.1021/es3017254, 2012.

De Haan, D.O., Pajunoja, A., Hawkins, L. N., Welsh, H.G., Jimenez, N. G., De Loera, A., Zauscher, M., Andretta, A. D., Joyce, B. W., De Haan, A. C., Riva, M., Cui, T., Surratt, J. D., Cazaunau, M., Formenti, P., Gratien, A., Pangui, E., and Doussin, J-F.: Methylamine's effects

on methylglyoxal-containing aerosol: chemical, physical, and optical changes, ACS Earth Space Chem., 3, 1706–1716, https://doi.org/10.1021/acsearthspacechem.9b00103, 2019.

Fleming, L. T., Lin, P., Laskin, A., Laskin, J., Weltman, R., Edwards, R. D., Arora, N. K., Yadav, A., Meinardi, S., Blake, D. R., Pillarisetti, A., Smith, K. R., and Nizkorodov, S. A.: Molecular composition of particulate matter emissions from dung and brushwood burning household cookstoves in Haryana, India, Atmos. Chem. Phys., 18, 2461–2480, https://doi.org/10.5194/acp-18-2461-2018, 2018.

Jiang, W., Misovich, M. V., Hettiyadura, A. P. S., Laskin, A., McFall, A. S., Anastasio, C., and Zhang, Q.: Photosensitized reactions of a phenolic carbonyl from wood combustion in the aqueous phase—chemical evolution and light absorption properties of aqSOA, Environ. Sci. Technol., 55, 5199–5211, https://doi.org/10.1021/acs.est.0c07581, 2021.

Laskin, J., Laskin, A., Nizkorodov, S. A., Roach, P., Eckert, P., Gilles, M. K., Wang, B., Lee, H. J., and Hu, Q.: Molecular selectivity of brown carbon chromophores, Environ. Sci. Technol., 48, 12047–12055, https://doi.org/10.1021/es503432r, 2014.

Lee, H. J., Aiona, P. K., Laskin, A., Laskin, J., and Nizkorodov, S. A.: Effect of solar radiation on the optical properties and molecular composition of laboratory proxies of atmospheric brown carbon, Environ. Sci. Technol., 48, 10217–10226, https://doi.org/10.1021/es502515r, 2014.

Leito, I., Herodes, K., Huopolainen, M., Virro, K., Künnapas, A., Kruve, A., and Tanner, R.: Towards the electrospray ionization mass spectrometry ionization efficiency scale of organic compounds, Rapid Commun. Mass Sp., 22, 379–384, https://doi.org/10.1002/rcm.3371, 2008.

Lin, P., Yu, J. Z., Engling, G., and Kalberer, M.: Organosulfates in humic-like substance fraction isolated from aerosols at seven locations in East Asia: a study by ultra-high-resolution mass spectrometry, Environ. Sci. Technol., 46, 13118–13127, https://doi.org/10.1021/es303570v, 2012.

Kebarle, P. A.: A brief overview of the mechanisms involved in electrospray mass spectrometry, J. Mass Spectrom., 35, 804–817, https://doi.org/10.1002/9783527628728.ch1, 2000.

Klodt, A.L., Romonosky, D.E., Lin, P., Laskin, J., Laskin, A., and Nizkorodov, S.A.: Aqueous photochemistry of secondary organic aerosol of α-pinene and α-humulene in the presence of hydrogen peroxide or inorganic salts, ACS Earth Space Chem., 3, 12, 2736–2746, https://doi.org/10.1021/acsearthspacechem.9b00222, 2019.

Kruve, A., Kaupmees, K., Liigand, J., and Leito, I.: Negative electrospray ionization via deprotonation: predicting the ionization efficiency, Anal. Chem., 86, 4822–4830, https://doi.org/10.1021/ac404066v, 2014.

Mabato, B. R. G., Lyu, Y., Ji, Y., Li, Y. J., Huang, D. D., Li, X., Nah, T., Lam, C. H., and Chan, C. K.: Aqueous secondary organic aerosol formation from the direct photosensitized oxidation of vanillin in the absence and presence of ammonium nitrate, Atmos. Chem. Phys., 22, 273–293, https://doi.org/10.5194/acp-22-273-2022, 2022.

Ning, C., Gao, Y., Zhang, H., Yu, H., Wang, L., Geng, N., Cao, R., and Chen, J.: Molecular characterization of dissolved organic matters in winter atmospheric fine particulate matters (PM2.5) from a coastal city of northeast China, Sci. Total Environ., 689, 312–321, https://doi.org/10.1016/j.scitotenv.2019.06.418, 2019.

Perry, R. H., Cooks, R. G., and Noll, R. J.: Orbitrap mass spectrometry: instrumentation, ion motion and applications, Mass Spectrom. Rev., 27, 661–699, https://doi.org/10.1002/mas.20186, 2008.

Romonosky, D. E., Li, Y., Shiraiwa, M., Laskin, A., Laskin, J., and Nizkorodov, S. A.: Aqueous photochemistry of secondary organic aerosol of α-Pinene and α-Humulene oxidized with ozone, hydroxyl radical, and nitrate radical, J. Phys. Chem. A, 121, 1298–1309, https://doi.org/10.1021/acs.jpca.6b10900, 2017.

Schmidt, A-C., Herzschuh, R., Matysik, F-M., and Engewald, W.: Investigation of the ionisation and fragmentation behaviour of different nitroaromatic compounds occurring as polar metabolites of explosives using electrospray ionisation tandem mass spectrometry, Rapid Commun. Mass Sp., 20, 2293–2302, https://doi.org/10.1002/rcm.2591, 2006.

Song, J., Li, M., Jiang, B., Wei, S., Fan, X., and Peng, P.: Molecular characterization of water-soluble humic like substances in smoke particles emitted from combustion of biomass materials and coal using ultrahigh-resolution electrospray ionization Fourier transform ion cyclotron resonance mass spectrometry, Environ. Sci. Technol., 52, 2575–2585, https://doi.org/10.1021/acs.est.7b06126, 2018.

Wang, K., Huang, R-J., Brüggemann, M., Zhang, Y., Yang, L., Ni, H., Guo, J., Wang, M., Han, J., Bilde, M., Glasius, M., and Hoffmann, T.: Urban organic aerosol composition in eastern China differs from north to south: molecular insight from a liquid chromatography–mass spectrometry (Orbitrap) study, Atmos. Chem. Phys., 21, 9089–9104, https://doi.org/10.5194/acp-21-9089-2021, 2021.

Wang, X., Hayeck, N., Brüggemann, M., Yao, L., Chen, H., Zhang, C., Emmelin, C., Chen, J., George, C., and Wang, L.: Chemical characterization of organic aerosols in Shanghai: A study by ultrahigh-performance liquid chromatography coupled with orbitrap mass spectrometry, J. Geophys. Res. Atmos., 122, 11703–11722, https://doi.org/10.1002/2017JD026930, 2017.

Yu, L., Smith, J., Laskin, A., Anastasio, C., Laskin, J., and Zhang, Q.: Chemical characterization of SOA formed from aqueous-phase reactions of phenols with the triplet excited state of carbonyl and hydroxyl radical, Atmos. Chem. Phys., 14, 13801–13816, https://doi.org/10.5194/acp-14-13801-2014, 2014.

Author Response for "Aqueous SOA formation from photosensitized guaiacol oxidation: Comparison between non-phenolic and phenolic methoxybenzaldehydes as photosensitizers in the absence and presence of ammonium nitrate" by Mabato et al.

We thank the Reviewer for their thorough comments. We have revised the manuscript accordingly, and below are our point-by-point responses (in blue) to the comments (in black) and changes to the manuscript (in red). In those changes that begin with line numbers, the original text is also in blue. In addition, please note that the line numbers in the responses correspond to those in the original manuscript.

Reviewer 2

This paper systematically investigated the physicochemical properties of aqueous SOA formed from the photosensitized guaiacol oxidation by using DMB and VL as photosensitizers in the presence and absence of AN. In general, this paper is well written, readable and logical. Before accepted for publication, some revisions should be made. The specific comments are listed as follows:

1. Why did not show aqSOA yields in this work? In my opinion, these data are very useful for readers to understand the importance of these oxidation processes. When these data were described in the paper, the comparison between these date and other similarly reported results should be made.

Response: Since this work mainly focused on the analyses of the reaction products and product distribution, we did not perform measurements of aqSOA mass yields. As similar aqSOA mass yields have been reported from the photosensitized oxidation of syringol (another non-carbonyl phenol) by ^{3}DMB* (111%) and ^{3}VL* (114%) (Smith et al., 2014, 2016) (mentioned in lines 57-59), we assumed that aqSOA mass yields from guaiacol photo-oxidation by ^{3}DMB* and ^{3}VL* would also be comparable.

2. As mentioned in section 2.1, the samples were collected every 30 min for 180 min for offline analyses. Therefore, authors can provide more information about the changes of signal-weighted distributions and visible light absorption of aqSOA formed under different conditions during the whole reaction processes. In addition, the concentration changes of small organic acids during the whole reaction processes should be also supplemented.

Response: Thank you for pointing this out. We apologize for the confusion regarding the samples subjected to offline analyses. In this work, the samples collected every 30 min were analyzed using only UHPLC-PDA and UV-Vis spectrophotometry for GUA and photosensitizers decay kinetics and absorbance changes, respectively. The absorbance enhancement from 0 to 180 min for all reaction systems studied have been added to Figure 4(a). Based on suggestions from Reviewer 4, the original Figure 4 (now Figure 4b) has also been replaced with the change in the rate of sunlight absorption (ΔR_{abs}) from 350-550 nm at 180 min during typical clear and haze days in Beijing, China. Moreover, the absorption spectra after 180 min of irradiation for each solution have been added to the supplement (Figure S7) based on suggestions from Reviewer 4.

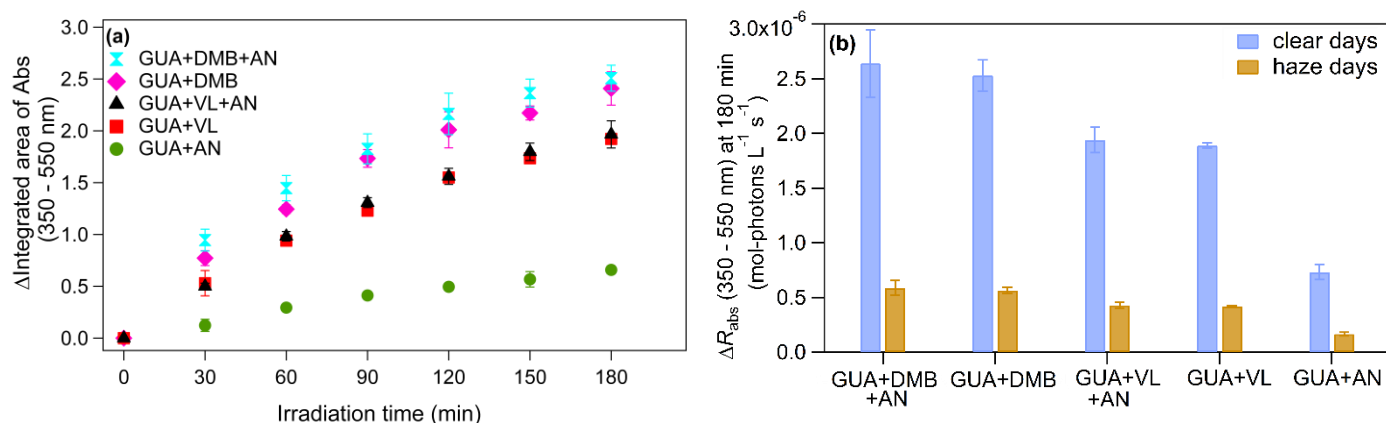The updated Figure 4 and added Figure S7 are shown below:

Figure 4. (a) Increase in light absorption throughout 180 min of irradiation for all reaction systems studied and (b) Change in the rate of sunlight absorption (ΔR_{abs}) from 350-550 nm at 180 min during typical clear and haze days in Beijing, China for aqSOA from GUA+DMB+AN, GUA+DMB, GUA+VL+AN, GUA+VL, and GUA+AN. ~~Increase in visible light absorption for aqSOA from GUA+DMB, GUA+VL, GUA+DMB+AN, and GUA+VL+AN.~~ Error bars represent one standard deviation of triplicate experiments.

Figure S7. UV-Vis absorption spectra of GUA+DMB+AN, GUA+DMB, GUA+VL+AN, GUA+VL, and GUA+AN after 180 min of irradiation. The inset is the expanded view from 350 to 550 nm.

The corresponding revisions in the text are as follows:

Lines 253-260: The increase in light absorption throughout 180 min of irradiation and the change in the rate of sunlight absorption (ΔR_{abs}) (Jiang et al., 2021) from 350 to 550 nm at 180 min during typical clear and haze days in Beijing, China for all the reaction systems studied are provided in Figure 4. Figure S7 shows the absorption spectra after 180 min of irradiation for each reaction system studied. In this work, the absorbance enhancement of GUA+DMB and GUA+VL (Fig. 4a) could be due to ~~correlates with~~ oligomers and functionalized monomers,

which are the highest contributors to the product signals. Identifying the chromophores responsible for the absorbance enhancement may be beneficial in understanding the impact of aqSOA on the Earth's radiative balance and determining the reactions that affect light absorption by aqSOA (Mabato et al., 2022). However, the detected products did not exhibit distinct peaks in the UHPLC-PDA chromatograms, likely due to the concentration of the chromophores being below the detection limit of PDA. Nevertheless, the higher absorbance enhancement and ΔR_{abs} for GUA+DMB than GUA+VL was ~~most likely associated with~~ probably due to the higher contribution and normalized abundance (by ~6 times) of oligomers in the former.

Line 353: The presence of AN also did not appreciably affect the absorbance enhancement and ΔR_{abs} for both GUA+DMB+AN and GUA+VL+AN (Fig. 4).

Moreover, the detection of products and small organic acids was performed only for the samples collected before and after irradiation (180 min). To clarify these differences, section 2.1 has been revised as follows:

Lines 132-137: Samples were collected every 30 min~~s~~ for 180 min~~s~~ for offline analyses of (1) GUA, DMB, and VL concentrations using ultra-high-performance liquid chromatography with photodiode array detector (UHPLC-PDA)~~;~~ and (4~~2~~) absorbance measurements using UV-Vis spectrophotometry. Moreover, the samples collected before and after irradiation (180 min) were analyzed for (2~~3~~) reaction products using UHPLC coupled with heated electrospray ionization Orbitrap mass spectrometry (UHPLC-HESI-Orbitrap-MS) operated in positive and negative ion modes~~;~~ and (4~~3~~) concentrations of small organic acids using ion chromatography (IC)~~;~~.

Other revisions in the text were as follows:

Line 213: The IC analyses also indicate the formation of small organic acids (e.g., formic acid), which appeared to have higher concentrations in the presence of DMB than in VL (Fig. S4~~3~~). Although no data is available for the concentration changes (every 30 min) of small organic acids during the reaction, it is likely that an increasing trend would be observed as fragmentation, which leads to the decomposition of initially formed oligomers and the generation of smaller oxygenated products, becomes important at longer irradiation times (Huang et al., 2018). This trend has also been observed in our previous work on the direct photosensitized oxidation of VL (Mabato et al., 2022), as well as other studies on photosensitized oxidation of non-carbonyl phenols and phenolic carbonyls (e.g., Yu et al., 2016; Jiang et al., 2021).

Line 382: The major aqSOA formation processes for GUA+DMB and GUA+VL were oligomerization and functionalization, but functionalization appeared to be more significant in GUA+VL due to VL transformation products. The photochemical evolution of aqSOA from GUA+DMB has been reported by Yu et al. (2016). Similar experiments for aqSOA from GUA+VL should be conducted in the future to better understand photosensitized reactions involving phenolic carbonyl photosensitizers.

3. Please provide the reason why selected the whole reaction times as 180 min.

Response: An irradiation time of 180 min was chosen for this work as it was sufficient to show the differences in the extent of reaction of GUA among the reaction systems studied. Moreover, the same irradiation time was applied to all experiments as we were trying to evaluate the product distributions after a certain time of photosensitization.

This information has been added to the discussion of the product distributions as follows:

Lines 194-197: The products detected using UHPLC-HESI-Orbitrap-MS were used to ~~represent~~ characterize the aqSOA formed in this work. The signal-weighted distributions of aqSOA calculated from combined positive (POS) and negative (NEG) ion modes MS results are summarized in Figure 2. The signal-weighted distributions calculated separately from POS and NEG ion modes MS results are available in Figures S2~~1~~ and S3~~2~~. It should be noted that in this work, the product distributions for all experiments were based on the same irradiation time of 180 min. An irradiation time of 180 min was chosen as it was sufficient to show the differences in the extent of reaction of GUA among the reaction systems studied. For reaction systems with precursors of different reactivities, chemical analysis at a fixed reaction time may be looking at different generations of products of each precursor, as Yu et al. (2014) reported. Measuring the product distribution at a fixed time might have missed the information on what/how many products are formed at the similar amounts of precursors reacted. The situation could be even more complicated if different precursors had major differences in pathways and dominant intermediates. However, comparing the product distributions after a certain time of light exposure, as is the case for this study, is useful to evaluate what products would form after a certain time of photosensitization.

4. There are still some language mistakes, please carefully check.

Response: Thank you for pointing this out. We have carefully checked the text for language mistakes.

References for responses to Reviewer 2:

Huang, D. D., Zhang, Q., Cheung, H. H. Y., Yu, L., Zhou, S., Anastasio, C., Smith, J. D., and Chan, C. K.: Formation and evolution of aqSOA from aqueous-phase reactions of phenolic carbonyls: comparison between ammonium sulfate and ammonium nitrate solutions, Environ. Sci. Technol., 52, 9215–9224, https://doi.org/10.1021/acs.est.8b03441, 2018.

Jiang, W., Misovich, M. V., Hettiyadura, A. P. S., Laskin, A., McFall, A. S., Anastasio, C., and Zhang, Q.: Photosensitized reactions of a phenolic carbonyl from wood combustion in the aqueous phase—chemical evolution and light absorption properties of aqSOA, Environ. Sci. Technol., 55, 5199–5211, https://doi.org/10.1021/acs.est.0c07581, 2021.

Mabato, B. R. G., Lyu, Y., Ji, Y., Li, Y. J., Huang, D. D., Li, X., Nah, T., Lam, C. H., and Chan, C. K.: Aqueous secondary organic aerosol formation from the direct photosensitized oxidation of vanillin in the absence and presence of ammonium nitrate, Atmos. Chem. Phys., 22, 273–293, https://doi.org/10.5194/acp-22-273-2022, 2022.

Smith, J. D., Sio, V., Yu, L., Zhang, Q., and Anastasio, C.: Secondary organic aerosol production from aqueous reactions of atmospheric phenols with an organic triplet excited state, Environ. Sci. Technol., 48, 1049–1057, https://doi.org/10.1021/es4045715, 2014.

Smith, J. D., Kinney, H., and Anastasio, C.: Phenolic carbonyls undergo rapid aqueous photodegradation to form low-volatility, light-absorbing products, Atmos. Environ., 126, 36–44, https://doi.org/10.1016/j.atmosenv.2015.11.035, 2016.

Yu, L., Smith, J., Laskin, A., Anastasio, C., Laskin, J., and Zhang, Q.: Chemical characterization of SOA formed from aqueous-phase reactions of phenols with the triplet excited state of carbonyl and hydroxyl radical, Atmos. Chem. Phys., 14, 13801–13816, https://doi.org/10.5194/acp-14-13801-2014, 2014.

Yu, L., Smith, J., Laskin, A., George, K. M., Anastasio, C., Laskin, J., Dillner, A. M., and Zhang, Q.: Molecular transformations of phenolic SOA during photochemical aging in the aqueous phase: competition among oligomerization, functionalization, and fragmentation, Atmos. Chem. Phys., 16, 4511–4527, https://doi.org/10.5194/acp-16-4511-2016.

Author Response for "Aqueous SOA formation from photosensitized guaiacol oxidation: Comparison between non-phenolic and phenolic methoxybenzaldehydes as photosensitizers in the absence and presence of ammonium nitrate" by Mabato et al.

We thank the Reviewer for their thorough comments. We have revised the manuscript accordingly, and below are our point-by-point responses (in blue) to the comments (in black) and changes to the manuscript (in red). In those changes that begin with line numbers, the original text is also in blue. In addition, please note that the line numbers in the responses correspond to those in the original manuscript.

Reviewer 3

This manuscript describes a comparative study of the photosensitization by phenolic and non-phenolic methoxybenzaldehydes in reactions of guaiacol (another phenolic compound, but without an aldehyde functional group), with and without the presence of ammonium nitrate salts. The experiments were conducted in bulk aqueous phase samples in a solar simulator.

The combination of photosensitizing reactions of methoxybenzaldehyde species with ammonium nitrate photochemistry in a series of experiments is especially interesting. The primary conclusion is that the non-phenolic species DNB is approximately 4 times more effective as a photosensitizer than the phenolic species vanillin, and produces slightly more brown carbon. The manuscript includes a great number of qualitative comparisons, but the authors highlight the most important ones in the abstract and conclusion. It will be of interest to atmospheric scientists studying mechanisms of formation of brown carbon and aqueous secondary organic aerosol.

(a) My first concern is that the authors may have oversimplified the complex task of comparing the photosensitizing abilities of VL and DNB, when VL is reacting away at ~20x the rate of DNB (a factor of 8 x 2.4). The reactivity of VL is so great that it successfully competes with GUA in the reaction with the VL triplet (3VL*), reacting with it 24% of the time over the course of the reaction even though the VL concentration is 10x less than GUA. (I estimated this reaction fraction from the stated 2.4x faster decay rate of VL times the VL / GUA concentration ratio of 0.01mM/0.1mM, resulting in a relative loss rate for VL of 0.24 if GUA loss rate = 1.) If one takes into account 3VL* reactions with both VL and GUA, DNB would be at most only 3 times faster than VL at promoting photosensitization reactions in general. A more nuanced kinetics analysis would thus be helpful for GUA + VL and GUA + VL + AN reactions. Furthermore, it could allow some qualitative statements in the paper, such as those in line 204 and 207, to become quantitative: (b) when integrated over the full course of the reaction, what is the impact of the loss of the reactant VL on the total amount of products generated?

Response: (a) Thank you for pointing this out. We would like to emphasize that the kinetics analysis and apparent quantum efficiency of GUA photodegradation suggested faster GUA oxidation in GUA+DMB vs. GUA+VL, which we attributed to two reasons: (1) DMB having a stronger photosensitizing ability than VL based on its higher quantum yield of $^3C^*$ formation and longer lifetime of $^3DMB^*$ compared to $^3VL^*$ (Felber et al., 2021) and (2) VL being highly reactive towards oxidation as it is also a phenolic compound, similar to GUA. However, these

trends **do not indicate that DMB is 4 times more effective as a photosensitizer** compared to VL. Also, during GUA oxidation, the calculated decay rate constant of VL was only 4.6 times higher (not ~20 times) than that of DMB (VL decay rate constant in GUA+VL: 3.6 min^{-1}/s^{-1} vs. DMB decay rate constant in GUA+DMB: 0.78 min^{-1}/s^{-1}; note that the decay rate constants were corrected for internal light screening due to DMB and VL light absorption, and normalized to the experimental photon flux).

The Reviewer is correct that comparing photosensitizing abilities is a complex task. However, a detailed quantitative analysis of the photosensitizing abilities which necessitates more experiments, e.g., determining the intersystem crossing quantum yield for VL (Smith et al., 2014) or using time-resolved absorption spectroscopy (Felber et al., 2021) is beyond the scope of the paper. Nonetheless, the estimated decay rate constants and apparent quantum efficiency of GUA photodegradation indicate that GUA oxidation in GUA+DMB was overall more efficient than in GUA+VL. These measurements can be useful for comparison with GUA oxidation by other oxidants or photosensitizers. Our kinetic analysis focused on the decay rate constants of the aqSOA precursor (GUA) and the photosensitizers (DMB and VL) during photosensitization under the same experimental conditions (same aqSOA precursor and concentration, same photosensitizer concentration, and same lamp photon flux). The effects of other factors (e.g., intersystem crossing efficiency) on the rate constants were not examined. Hence, lacking rate constants that are either universal or specific for a number of experimental conditions in the literature, we hope that these parameters obtained in our study can provide first-order estimates for modeling since the experimental conditions (GUA+DMB, GUA+VL, GUA+DMB+AN, GUA+VL+AN, and GUA+AN based on concentrations relevant to cloud and fog conditions at pH 4 in air) are atmospherically relevant. Explicit kinetic studies (e.g., Smith et al., 2014, 2015) that measure second-order rate constants should be conducted in the future to extend the applicability of the kinetic parameters to other conditions.

The following sentences have been added at the end of Sect. 3.1.1 to clarify these:

Line 192: It should be noted that the differences in the GUA decay rate constants among different reaction systems are not quantitatively equivalent to photosensitizing efficiencies, and a detailed quantitative analysis of which is beyond the scope of this study. Nonetheless, these results suggested that GUA oxidation in GUA+DMB was overall more efficient than in GUA+VL. Our kinetic analysis focused on the decay rate constants of the aqSOA precursor (GUA) and the photosensitizers (DMB and VL) during photosensitization under the same experimental conditions (same aqSOA precursor and concentration, same photosensitizer concentration, and same lamp photon flux). The effects of other factors (e.g., intersystem crossing efficiency) on the rate constants were not examined. Explicit kinetic studies (e.g., Smith et al., 2014, 2015) that measure second-order rate constants should be conducted in the future to extend the applicability of the kinetic parameters to other conditions.

Moreover, it should be noted that in this work, we mainly focused on the analyses of the reaction products and product distributions.

The title of the paper has been revised to 'Comparison of aqueous SOA product distributions from guaiacol oxidation by non-phenolic and phenolic methoxybenzaldehydes as

photosensitizers in the absence and presence of ammonium nitrate' to better reflect the focus of the work.

Furthermore, the following sentences have been added to the text to clarify the focus of this work:

Line 96: The precursor and photosensitizer decay kinetics, detected products, and absorbance enhancement were used to characterize the reactions. However, it should be noted that we mainly focused on the analyses of the reaction products and product distribution.

(b) We have given a lot of thought to this comment. We assumed that the question pertains to the normalized abundance of products. The calculation of the normalized abundance of products involves the absolute GUA concentration changes measured before and after irradiation using UHPLC-PDA, which is related to the loss of the photosensitizers. Therefore, the estimated normalized abundance of products already covers the loss of the photosensitizers. The following are mentioned in lines 207-208: "In addition, the normalized product abundance for GUA+DMB was ~4 times higher than that for GUA+VL (Table 1), further suggesting more efficient photosensitized GUA oxidation by ^{3}DMB* than by ^{3}VL*." However, we would like to emphasize that the normalized abundance of products in this work represents a semi-quantitative analysis of products in different experiments rather than absolute concentration of products.

Other comments:

1. Line 95: How are products counted if they appear in both positive and negative modes of ionization?

Response: For the signal-weighted distributions in Figure 2, the peak area of each product (whether it appeared in either positive or negative ion mode only, or it appeared in both ion modes) was normalized to the total signal areas summed from positive and negative ion modes. For reference, the signal-weighted distributions calculated separately from positive and negative ion modes are provided in Figures S2 and S3 (formerly Figures S1 and S2).

2. Line 335: What could highly oxidized species decompose into, that would not be detected and therefore not contribute to the measured O/C ratio? Is this statement alluding to CO2 production?

Response: We apologize for the confusion. Lines 334-335 are based on an earlier work on photo-oxidation of phenolic carbonyls in ammonium nitrate (AN) and ammonium sulfate solutions using a time-of-flight aerosol mass spectrometer (AMS) and therefore involved the aerosolization of samples before analysis (Huang et al., 2018). In that study, highly oxidized species such as small carboxylic acids with O:C =1 (e.g., acetic acid) possibly formed but may have evaporated during aerosolization as they are too volatile. As a result, these species cannot be detected by the AMS. Solutions with AN had a higher concentration of organic acids (without atomization) in the aqueous samples compared to ammonium sulfate solutions, ascribable to nitrate photolytic products promoting the reactions. In brief, the study by Huang et al. (2018) suggested that AN promoted the formation of oxygenated and oxidized products.

As mentioned in lines 340-342, AN generally increased the average OS_c values for both GUA+DMB and GUA+VL, indicating the formation of more oxidized products, similar to the findings by Huang et al. (2018). In this work, AN also possibly promoted the formation of oxygenated products. The lower average O:C for GUA+DMB+AN and GUA+VL+AN than those in the absence of AN could be due to the formation of N-heterocycles, altering the elemental ratios.

The corresponding revisions in the text are as follows:

Line 334: The ⟨O:C⟩ for GUA+DMB+AN and GUA+VL+AN were lower than those in the absence of AN (Table 1), ~~likely due to the rapid formation of highly oxidized species followed by their decomposition (Huang et al., 2018)~~ possibly due to the formation of N-heterocycles, altering the elemental ratios.

Line 340: Nonetheless, AN generally increased the ⟨OS_C⟩ for both GUA+DMB and GUA+VL, with a more noticeable increase for the former, suggesting more oxidized products. Similarly, in a previous work, the more oxygenated and oxidized aqSOA from the photo-oxidation of phenolic carbonyls in AN solutions than in ammonium sulfate solutions has been ascribed to nitrate photolytic products promoting the reactions (Huang et al., 2018).

3. Figure 3: at the top right, C12 and C11 products are referred to as functionalized monomers. How is this different from a ring-opened dimer? How exactly do the authors distinguish functionalization from dimerization?

Response: The dimers in this work have minimum carbon atoms of 12 for 2 benzene rings, and considering demethylation of both -OCH$_3$ groups of typical guaiacol dimer (C$_{14}$H$_{14}$O$_4$; #1 to C$_{12}$H$_{10}$O$_4$; #17; Table S1). The C12 and C11 products in Figure 3 were referred to as functionalized monomers and not ring-opened dimers as the substituents (other than -OH and -OCH$_3$) in these products have carbon atoms <6 which were not enough to form another aromatic ring. These substituents were more likely to be highly oxygenated small species (carbon atoms <6) from oxidation and fragmentation reactions which have also been reported in previous studies on similar reaction systems (e.g., Yu et al., 2014, 2016).

Functionalization involves the addition of polar oxygenated functional groups (e.g., hydroxyl, carbonyl, carboxyl etc.) as well as highly oxygenated small species (carbon atoms < 6) from oxidation and fragmentation reactions to the aromatic ring. Dimerization is characterized by two covalently bound units of the aromatic compounds studied.

4. Figure 4: In this graph, does 1 or zero = no change in integrated absorbance? In other words, is it normalized somehow?

Response: In the original Figure 4, a value of zero means that at 180 min, there was no change in the integrated area of absorbance from 350 to 550 nm compared to 0 min (before irradiation). The integrated area of absorbance from 350 to 550 nm at 180 min was normalized by subtracting the corresponding values at 0 min (before irradiation). For all experiments in this work, we measured the absorbance every 30 min from 0 to 180 min and observed an increase in visible light absorption from 350 to 550 nm.

The absorbance enhancement from 0 to 180 min for all reaction systems studied have been added to Figure 4(a). Based on suggestions from Reviewer 4, the original Figure 4 (now Figure 4b) has also been replaced with the change in the rate of sunlight absorption (ΔR_{abs}) from 350-550 nm at 180 min during typical clear and haze days in Beijing, China. Moreover, the absorption spectra after 180 min of irradiation for each reaction system have been added to the supplement (Figure S7) based on suggestions from Reviewer 4.

The updated Figure 4 and added Figure S7 are shown below:

Figure 4. (a) Increase in light absorption throughout 180 min of irradiation for all reaction systems studied and (b) Change in the rate of sunlight absorption (ΔR_{abs}) from 350-550 nm at 180 min during typical clear and haze days in Beijing, China for aqSOA from GUA+DMB+AN, GUA+DMB, GUA+VL+AN, GUA+VL, and GUA+AN. ~~Increase in visible light absorption for aqSOA from GUA+DMB, GUA+VL, GUA+DMB+AN, and GUA+VL+AN.~~ Error bars represent one standard deviation of triplicate experiments.

Figure S7. UV-Vis absorption spectra of GUA+DMB+AN, GUA+DMB, GUA+VL+AN, GUA+VL, and GUA+AN after 180 min of irradiation. The inset is the expanded view from 350 to 550 nm. The corresponding revisions in the text are as follows:

Lines 253-260: The increase in light absorption throughout 180 min of irradiation and the change in the rate of sunlight absorption (ΔR_{abs}) (Jiang et al., 2021) from 350 to 550 nm at 180 min during typical clear and haze days in Beijing, China for all the reaction systems studied

are provided in Figure 4. Figure S7 shows the absorption spectra after 180 min of irradiation for each reaction system studied. In this work, the absorbance enhancement of GUA+DMB and GUA+VL (Fig. 4a) could be due to ~~correlates with~~ oligomers and functionalized monomers, which are the highest contributors to the product signals. Identifying the chromophores responsible for the absorbance enhancement may be beneficial in understanding the impact of aqSOA on the Earth's radiative balance and determining the reactions that affect light absorption by aqSOA (Mabato et al., 2022). However, the detected products did not exhibit distinct peaks in the UHPLC-PDA chromatograms, likely due to the concentration of the chromophores being below the detection limit of PDA. Nevertheless, the higher absorbance enhancement and ΔR_{abs} for GUA+DMB than GUA+VL was ~~most likely associated with~~ probably due to the higher contribution and normalized abundance (by ~6 times) of oligomers in the former.

Line 353: The presence of AN also did not appreciably affect the absorbance enhancement and ΔR_{abs} for both GUA+DMB+AN and GUA+VL+AN (Fig. 4).

Technical corrections

1. Line (1)94: "represent" should be "characterize"

Response: Thank you for the correction. "represent" has been replaced by "characterize"

2. Line 328: should this say "likely has a furanone group"? Otherwise, how do the authors know this is the correct structure from the many possibilities?

Response: The Reviewer is correct. The text has been revised accordingly.

References for responses to Reviewer 3:

Felber, T., Schaefer, T., He, L., and Herrmann, H.: Aromatic carbonyl and nitro compounds as photosensitizers and their photophysical properties in the tropospheric aqueous phase, J. Phys. Chem. A, 125, 5078–5095, https://doi.org/10.1021/acs.jpca.1c03503, 2021.

Huang, D. D., Zhang, Q., Cheung, H. H. Y., Yu, L., Zhou, S., Anastasio, C., Smith, J. D., and Chan, C. K.: Formation and evolution of aqSOA from aqueous-phase reactions of phenolic carbonyls: comparison between ammonium sulfate and ammonium nitrate solutions, Environ. Sci. Technol., 52, 9215–9224, https://doi.org/10.1021/acs.est.8b03441, 2018.

Jiang, W., Misovich, M. V., Hettiyadura, A. P. S., Laskin, A., McFall, A. S., Anastasio, C., and Zhang, Q.: Photosensitized reactions of a phenolic carbonyl from wood combustion in the aqueous phase—chemical evolution and light absorption properties of aqSOA, Environ. Sci. Technol., 55, 5199–5211, https://doi.org/10.1021/acs.est.0c07581, 2021.

Mabato, B. R. G., Lyu, Y., Ji, Y., Li, Y. J., Huang, D. D., Li, X., Nah, T., Lam, C. H., and Chan, C. K.: Aqueous secondary organic aerosol formation from the direct photosensitized oxidation of

vanillin in the absence and presence of ammonium nitrate, Atmos. Chem. Phys., 22, 273–293, https://doi.org/10.5194/acp-22-273-2022, 2022.

Smith, J. D., Sio, V., Yu, L., Zhang, Q., and Anastasio, C.: Secondary organic aerosol production from aqueous reactions of atmospheric phenols with an organic triplet excited state, Environ. Sci. Technol., 48, 1049–1057, https://doi.org/10.1021/es4045715, 2014.

Smith, J. D., Kinney, H., and Anastasio, C.: Aqueous benzene-diols react with an organic triplet excited state and hydroxyl radical to form secondary organic aerosol, Phys. Chem. Chem. Phys., 17, 10227–10237, https://doi.org/10.1039/C4CP06095D, 2015.

Yu, L., Smith, J., Laskin, A., Anastasio, C., Laskin, J., and Zhang, Q.: Chemical characterization of SOA formed from aqueous-phase reactions of phenols with the triplet excited state of carbonyl and hydroxyl radical, Atmos. Chem. Phys., 14, 13801–13816, https://doi.org/10.5194/acp-14-13801-2014, 2014.

Yu, L., Smith, J., Laskin, A., George, K. M., Anastasio, C., Laskin, J., Dillner, A. M., and Zhang, Q.: Molecular transformations of phenolic SOA during photochemical aging in the aqueous phase: competition among oligomerization, functionalization, and fragmentation, Atmos. Chem. Phys., 16, 4511–4527, https://doi.org/10.5194/acp-16-4511-2016.

Author Response for "Aqueous SOA formation from photosensitized guaiacol oxidation: Comparison between non-phenolic and phenolic methoxybenzaldehydes as photosensitizers in the absence and presence of ammonium nitrate" by Mabato et al.

We thank the Reviewer for their thorough comments. We have revised the manuscript accordingly, and below are our point-by-point responses (in blue) to the comments (in black) and changes to the manuscript (in red). In those changes that begin with line numbers, the original text is also in blue. In addition, please note that the line numbers in the responses correspond to those in the original manuscript.

Reviewer 4

Mabato and co-authors studied the aqueous photochemical reactions of guaiacol (GUA), a methoxyphenol from wood burning, in the presence of vanillin (VL; a phenolic carbonyl), dimethoxybenzaldehyde (DMB; a non-phenolic carbonyl), and/or ammonium nitrate (AN). They examined photochemistry in five different reaction solutions: (1) GUA + AN, (2) GUA + DMB, (3) GUA + DMB + AN, (4) GUA + VL, and (5) GUA + VL + AN. For each system, they give the kinetics of loss, information about the products formed, and some very cursory information about light absorption from the resulting reaction mixture.

There are a few interesting pieces in the manuscript, most notably the suggested interaction of AN photoproducts with triplet photoproducts, which I wish the authors had explored more. But, otherwise, the research seems to largely repeat ideas and experiments that have been reported previously. I don't see new, interesting questions that are driving the current work. In addition, I see several other important weaknesses, as described below.

Response: Thank you for the comprehensive review. In this work, our focuses were 1) to **compare** aqSOA formation from **photosensitization by non-phenolic and phenolic methoxybenzaldehydes** as photosensitizers using GUA as the dominant aqSOA precursor and 2) to examine the **effects of AN** on these reactions. Biomass burning smoke has been reported to have comparable concentrations of phenolic and non-phenolic carbonyls (Simoneit et al., 1993; Anastasio et al., 1997), and certain phenolic carbonyls including VL, have been shown to be capable of photosensitization, contributing to aqSOA formation (Smith et al., 2016; Mabato et al., 2022). However, compared to DMB (a non-phenolic carbonyl), the most commonly used photosensitizer in related studies, aqSOA formation using phenolic carbonyls as photosensitizers is less understood. DMB and VL were chosen to represent non-phenolic and phenolic methoxybenzaldehydes photosensitizers because (1) their structures differ only by one functional group ($-OCH_3$ for the former and $-OH$ for the latter), (2) they are both abundant in biomass burning emissions, and (3) there is available information on their photophysical properties (e.g., quantum yield of $^3C^*$ formation and $^3C^*$ lifetime) (Felber et al., 2021). Moreover, aromatic carbonyls and phenols may coexist with AN in biomass burning aerosols. However, aqSOA formation **studies have investigated either photosensitization or nitrate-mediated photo-oxidation, even though these reactions can occur simultaneously**. In general, **studies** on the **effects of inorganic nitrate on aqSOA formation remain very limited**. We believe that **this work is one of the very few in the literature that examines this complex system. The Reviewer has given us a lot of valuable comments highlighting the complexity of the photosensitization reactions** when even just a photosensitizer and a non-

phenolic carbonyl are involved in the reactions, let alone the addition of AN in the system. **It is** understood that **much more work needs to be done to fully unravel the interactions of photosensitization and nitrate photolysis.** We hope this work can **stimulate researchers to look into these important but rarely explored interactions in the photochemistry of aerosols.** Further information on the novelty of this work is given in the response to major comment #1.

Major Comments

1. It is not clear what is novel enough about this work that it deserves to be published in ACP. (a) A number of the systems or parts of the manuscript have been reported previously, both by this group and other groups. For example, Mabato et al. (2022) reported results for GUA + VL, while Smith et al. and Yu et al. reported results for GUA + DMB and for another phenol (SYR) with VL. (b) The addition of ammonium nitrate in the manuscript has no significant impact on kinetics or normalized product amounts, but does lead to incorporation of N into the aqSOA, a point made for VL + AN by Mabato et al. (2022) and for general carbonyl + ammonium systems by several past authors. (c) One result is that there is significant repetition of past work. Some examples: (1) the first two paragraphs on page 8 largely repeat what has been shown in previous work, (2) there's nothing new in Figure 1, as all of these molar absorptivities have been shown by previous groups, and (3) most of the pieces of Figure 3 have been shown in Mabato et al. (2022) or in past work by the Zhang group.

Response: (a) The Reviewer is correct that GUA+DMB and GUA+VL have been explored in earlier studies. Our previous study (Mabato et al., ACP, 2022) focused on aqSOA formation from the direct photosensitized oxidation of VL. GUA+VL in that study was compared with direct GUA photodegradation. We discussed the decay kinetics of both VL and GUA, absorbance changes, and a few detected products **but not product distribution**. Smith et al. (2014) and Yu et al. (2014, 2016) provided valuable information on GUA+DMB, focusing on the decay kinetics of GUA, aqSOA mass yields, product characterization, photochemical evolution of aqSOA, and aqSOA formation pathways. For VL+syringol, SYR (another non-carbonyl phenol), Smith et al. (2016) reported VL and SYR decay kinetics and absorbance changes. **However, as stated in the original manuscript, our previous experiments were performed at a higher concentration of VL (0.1 mM) compared to DMB concentration (0.005 to 0.01 mM) used by Smith et al. (2014) and Yu et al. (2014, 2016).** Moreover, different instruments were used to characterize the products in these earlier works. Thus, direct comparisons between GUA+DMB and GUA+VL based on atmospherically relevant conditions cannot be made using the above studies. **This paper is the first, to the best of our knowledge, to make such comparisons at the same concentration range with the same analytical techniques systematically.**

Moreover, previous aqSOA formation studies involving aromatic carbonyls and non-carbonyl phenols have examined either photosensitization or nitrate-mediated photo-oxidation **separately, even though these reactions can occur simultaneously**. In general, aqSOA formation **studies on multicomponent reaction systems w**here inorganic and organic species are present **remain limited. In the current work,** we attempted to **address this gap by introducing AN, a common aerosol component** that is also abundant in cloud and fog waters, **into the reaction systems studied.**

We would like to emphasize that the novelty of the current work includes: 1) a thorough comparison of aqSOA formation from photosensitization by non-phenolic and phenolic methoxybenzaldehydes as photosensitizers using GUA as the dominant aqSOA precursor based on GUA and photosensitizers decay kinetics, detected products, and absorbance enhancement and 2) the examination of the effects of AN on these reactions. Despite some similar findings with earlier studies, our results offer new insights into the reaction systems examined. For instance, our results demonstrate that **the structural features of photosensitizers affect aqSOA formation** via GUA (non-carbonyl phenol) oxidation. Moreover, we found that **photosensitization by non-phenolic and phenolic methoxybenzaldehydes may be differently influenced by AN photolysis.** For example, compared to GUA+VL, the more extensive fragmentation in GUA+DMB likely resulted in a higher contribution of ring-opening products. These ring-opening species reacted with ammonia resulting in higher contributions of N-heterocycles and N-oligomers and yielding an overall higher contribution of N-containing products in GUA+DMB+AN than in GUA+VL+AN. The increase in oligomers in GUA+VL+AN could be due to the generation of phenoxy radicals from VL via H-atom abstraction by $^{\bullet}$OH or $^{\bullet}$NO$_2$ from nitrate photolysis. Furthermore, our results suggest that **photosensitization may promote reactions by nitrate photolysis.** In particular, $^{\bullet}$OH and O$_2^{\bullet-}$ (secondary oxidants from ^{3}DMB* or ^{3}VL*) can react with NO$_2^-$ from nitrate photolysis to increase the formation of $^{\bullet}$NO$_2$ (Pang et al., 2019; Mabato et al., 2022).

(b) The Reviewer is right that the formation of N-heterocycles which indicates the participation of ammonium in the reactions has also been reported in our previous experiments on VL+AN (Mabato et al., 2022) and for smaller carbonyls + ammonium systems in several past works (e.g., De Haan et al., 2009; Galloway et al., 2009; Nozière et al., 2009; Shapiro et al., 2009; Yu et al., 2011; Kampf et al., 2012; Gen et al., 2018; Mabato et al., 2019). **However, our present study also demonstrated that photosensitized aqSOA formation involving non-phenolic and phenolic methoxybenzaldehydes as photosensitizers may be differently influenced by AN photolysis.** In addition, we also found that **photosensitized reactions may promote nitrate-mediated photolytic reactions.** Overall, our conclusions provide a clear path forward for further work on other types of photosensitizers for aqSOA formation, which to date is **limited mainly to DMB, and indicate a potential interplay between photosensitized reactions and AN photolysis, beyond the formation of nitrated compounds.** We also revised the abstract to further highlight the novelty of the work, as shown below:

Abstract:

Aromatic carbonyls (e.g., methoxybenzaldehydes), an important class of photosensitizers, are abundant in the atmosphere. Photosensitization and nitrate-mediated photo-oxidation can occur simultaneously, yet studies about their interactions, particularly for aqueous secondary organic aerosol (aqSOA) formation, remain limited. This study compared non-phenolic (3,4-dimethoxybenzaldehyde, DMB) and phenolic (vanillin, VL) methoxybenzaldehydes as photosensitizers for ~~aqueous secondary organic aerosol (~~aqSOA~~)~~ formation via guaiacol (GUA) oxidation in the absence and presence of ammonium nitrate (AN) under atmospherically relevant cloud and fog conditions…

(c) We thank the Reviewer for highlighting these three areas that contain a lot of information based on the literature. However, they mainly **provide background for the readers to follow the results and discussions.** We are unsure if they are the best examples for evaluating the novelty of this paper.

(1) The first 2 paragraphs on page 8 compare **the major products, average elemental ratios, and elemental distributions of products** from GUA+DMB and GUA+VL. In addition, we **discussed how this information relates to the differences in the product distributions, which are not available in previous works.**

(2) Aside from showing molar absorptivities, Figure 1 provides the structures of the compounds studied in this work, the photon flux in the photoreactor, and photon fluxes on clear or haze days. **This figure is meant to provide sufficient background information for readers. It is not a "result" figure.**

(3) The related figure by Yu et al. (2014) shows the **main pathways of aqSOA formation via photosensitized oxidation of non-carbonyl phenols by ^{3}DMB* only**. Also, the related figure in our previous work (Mabato et al., 2022) shows the potential aqSOA formation pathways for the direct photosensitized oxidation of VL and VL+AN. **The comparisons about N-containing products in that work pertained to pH effects, not photosensitizers**. In addition, the aqSOA precursor (and photosensitizer) in that study is VL, whereas here, it is GUA. Figure 3 illustrates the **differences between GUA oxidation by ^{3}DMB* and ^{3}VL* in the absence and presence of AN, highlighting the major products detected in this work**. **The comparisons are based on the product distributions which have not been reported for GUA+VL. Moreover, the effects of AN on the product distributions of aqSOA from photosensitized reactions have not been examined previously.**

2. The results aren't quantitative in a way that they could be used to model aqSOA formation from 3VL*. For example, the rate constants for decay of GUA given in Table 1 are probably specific for the experimental conditions used here. The same is true for the quantum yields given in the text - these are almost certainly a function of GUA concentration. It would be much more useful to measure fundamental quantities (e.g., second-order rate constants for 3VL* + GUA) that can be used across a wide range of conditions. Can the current set of data be used to determine some fundamental quantities that are widely applicable? If not, how will people use these data to quantitatively understand these reaction systems?

Response: Agreed. Having said that, we believe this is a common limitation of laboratory kinetic studies in complex chemical systems. While there are some studies (e.g., Smith et al., 2015) citing various kinetic parameters on photosensitization based on selected experimental studies, we are unsure if there are kinetic parameters that are **proven universal** in photosensitization studies. Moreover, it should be noted that in this work, we mainly focused on the analyses of the reaction products and product distributions. Our kinetic analysis focused on the decay rate constants of the aqSOA precursor (GUA) and the photosensitizers (DMB and VL) during photosensitization under the same experimental conditions (same aqSOA precursor and concentration, same photosensitizer concentration, and same lamp photon flux). The effects of other factors (e.g., intersystem crossing efficiency) on the rate constants were not examined. Hence, lacking rate constants that are either universal or

specific for a number of experimental conditions in the literature, we hope that these parameters obtained in our study can provide first-order estimates for modeling since the experimental conditions (GUA+DMB, GUA+VL, GUA+DMB+AN, GUA+VL+AN, and GUA+AN based on concentrations relevant to cloud and fog conditions at pH 4 in air) are atmospherically relevant. Explicit kinetic studies (e.g., Smith et al., 2014, 2015) that measure second-order rate constants should be conducted in the future to extend the applicability of the kinetic parameters to other conditions.

We agree with the Reviewer that the apparent quantum efficiency of GUA photodegradation in the presence of DMB and likely VL as well is dependent on GUA concentration based on an earlier work (Anastasio et al., 1997). Regardless, this information would still be useful for comparison with GUA oxidation by other oxidants or photosensitizers.

The title of the paper has been revised to 'Comparison of aqueous SOA product distributions from guaiacol oxidation by non-phenolic and phenolic methoxybenzaldehydes as photosensitizers in the absence and presence of ammonium nitrate' to better reflect the focus of the work.

Furthermore, the following sentences have been added to the text to clarify the focus of this work:

Line 96: The precursor and photosensitizer decay kinetics, detected products, and absorbance enhancement were used to characterize the reactions. However, it should be noted that we mainly focused on the analyses of the reaction products and product distribution.

Line 192: Our kinetic analysis focused on the decay rate constants of the aqSOA precursor (GUA) and the photosensitizers (DMB and VL) during photosensitization under the same experimental conditions (same aqSOA precursor and concentration, same photosensitizer concentration, and same lamp photon flux). The effects of other factors (e.g., intersystem crossing efficiency) on the rate constants were not examined. Explicit kinetic studies (e.g., Smith et al., 2014, 2015) that measure second-order rate constants should be conducted in the future to extend the applicability of the kinetic parameters to other conditions.

3. (a) I don't see the utility of [P], the normalized product abundance. In the big picture, what does [P] indicate about a certain reaction system and what do differences in [P] between reaction systems indicate? (b) The authors present it as an equation without any in-depth discussion of its strengths and weaknesses. Since [GUA]t/[GUA]0 is the inverse of the fraction of initial GUA that is present at time t, Equation 2 for [P] could be simplified as A(P,t)/A(GUA,0). Thus [P] depends on at least three variables: (1) the extent of reaction, since A(P,t) probably rises initially and later falls, (2) the fraction of products that give a signal in the HPLC-Orbitrap (e.g., small organic acids probably do not), and (3) the ionization efficiency of each product in the Orbitrap. These issues need to be described in the manuscript; as part of this, the authors should say something about the IE values for the different classes of products that they see. (c) [P] also depends on what is used to normalize peak areas, e.g., VL in Mabato et al. (2022) and GUA here (making it very difficult to compare across the papers), and probably the initial concentration of the normalizing species. Given all of these variables, what do we learn from the Table 1 data of [P] after 180 min of illumination? If they authors

want to use [P] to describe products, they need to state what they think this parameter indicates, give us some experimental evidence that it's useful, and say something about its strengths and weaknesses. As it currently stands, the reported values of [P] seem to have no real utility.

Response: (a) The normalized abundance of products in this work is a semi-quantitative analysis intended to provide an overview of how the mass spectrometry (MS) signal intensities varied under different experimental conditions, but it does not quantify the absolute concentration of products from reaction systems. As demonstrated in our previous work (Mabato et al., 2022) and the current study, a higher normalized abundance of products correlates with higher efficiency of oxidation.

(b) Thank you for the suggestion. In this work and in our previous study (Mabato et al., 2022), we measured the absolute concentration changes of the precursor and photosensitizers using UHPLC-PDA. As we already have this quantitative data and given that it is a direct quantification of GUA concentration, we included the GUA concentration changes measured using UHPLC-PDA in the calculation of normalized product abundance to lessen its overall uncertainties. The simplification of the equation suggested by the Reviewer would yield the same trends in the original manuscript and would not change the conclusions. Therefore, we would like to retain the equation and the values presented in the original manuscript.

(1) We agree with the Reviewer that the [P] would depend on the extent of the reaction. However, in this work, the same irradiation time (180 min) was applied to all experiments as we were trying to compare the product distributions after a certain time of light photosensitization. An irradiation time of 180 min was chosen as it was sufficient to show the differences in the extent of reaction of GUA among the reaction systems studied. Moreover, our analysis of product distribution was focused only on aqSOA generated after 180 min of irradiation.

This has been clarified in the text are follows:

Lines 194-197: The products detected using UHPLC-HESI-Orbitrap-MS were used to ~~represent~~ characterize the aqSOA formed in this work. The signal-weighted distributions of aqSOA calculated from combined positive (POS) and negative (NEG) ion modes MS results are summarized in Figure 2. The signal-weighted distributions calculated separately from POS and NEG ion modes MS results are available in Figures S~~1~~2 and S~~2~~3. It should be noted that in this work, the product distributions for all experiments were based on the same irradiation time of 180 min. An irradiation time of 180 min was chosen as it was sufficient to show the differences in the extent of reaction of GUA among the reaction systems studied. For reaction systems with precursors of different reactivities, chemical analysis at a fixed reaction time may be looking at different generations of products of each precursor, as Yu et al. (2014) reported. Measuring the product distribution at a fixed time might have missed the information on what/how many products are formed at the similar amounts of precursors reacted. The situation could be even more complicated if different precursors had major differences in pathways and dominant intermediates. However, comparing the product distributions after a certain time of light exposure, as is the case for this study, is useful to evaluate what products would form after a certain time of photosensitization.

(2) We agree with the Reviewer that certain products may not give signals (or may have weak signals) in the UHPLC-Orbitrap. We mentioned in the discussion of product distributions that the products detected using UHPLC-HESI-Orbitrap-MS were used to characterize the aqSOA formed in this work (line 194). Moreover, as stated in the footnote of Table 1, the normalized abundance of products was calculated using only the positive ion mode data as the GUA signal from the negative ion mode was weak and thus may present large uncertainties during normalization. Therefore, products that may not give signals or may have weak signals in the positive ion mode were possibly underestimated in the normalized product abundance. For example, small organic acids are more likely to be detected in the negative ion mode as this mode is more sensitive to deprotonatable compounds (Ho et al., 2003).

To clarify this, the following has been added to the description of normalized abundance of products (Sect 2.2):

It should be noted that the normalized abundance of products was calculated using only the positive ion mode data as the GUA signal from the negative ion mode was weak and thus may present large uncertainties during normalization. Therefore, products that may not give signals or may have weak signals in the positive ion mode were possibly underestimated in the normalized product abundance.

(3) It is very common to compare the relative abundance of products based on peak areas from MS results (e.g., Lee et al., 2014; Romonosky et al., 2017; Wang et al., 2017; Fleming et al., 2018; Song et al., 2018; Klodt et al., 2019; Ning et al., 2019) to show the relative importance of different types of compounds (K. Wang et al., 2021). However, comparisons of relative abundance among different compounds can be subject to uncertainties as ionization efficiencies in soft ionization, such as ESI, may significantly vary between different compounds (Kebarle, 2000; Schmidt et al., 2006; Leito et al., 2008; Perry et al., 2008; Kruve et al., 2014). **In our previous work (Mabato et al., 2022), we introduced the normalized abundance of products ([P], unitless).** The calculation assumes equal ionization efficiencies of different compounds, which is commonly used for the estimation of O:C ratios of SOA (e.g., Bateman et al., 2012; Lin et al., 2012; Laskin et al., 2014; De Haan et al., 2019). **This allows us to have a better comparison with the literature results.** It is therefore emphasized that the normalized abundance of products is a semi-quantitative analysis of the detected products under different experimental conditions, instead of absolute concentrations of them. As stated in the footnote of Table 1, the uncertainties were propagated from the changes in [GUA] measured using UHPLC-PDA and the MS signal intensities.

Unfortunately, there is limited availability of measured relative ionization efficiencies (RIE) for different compounds in the literature. We are in no position to provide the RIE values for the detected products. While ESI ionization is not ideal for quantification analysis of products, Nguyen et al. (2013) (https://doi.org/10.1039/C2AY25682G) demonstrated a positive correlation between ESI signal and "adjusted mass" (= molecular mass × H:C). According to that study, the uncertainty would be a factor of 2 – 4 if only the "adjusted mass" is considered, and further complications of matrix effect and polarity are ignored. **However, what we compared is not the absolute concentrations (or contributions) of the detected products. The comparison was based on how the signal intensities (as normalized in Eq. 2) varied under different experimental conditions so that the responses of the same class of products**

(e.g., monomers, dimers, etc.) could be compared as the conditions varied. The ionization efficiency might not be very different within the same class according to the "adjusted mass" concept by Nguyen et al. (2013). We hope that the above discussion has addressed the Reviewer's question.

(c) In this work, GUA was used to normalize the product peak areas as it is found in all samples, enabling comparisons among different experiments. In our previous study (Mabato et al., 2022), VL was used as it was both the dominant aqSOA precursor and the photosensitizer. Although the normalized abundance of products has inherent uncertainties due to the variability in ionization efficiencies for different compounds, **it can be used as a semi-quantitative analysis of the detected products that provides an overview of how the MS signal intensities varied under different experimental conditions.** As demonstrated in our previous work (Mabato et al., 2022) and the current study, a higher normalized abundance of products generally correlates with higher efficiency of oxidation. For instance, in our earlier study on the direct photosensitized oxidation of VL (Mabato et al., 2022), we found higher VL decay rate constants and higher normalized abundance of products under air-saturated conditions vs. nitrogen-saturated conditions. In this study, a higher GUA decay rate constant and higher normalized abundance of products was noted for GUA+DMB vs. GUA+VL.

Based on the responses above, Sect. 2.2 has been amended to give more information about the normalized abundance of products as follows:

Section 2.2 Calculation of ~~the~~ normalized abundance of products

Several recent studies have used comparisons of relative abundance of products based on peak areas from mass spectrometry (MS) results (e.g., Lee et al., 2014; Romonosky et al., 2017; Wang et al., 2017; Fleming et al., 2018; Song et al., 2018; Klodt et al., 2019; Ning et al., 2019) to show the relative importance of different types of compounds (K. Wang et al., 2021). However, comparisons of relative abundance among different compounds can be subject to uncertainties as ionization efficiencies in soft ionization, such as ESI, may significantly vary between different compounds (Kebarle, 2000; Schmidt et al., 2006; Leito et al., 2008; Perry et al., 2008; Kruve et al., 2014). ~~The normalized abundance of products ([P], unitless) was introduced in our previous work (Mabato et al., 2022).~~ In our previous work (Mabato et al., 2022), we introduced the normalized abundance of products ([P], unitless) (Eq. 2) as ~~Nevertheless, it is~~ a semi-quantitative analysis that gives an overview of how the signal intensities changed under different experimental conditions but not the quantification of the absolute product concentration. ~~Briefly,~~ The calculation assumes equal ionization efficiencies of different compounds, which is commonly used to estimate O:C ratios of SOA (Bateman et al., 2012; Lin et al., 2012; Laskin et al., 2014; De Haan et al., 2019) ~~was assumed for the calculation~~:

$$[P] = \frac{A_{P,t}}{A_{GUA,t}} \cdot \frac{[GUA]_t}{[GUA]_0} \qquad \text{(Eq. 2)}$$

where $A_{P,t}$ and $A_{GUA,t}$ are the extracted ion chromatogram (EIC) peak areas of the product P and GUA from UHPLC-HESI-Orbitrap-MS analyses at time t, respectively; $[GUA]_t$ and $[GUA]_0$ are the GUA concentrations (µM) determined using UHPLC-PDA at time t and 0, respectively. Note that the normalized abundance of products has intrinsic uncertainties due to the

variability in ionization efficiencies for various compounds. Moreover, it should be noted that the normalized abundance of products was calculated using only the positive ion mode data as the GUA signal from the negative ion mode was weak and thus may present large uncertainties during normalization. Therefore, products that may not give signals or may have weak signals in the positive ion mode were possibly underestimated in the normalized product abundance. Nevertheless, it enables the comparison of MS results among different experiments. As demonstrated in our previous work (Mabato et al., 2022) and the current study, a higher normalized abundance of products generally correlates with higher efficiency of oxidation. The reported uncertainties were propagated from the changes in [GUA] measured using UHPLC-PDA and the MS signal intensities.

4. In each of the five systems, products were measured after 180 min of illumination. But this approach ignores the fact that the systems have different reactivities and so a fixed time of analysis is looking at different generations of products in the different systems (as shown by Yu et al.). This is important because the relative amounts of products are a function of oxidation time in any given solution. So it is difficult to meaningfully compare across different solutions unless the GUA fraction reacted is very similar. This is further complicated by the much faster decay of VL compared to DMB.

Response: The Reviewer raised a good point. However, in this work, the same irradiation time was applied to all experiments as we were trying to evaluate the product distributions after a certain time of photosensitization. An irradiation time of 180 min was chosen for this work as it was sufficient to show the differences in the extent of reaction of GUA among the reaction systems studied. It is true that for reaction systems with precursors of different reactivities, chemical analysis at a fixed reaction time may be looking at different generations of products of each precursor, as Yu et al. (2014) reported. Measuring the product distribution at a fixed time might have missed the information on what/how many products are formed at the similar amounts of precursors reacted. The situation could be even more complicated if different precursors had major differences in pathways and dominant intermediates. However, comparing the product distributions after a certain time of light exposure, as is the case for this study, is useful to evaluate what products would form after a certain time of photosensitization. The corresponding changes in the text (lines 194-197) are shown in our response to major comment #3.

5. The presentation of light absorption data for the reaction products is insufficient. There is one figure (Fig. 4) that sums absorbance values across 350 – 550 nm. This is interesting in that it shows the presence of ammonium nitrate doesn't affect overall absorbance, but this is too coarse a tool to describe the brown carbon products by itself. It would be helpful to show spectra for each solution at 180 min in the supplement. Also, Fig. 4 should be improved by weighting each absorbance spectrum by the spectral actinic flux to properly describe light absorption. This could also be done by calculating the rate of sunlight absorption by each aqSOA for some standard sunlight condition. This matters because the number of solar photons increases enormously from 350 to 550 nm.

Response: Thank you for the suggestions. The absorption spectra after 180 min of irradiation for each reaction system have been added to the supplement (Figure S7) as shown below:
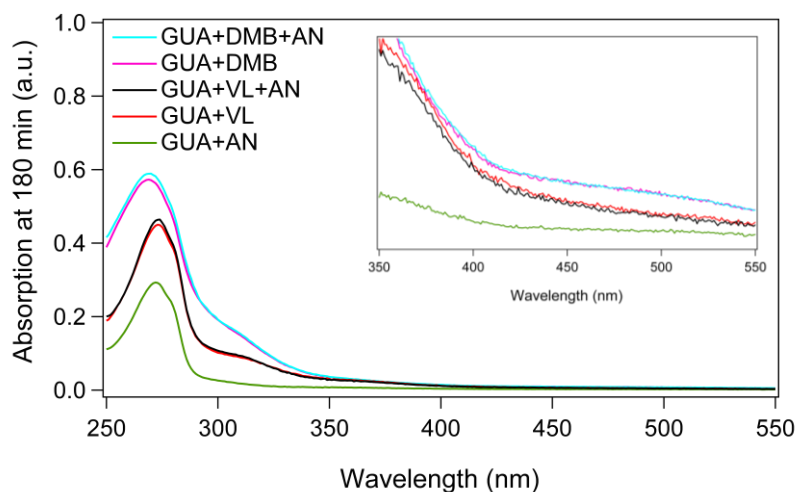
Figure S7. UV-Vis absorption spectra of GUA+DMB+AN, GUA+DMB, GUA+VL+AN, GUA+VL, and GUA+AN after 180 min of irradiation. The inset is the expanded view from 350 to 550 nm.

Moreover, the absorbance enhancement from 0 to 180 min for all reaction systems studied have been added to Figure 4(a), based on suggestions from Reviewers 1 and 2. The original Figure 4 (now Figure 4b) has also been replaced with the change in the rate of sunlight absorption (ΔR_{abs}) from 350-550 nm at 180 min during typical clear and haze days in Beijing, China. The updated Figure 4 is shown below:
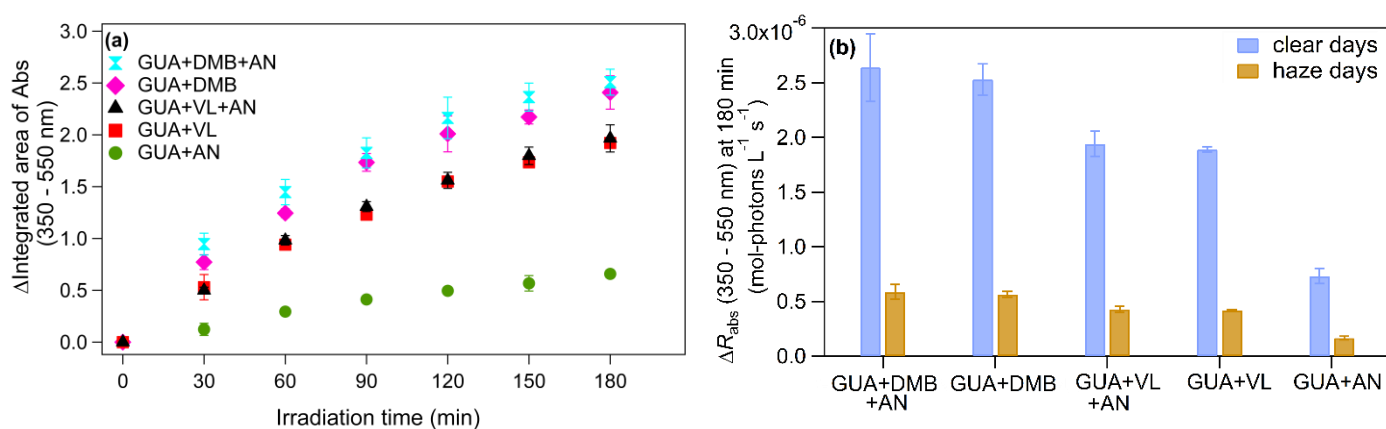
Figure 4. (a) Increase in light absorption throughout 180 min of irradiation for all reaction systems studied and (b) Change in the rate of sunlight absorption (ΔR_{abs}) from 350-550 nm at 180 min during typical clear and haze days in Beijing, China for aqSOA from GUA+DMB+AN, GUA+DMB, GUA+VL+AN, GUA+VL, and GUA+AN. ~~Increase in visible light absorption for aqSOA from GUA+DMB, GUA+VL, GUA+DMB+AN, and GUA+VL+AN.~~ Error bars represent one standard deviation of triplicate experiments.

The corresponding revisions in the text are as follows:

Lines 253-260: The increase in light absorption throughout 180 min of irradiation and the change in the rate of sunlight absorption (ΔR_{abs}) (Jiang et al., 2021) from 350 to 550 nm at 180 min during typical clear and haze days in Beijing, China for all the reaction systems studied

are provided in Figure 4. Figure S7 shows the absorption spectra after 180 min of irradiation for each reaction system studied. In this work, the absorbance enhancement of GUA+DMB and GUA+VL (Fig. 4a) could be due to ~~correlates with~~ oligomers and functionalized monomers, which are the highest contributors to the product signals. Identifying the chromophores responsible for the absorbance enhancement may be beneficial in understanding the impact of aqSOA on the Earth's radiative balance and determining the reactions that affect light absorption by aqSOA (Mabato et al., 2022). However, the detected products did not exhibit distinct peaks in the UHPLC-PDA chromatograms, likely due to the concentration of the chromophores being below the detection limit of PDA. Nevertheless, the higher absorbance enhancement and ΔR_{abs} for GUA+DMB than GUA+VL was ~~most likely associated with~~ probably due to the higher contribution and normalized abundance (by ~6 times) of oligomers in the former.

Line 353: The presence of AN also did not appreciably affect the absorbance enhancement and ΔR_{abs} for both GUA+DMB+AN and GUA+VL+AN (Fig. 4).

Other Comments

1. Line 125. Just a note: you don't need to bubble air through a solution to make it air saturated. Shaking the solution with air in the headspace, then opening the container, and repeating this several times is sufficient. The downside to bubbling synthetic air is that you can introduce water-soluble contaminants from the air into the solution.

Response: Thank you for the suggestion. We will keep this in mind for our future work. We performed continuous bubbling of air into the reactor to ensure that the reactions would not be limited by oxygen availability.

2. Line 126. What was the flow rate of air through the solutions during illumination. Is it fast enough to be a significant loss mechanism for volatile compounds (e.g,. NOx, small organics, etc.)?

Response: The flow rate used in this work was 0.5 dm^3/min. We have added the flow rate used as well as the initial volume of the solutions in the text as follows:

Line 125: The solutions (initial volume of 500 mL) were bubbled with synthetic air (0.5 dm^3/min) for 30 min before irradiation and throughout the reactions to achieve air-saturated conditions (Du et al., 2011; Chen et al., 2020) and were continuously magnetically stirred.

Our control experiment of bubbling air through 0.01 mM formic acid for 6 hours did not result in a significant change ($p > 0.05$) in concentration. Based on this, we believe that the flow rate used in this work is not fast enough to be a significant loss mechanism for volatile compounds (e.g., NOx, small organics, etc.).

3. Line 129. (a) What was the pathlength of the photoreactor? (b) What were the corresponding light screening factors for each solution? (c) Are corrections for light screening required to correct the rate constants?

Response: (a) The path length of the photoreactor is 8.5 cm.

(b) Following Smith et al. (2014, 2016), the values of the internal light screening factor (S_λ) determined around the peak in the light absorption action spectrum (DMB: 310-335 nm, VL: 304-364 nm, and nitrate: 300-331 nm) for an 8.5 cm cell were as follows:

Reaction conditions	Internal light screening factor (S_λ)
GUA+AN	0.95
GUA+DMB	0.51
GUA+DMB+AN	0.54
GUA+VL	0.57
GUA+VL+AN	0.59

(c) Thank you for pointing this out. The decay rate constants were initially not corrected for light screening as the same concentration was used for DMB and VL. However, given the significant difference between the S_λ of GUA+AN and those of other reaction conditions, we corrected the decay rate constants for S_λ in Table 1. The following information has been added to the text to reflect these changes:

Line 143: The decay rate constants were normalized to the photon flux measured for each experiment through dividing k' by the measured 2-nitrobenzaldehyde (2NB; a chemical actinometer) decay rate constant, j(2NB) (Mabato et al., 2022). In addition, the decay rate constants were corrected for the internal light screening due to DMB, VL, and AN (Leifer, 1988; Zhang and Anastasio, 2003; Smith et al., 2014, 2016). The values of the internal light screening factor (S_λ) determined around the peak in the light absorption action spectrum (DMB: 310-335 nm, VL: 304-364 nm, nitrate: 300-331 nm) (Smith et al., 2014, 2016) for an 8.5 cm cell were 0.95 for GUA+AN, 0.51 for GUA+DMB, 0.54 for GUA+DMB+AN, 0.57 for GUA+VL, and 0.59 for GUA+VL+AN.

Footnote of Table 1: [a]The data fitting was performed in the initial linear region. Each value is the average of results from triplicate experiments, corrected for internal light screening due to DMB, VL, and AN, and normalized to the experimental photon flux. Errors represent one standard deviation.

4. Line 141. Were the decays of GUA, VL, and DMB always first-order? It seems unlikely given that the reactions proceeded for many half-lives of some of the compounds (e.g., VL). It would be helpful to show both examples of good (first-order) and not so good kinetics in the supplement.

Response: In this work, the decay of GUA, DMB, and VL were treated as pseudo-first-order, and the reported decay rate constants were obtained by performing the data fitting in the initial linear region, as noted in the original text (line 176) and Table 1. This is based on the consideration that the exact composition of the solutions during the reactions is unknown (e.g., due to the generation of intermediates).

The plots of the GUA, DMB, and VL decay (shown below) have now been added to Figure S1. The corresponding changes in the text are as follows:

Line 180: Figure S1 shows the decay of GUA, DMB, and VL under different experimental conditions.
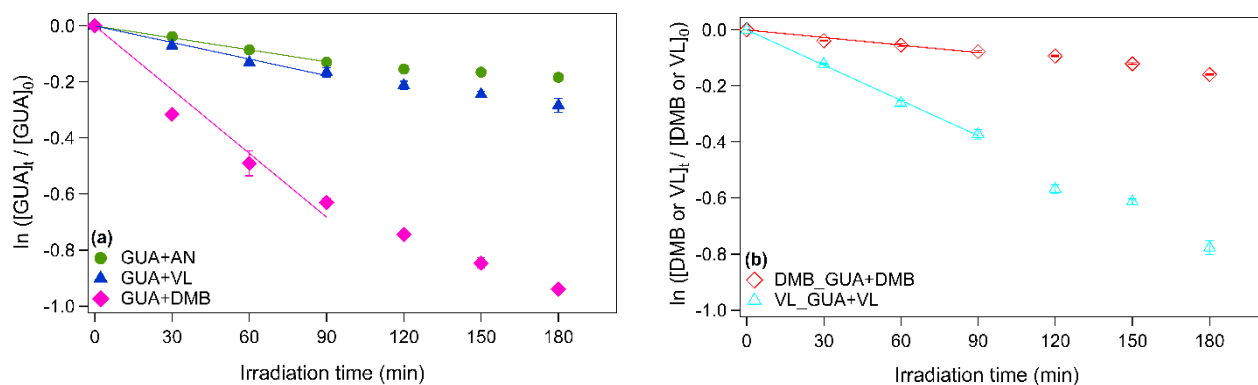
Figure S1. (a) The decay of GUA during (ammonium) nitrate-mediated photo-oxidation (GUA+AN) and photosensitized oxidation by ^{3}VL* (GUA+VL) or ^{3}DMB* (GUA+DMB). (b) The decay of DMB or VL during GUA photo-oxidation in GUA+DMB and GUA+VL, respectively. No statistically significant difference ($p > 0.05$) was noted between GUA+DMB and GUA+DMB+AN and between GUA+VL and GUA+VL+AN. Error bars represent 1 standard deviation; most error bars are smaller than the markers.

5. Line 234. These two sentences seem contradictory: GUA+DMB had more compounds with higher O:C, but GUA+VL had a higher average OS(C). How to reconcile this apparent discrepancy?

Response: We apologize that we may have misled the Reviewer. They are not inconsistent. The statement on GUA+DMB indicates having more compounds in terms of quantity or number with higher O:C than in GUA+VL. However, overall, the average O:C and OS_C calculated using the signal-weighted method (Bateman et al., 2012) were higher for GUA+VL than for GUA+DMB. This is probably due to the more significant functionalization in GUA+VL (as mentioned in line 236).

6. Line 254. Is this statement based only on the higher amounts of oligomers and functionalized monomers in the GUA+DMB case compared to the GUA+VL case? If so, this is weak evidence and really not a "correlation".

Response: Line 254 does not compare the absorbance enhancement for GUA+DMB vs. GUA+VL. Rather, it is about attributing the absorbance enhancement for both GUA+DMB and GUA+VL to oligomers and functionalized monomers which are the highest signal contributors. Regardless, we revised the text as follows:

Line 254: In this work, the absorbance enhancement of GUA+DMB and GUA+VL (Fig. 4a) could be due to ~~correlates with~~ oligomers and functionalized monomers, which are the highest contributors to the product signals.

7. Table 1. (a) Are these rate constants normalized to a specific j(2NB) value? Line 144 indicates that rate constants were normalized by dividing by j(2NB), but this does not appear to have been done to the Table 1 rate constants based on their units. If the authors aren't going to normalize the rate constants, they should discuss the variation in j(2NB) across their samples and give average j(2NB) values for each reaction condition. (b) In the presence of AN, GUA has a rate constant of 8.1E-3 min-1, which is appreciable. But the addition of AN to the DMB or VL solutions has no apparent impact on the rate constant for GUA loss, with a difference much less than the addition increment expected of 8E-3 min-1. How to explain this discrepancy in the kinetics? Is light screening an issue? (c) Experiment #4 is labeled as a second #3.

Response: (a) Thank you for pointing this out. Yes, these rate constants were normalized to the photon flux measured for each experiment, but we inadvertently used the wrong unit for 2-nitrobenzaldehyde (2NB) decay rate constants during normalization. Table 1 now shows the correct photon flux-normalized rate constants, which were also corrected for internal light screening due to DMB, VL, and AN, based on the Reviewer's other comment #3. We apologize for the confusion.

(b) The addition of AN to GUA+DMB and GUA+VL had no significant effect on the decay rate constants, likely due to the higher molar absorptivities of DMB and VL compared to that of nitrate. This indicates that the chemistry of ^{3}DMB* and ^{3}VL* dominated that of nitrate photolysis. This information was already provided in lines 277-279. The estimated light-absorbing fraction (molar absorptivities from 300 to ~360 nm × concentration) of DMB, VL, and nitrate in these multicomponent systems were: 95.50% DMB and 4.50% nitrate for GUA+DMB+AN; and 95.12% VL and 4.88% nitrate for GUA+VL+AN. Similarly, in our previous work, we estimated comparable VL decay constants for the direct photosensitized oxidation of VL in the absence and presence of AN (Mabato et al., 2022). We do not think that this is a light screening issue as S_λ for GUA+DMB (0.51) and GUA+DMB+AN (0.54) (also for GUA+VL, 0.57, and GUA+VL+AN, 0.59) were comparable. However, although AN did not significantly affect the oxidation kinetics, it had distinct effects on the product distributions.

(c) Thank you for catching this error. The labeling has been corrected in Table 1.

Minor Comments

1. Line 87. The Henry's law constant listed for DMB (5.4E1 M/atm) is far too low. This is either a typo or a problem in the source reference.

Response: The initially provided Henry's law constant for DMB (5.4×10^1 M atm^{-1}) is based on the group method estimate from EPI Suite. We have updated the listed Henry's law constant based on vapor pressure/water solubility estimate, which is more accurate compared to the group and bond methods:

Line 87: DMB and VL (Henry's law constants of ~~5.4×10^1~~ 7.3×10^3 M atm^{-1} and 4.7×10^5 M..

2. Line 108. "…AN generated more N-containing products…" More than what condition?

Response: We apologize for the confusion. AN generated more N-containing products in GUA+DMB+AN than in GUA+VL+AN. This has been corrected in the text as follows:

Line 107: In particular, AN generated more N-containing products in GUA+DMB+AN than in GUA+VL+AN, and increased the oligomers in GUA+VL+AN.

3. Line 129. To better simulate sunlight, I recommend the authors add an airmass filter to their illumination system for future work.

Response: Thank you for the suggestion. We will keep this in mind for our future work.

4. Line 191. The authors posit that the OH + VL rate constant is larger than the OH + DMB rate constant, but it seems unlikely that the difference is large given that they are probably both very fast. Have the authors looked for these rate constants?

Response: This statement is based on the -OH group (in VL) being more activating than the -OCH$_3$ group (in DMB). The second-order rate constant for the reaction between $^\bullet$OH and VL has been reported to be 4×10^8 M^{-1} s^{-1} (Li et al., 2014), while we are unaware of any data for $^\bullet$OH + DMB. To avoid confusion, we omitted this phrase in the text.

5. Line 377. Should clarify that this is referring to stronger light absorption by the products.

Response: Thank you for the suggestion. This has been clarified in the text as follows:

Line 377: Compared to GUA+VL, faster GUA oxidation and stronger light absorption by the products were observed in GUA+DMB.

Line 271: In summary, ^{3}DMB* and ^{3}VL* can oxidize GUA resulting in aqSOA and BrC formation, but GUA+DMB products exhibited stronger light absorption.

Recommendation

This is a difficult manuscript to rate, as it has a few interesting points but some major issues. However, given that there is not a lot that is novel about the work, I am sorry to recommend that it be rejected.

References for responses to Reviewer 4:

Anastasio, C., Faust, B. C., and Rao, C. J.: Aromatic carbonyl compounds as aqueous-phase photochemical sources of hydrogen peroxide in acidic sulfate aerosols, fogs, and clouds. 1. Non-phenolic methoxybenzaldehydes and methoxyacetophenones with reductants (phenols), Environ. Sci. Technol., 31, 218–232, https://doi.org/10.1021/es960359g, 1997.

Bateman, A. P., Laskin, J., Laskin, A., and Nizkorodov, S. A.: Applications of high-resolution electrospray ionization mass spectrometry to measurements of average oxygen to carbon ratios in secondary organic aerosols, Environ. Sci. Technol., 46, 8315–8324, https://doi.org/10.1021/es3017254, 2012.

Chen, Y., Li, N., Li, X., Tao, Y., Luo, S., Zhao, Z., Ma, S., Huang, H., Chen, Y., Ye, Z., and Ge, X.: Secondary organic aerosol formation from $^3C*$-initiated oxidation of 4-ethylguaiacol in atmospheric aqueous-phase, Sci. Total Environ., 723, 137953, https://doi.org/10.1016/j.scitotenv.2020.137953, 2020.

De Haan, D. O., Tolbert, M. A., and Jimenez, J. L.: Atmospheric condensed-phase reactions of glyoxal with methylamine, Geophys. Res. Lett., 36, No. L11819, https://doi.org/10.1029/2009GL037441, 2009.

De Haan, D.O., Pajunoja, A., Hawkins, L. N., Welsh, H.G., Jimenez, N. G., De Loera, A., Zauscher, M., Andretta, A. D., Joyce, B. W., De Haan, A. C., Riva, M., Cui, T., Surratt, J. D., Cazaunau, M., Formenti, P., Gratien, A., Pangui, E., and Doussin, J-F.: Methylamine's effects on methylglyoxal-containing aerosol: chemical, physical, and optical changes, ACS Earth Space Chem., 3, 1706–1716, https://doi.org/10.1021/acsearthspacechem.9b00103, 2019.

Du, Y., Fu, Q. S., Li, Y., and Su, Y.: Photodecomposition of 4-chlorophenol by reactive oxygen species in UV/air system, J. Hazard. Mater., 186, 491–496, https://doi.org/10.1016/j.jhazmat.2010.11.023, 2011.

Felber, T., Schaefer, T., He, L., and Herrmann, H.: Aromatic carbonyl and nitro compounds as photosensitizers and their photophysical properties in the tropospheric aqueous phase, J. Phys. Chem. A, 125, 5078–5095, https://doi.org/10.1021/acs.jpca.1c03503, 2021.

Fleming, L. T., Lin, P., Laskin, A., Laskin, J., Weltman, R., Edwards, R. D., Arora, N. K., Yadav, A., Meinardi, S., Blake, D. R., Pillarisetti, A., Smith, K. R., and Nizkorodov, S. A.: Molecular composition of particulate matter emissions from dung and brushwood burning household cookstoves in Haryana, India, Atmos. Chem. Phys., 18, 2461–2480, https://doi.org/10.5194/acp-18-2461-2018, 2018.

Galloway, M. M., Chhabra, P. S., Chan, A. W. H., Surratt, J. D., Flagan, R. C., Seinfeld, J. H., and Keutsch, F. N.: Glyoxal uptake on ammonium sulphate seed aerosol: reaction products and reversibility of uptake under dark and irradiated conditions, Atmos. Chem. Phys., 9, 3331–3345, https://doi.org/10.5194/acp-9-3331-2009, 2009.

Gen, M., Huang, D. D., and Chan, C. K.: Reactive uptake of glyoxal by ammonium-containing salt particles as a function of relative humidity, Environ. Sci. Technol., 52, 6903–6911, https://doi.org/10.1021/acs.est.8b00606, 2018.

Ho, C. S., Lam, C. W. K., Chan, M. H. M., Cheung, R. C. K., Law, L. K., Suen, M. W. M., and Tai, H. L.: Electrospray ionization mass spectrometry: principles and clinical application, Clin. Biochem. Rev., 24, 3–12, 2003.

Jiang, W., Misovich, M. V., Hettiyadura, A. P. S., Laskin, A., McFall, A. S., Anastasio, C., and Zhang, Q.: Photosensitized reactions of a phenolic carbonyl from wood combustion in the aqueous phase—chemical evolution and light absorption properties of aqSOA, Environ. Sci. Technol., 55, 5199–5211, https://doi.org/10.1021/acs.est.0c07581, 2021.

Kampf, C. J., Jakob, R., and Hoffmann, T.: Identification and characterization of aging products in the glyoxal/ammonium sulfate system – implications for light-absorbing material in atmospheric aerosols, Atmos. Chem. Phys., 12, 6323–6333, https://doi.org/10.5194/acp-12-6323-2012, 2012.

Kebarle, P. A.: A brief overview of the mechanisms involved in electrospray mass spectrometry, J. Mass Spectrom., 35, 804–817, https://doi.org/10.1002/9783527628728.ch1, 2000.

Klodt, A.L., Romonosky, D.E., Lin, P., Laskin, J., Laskin, A., and Nizkorodov, S.A.: Aqueous photochemistry of secondary organic aerosol of α-pinene and α-humulene in the presence of hydrogen peroxide or inorganic salts, ACS Earth Space Chem., 3, 12, 2736–2746, https://doi.org/10.1021/acsearthspacechem.9b00222, 2019.

Kruve, A., Kaupmees, K., Liigand, J., and Leito, I.: Negative electrospray ionization via deprotonation: predicting the ionization efficiency, Anal. Chem., 86, 4822–4830, https://doi.org/10.1021/ac404066v, 2014.

Laskin, J., Laskin, A., Nizkorodov, S. A., Roach, P., Eckert, P., Gilles, M. K., Wang, B., Lee, H. J., and Hu, Q.: Molecular selectivity of brown carbon chromophores, Environ. Sci. Technol., 48, 12047–12055, https://doi.org/10.1021/es503432r, 2014.

Lee, H. J., Aiona, P. K., Laskin, A., Laskin, J., and Nizkorodov, S. A.: Effect of solar radiation on the optical properties and molecular composition of laboratory proxies of atmospheric brown carbon, Environ. Sci. Technol., 48, 10217–10226, https://doi.org/10.1021/es502515r, 2014.

Leifer, A.: The Kinetics of environmental aquatic photochemistry: Theory and practice, American Chemical Society, Washington, DC, 1988.

Leito, I., Herodes, K., Huopolainen, M., Virro, K., Künnapas, A., Kruve, A., and Tanner, R.: Towards the electrospray ionization mass spectrometry ionization efficiency scale of organic compounds, Rapid Commun. Mass Sp., 22, 379–384, https://doi.org/10.1002/rcm.3371, 2008.

Li, Y. J., Huang, D. D., Cheung, H. Y., Lee, A. K. Y., and Chan, C. K.: Aqueous-phase photochemical oxidation and direct photolysis of vanillin - a model compound of methoxy phenols from biomass burning, Atmos. Chem. Phys., 14, 2871–2885, https://doi.org/10.5194/acp-14-2871-2014, 2014.

Lin, P., Yu, J. Z., Engling, G., and Kalberer, M.: Organosulfates in humic-like substance fraction isolated from aerosols at seven locations in East Asia: a study by ultra-high-resolution mass spectrometry, Environ. Sci. Technol., 46, 13118–13127, https://doi.org/10.1021/es303570v, 2012.

Mabato, B. R. G., Gen, M., Chu, Y., and Chan, C. K.: Reactive uptake of glyoxal by methylaminium-containing salts as a function of relative humidity, ACS Earth Space Chem., 3, 150–157, https://doi.org/10.1021/acsearthspacechem.8b00154, 2019.

Mabato, B. R. G., Lyu, Y., Ji, Y., Li, Y. J., Huang, D. D., Li, X., Nah, T., Lam, C. H., and Chan, C. K.: Aqueous secondary organic aerosol formation from the direct photosensitized oxidation of vanillin in the absence and presence of ammonium nitrate, Atmos. Chem. Phys., 22, 273–293, https://doi.org/10.5194/acp-22-273-2022, 2022.

Nguyen, T. B., Nizkorodov, S. A., Laskin, A., and Laskin, J.: An approach toward quantification of organic compounds in complex environmental samples using high-resolution electrospray ionization mass spectrometry, Anal. Methods, 5, 72–80, https://doi.org/10.1039/C2AY25682G, 2013.

Ning, C., Gao, Y., Zhang, H., Yu, H., Wang, L., Geng, N., Cao, R., and Chen, J.: Molecular characterization of dissolved organic matters in winter atmospheric fine particulate matters (PM2.5) from a coastal city of northeast China, Sci. Total Environ., 689, 312–321, https://doi.org/10.1016/j.scitotenv.2019.06.418, 2019.

Nozière, B., Dziedzic, P., and Córdova, A.: Products and kinetics of the liquid-phase reaction of glyoxal catalyzed by ammonium ions (NH$_4^+$), J. Phys. Chem. A, 113, 231–237, https://doi.org/10.1021/jp8078293, 2009.

Pang, H., Zhang, Q., Lu, X., Li, K., Chen, H., Chen, J., Yang, X., Ma, Y., Ma, J., and Huang, C.: Nitrite-mediated photooxidation of vanillin in the atmospheric aqueous phase, Environ. Sci. Technol., 53, 14253–14263, https://doi.org/10.1021/acs.est.9b03649, 2019.

Perry, R. H., Cooks, R. G., and Noll, R. J.: Orbitrap mass spectrometry: instrumentation, ion motion and applications, Mass Spectrom. Rev., 27, 661–699, https://doi.org/10.1002/mas.20186, 2008.

Romonosky, D. E., Li, Y., Shiraiwa, M., Laskin, A., Laskin, J., and Nizkorodov, S. A.: Aqueous photochemistry of secondary organic aerosol of α-Pinene and α-Humulene oxidized with ozone, hydroxyl radical, and nitrate radical, J. Phys. Chem. A, 121, 1298–1309, https://doi.org/10.1021/acs.jpca.6b10900, 2017.

Schmidt, A-C., Herzschuh, R., Matysik, F-M., and Engewald, W.: Investigation of the ionisation and fragmentation behaviour of different nitroaromatic compounds occurring as polar metabolites of explosives using electrospray ionisation tandem mass spectrometry, Rapid Commun. Mass Sp., 20, 2293–2302, https://doi.org/10.1002/rcm.2591, 2006.

Shapiro, E. L., Szprengiel, J., Sareen, N., Jen, C. N., Giordano, M. R., and McNeill, V. F.: Light-absorbing secondary organic material formed by glyoxal in aqueous aerosol mimics, Atmos. Chem. Phys., 9, 2289–2300, https://doi.org/10.5194/acp-9-2289-2009, 2009.

Simoneit, B. R. T., Rogge, W. F., Mazurek, M. A., Standley, L. J., Hildemann, L. M., and Cass, G. R.: Lignin pyrolysis products, lignans, and resin acids as specific tracers of plant classes in emissions from biomass combustion, Environ. Sci. Technol., 27, 2533–2541, https://doi.org/10.1021/es00048a034, 1993.

Smith, J. D., Sio, V., Yu, L., Zhang, Q., and Anastasio, C.: Secondary organic aerosol production from aqueous reactions of atmospheric phenols with an organic triplet excited state, Environ. Sci. Technol., 48, 1049–1057, https://doi.org/10.1021/es4045715, 2014.

Smith, J. D., Kinney, H., and Anastasio, C.: Aqueous benzene-diols react with an organic triplet excited state and hydroxyl radical to form secondary organic aerosol, Phys. Chem. Chem. Phys., 17, 10227–10237, https://doi.org/10.1039/C4CP06095D, 2015.

Smith, J. D., Kinney, H., and Anastasio, C.: Phenolic carbonyls undergo rapid aqueous photodegradation to form low-volatility, light-absorbing products, Atmos. Environ., 126, 36–44, https://doi.org/10.1016/j.atmosenv.2015.11.035, 2016.

Song, J., Li, M., Jiang, B., Wei, S., Fan, X., and Peng, P.: Molecular characterization of water-soluble humic like substances in smoke particles emitted from combustion of biomass materials and coal using ultrahigh-resolution electrospray ionization Fourier transform ion cyclotron resonance mass spectrometry, Environ. Sci. Technol., 52, 2575–2585, https://doi.org/10.1021/acs.est.7b06126, 2018.

Wang, K., Huang, R-J., Brüggemann, M., Zhang, Y., Yang, L., Ni, H., Guo, J., Wang, M., Han, J., Bilde, M., Glasius, M., and Hoffmann, T.: Urban organic aerosol composition in eastern China differs from north to south: molecular insight from a liquid chromatography–mass spectrometry (Orbitrap) study, Atmos. Chem. Phys., 21, 9089–9104, https://doi.org/10.5194/acp-21-9089-2021, 2021.

Wang, X., Hayeck, N., Brüggemann, M., Yao, L., Chen, H., Zhang, C., Emmelin, C., Chen, J., George, C., and Wang, L.: Chemical characterization of organic aerosols in Shanghai: A study by ultrahigh-performance liquid chromatography coupled with orbitrap mass spectrometry, J. Geophys. Res. Atmos., 122, 11703–11722, https://doi.org/10.1002/2017JD026930, 2017.

Yu, G., Bayer, A. R., Galloway, M. M., Korshavn, K. J., Fry, C. G., and Keutsch, F. N.: Glyoxal in aqueous ammonium sulfate solutions: products, kinetics and hydration effects, Environ. Sci. Technol., 45, 6336–6342, https://doi.org/10.1021/es200989n, 2011.

Yu, L., Smith, J., Laskin, A., Anastasio, C., Laskin, J., and Zhang, Q.: Chemical characterization of SOA formed from aqueous-phase reactions of phenols with the triplet excited state of carbonyl and hydroxyl radical, Atmos. Chem. Phys., 14, 13801–13816, https://doi.org/10.5194/acp-14-13801-2014, 2014.

Yu, L., Smith, J., Laskin, A., George, K. M., Anastasio, C., Laskin, J., Dillner, A. M., and Zhang, Q.: Molecular transformations of phenolic SOA during photochemical aging in the aqueous phase: competition among oligomerization, functionalization, and fragmentation, Atmos. Chem. Phys., 16, 4511–4527, https://doi.org/10.5194/acp-16-4511-2016.

Zhang, Q. and Anastasio, C.: Conversion of fogwater and aerosol organic nitrogen to ammonium, nitrate, and NOx during exposure to simulated sunlight and ozone, Environ. Sci. Technol., 37, 3522–3530, https://doi.org/10.1021/es034114x, 2003.

Comparison of aAqueous SOA product distributions formation from photosensitized guaiacol oxidation by: Comparison between non-phenolic and phenolic methoxybenzaldehydes as photosensitizers in the absence and presence of ammonium nitrate

Beatrix Rosette Go Mabato[1,2], Yong Jie Li[3], Dan Dan Huang[4], Yalin Wang[3], and Chak K. Chan[1,2]*

[1]School of Energy and Environment, City University of Hong Kong, Hong Kong, China
[2]City University of Hong Kong Shenzhen Research Institute, Shenzhen, China
[3]Department of Civil and Environmental Engineering, and Centre for Regional Ocean, Faculty of Science and Technology, University of Macau, Macau, China
[4]Shanghai Academy of Environmental Sciences, Shanghai 200233, China

Correspondence to: Chak K. Chan (Chak.K.Chan@cityu.edu.hk)

Abstract. Aromatic carbonyls (e.g., methoxybenzaldehydes), an important class of photosensitizers, are abundant in the atmosphere. Photosensitization and nitrate-mediated photo-oxidation can occur simultaneously, yet studies about their interactions, particularly for aqueous secondary organic aerosol (aqSOA) formation, remain limited. This study compared non-phenolic (3,4-dimethoxybenzaldehyde, DMB) and phenolic (vanillin, VL) methoxybenzaldehydes as photosensitizers for aqueous secondary organic aerosol (aqSOA) formation via guaiacol (GUA) oxidation in the absence and presence of ammonium nitrate (AN) under atmospherically relevant cloud and fog conditions. The effects of ammonium nitrate (AN) on these reactions were also explored. GUA oxidation by triplet excited states of DMB (^{3}DMB*) (GUA+DMB) was ~4 times faster and exhibited greater light absorption than oxidation by ^{3}VL* (GUA+VL). Both GUA+DMB and GUA+VL formed aqSOA composed of oligomers, functionalized monomers, oxygenated ring-opening species, and N-containing products in the presence of AN. The observation of N-heterocycles such as imidazoles indicates the participation of ammonium in the reactions. The majority of generated aqSOA are potential brown carbon (BrC) chromophores. Oligomerization and functionalization dominated in GUA+DMB and GUA+VL, but functionalization appeared to be more important in GUA+VL due to contributions from VL itself. AN did not significantly affect the oxidation kinetics, but it had distinct effects on the product distributions, likely due to differences in the photosensitizing abilities and structural features of DMB and VL. In particular, the more extensive fragmentation in GUA+DMB than in GUA+VL likely generated more N-containing products in GUA+DMB+AN. In GUA+VL+AN, the increased oligomers may be due to VL-derived phenoxy radicals induced by $^\bullet$OH or $^\bullet$NO$_2$ from nitrate photolysis. Furthermore, increased nitrated products observed in the presence of both DMB or VL and AN than in AN alone implies that photosensitized reactions may promote nitration. This work demonstrates how the structural features of photosensitizers affect aqSOA formation via non-carbonyl phenol oxidation.

1

32   Potential interactions between photosensitization and AN photolysis were also elucidated. These findings facilitate a better

33   understanding of photosensitized aqSOA formation and highlight the importance of ~~ammonium nitrate~~AN photolysis in

34   these reactions.

1 Introduction

36   Photosensitized reactions involving triplet excited states of organic compounds (^{3}C*) are efficient pathways for the

37   formation of secondary organic aerosol in the aqueous phase (aqSOA; Smith et al., 2014, 2016; Yu et al., 2014, 2016; Chen

38   et al., 2020; Jiang et al., 2021; Misovich et al., 2021; Mabato et al., 2022). Upon irradiation by solar radiation,

39   photosensitizers form an excited triplet state that directly reacts with substrates (e.g., phenols), and can generate singlet

40   oxygen (^{1}O$_2$), superoxide (O$_2^{\bullet-}$) or hydroperoxyl ($^{\bullet}$HO$_2$) radicals, and hydroxyl radicals ($^{\bullet}$OH) upon reactions with O$_2$ and

41   substrates (George et al., 2018; Chen et al., 2020), thereby facilitating the oxidation of rather volatile species and

42   contributing to aqSOA formation. An important class of photosensitizers is aromatic carbonyls (e.g.,

43   methoxybenzaldehydes) which are abundant in aerosol particles, cloud waters, and fog waters (Anastasio et al., 1997; Felber

44   et al., 2021). Aromatic carbonyls can be emitted from anthropogenic sources and biomass burning (BB; Lipari et al.,1984;

45   Edye and Richards, 1991; Hawthorne et al., 1992; Simoneit et al., 1993, 1999; Anastasio et al., 1997; Felber et al., 2021), or

46   formed via atmospheric oxidation of aromatic hydrocarbons (Hoshino et al., 1978; Calvert and Madronich, 1987; Anastasio

47   et al., 1997; Felber et al., 2021). BB is also a significant source of phenols through lignin pyrolysis (Simpson et al., 2005).

48   Phenolic carbonyls have a hydroxyl (–OH) group on the aromatic ring, whereas non-phenolic carbonyls do not. BB smoke

49   has been reported to have comparable concentrations of phenolic and non-phenolic carbonyls (Simoneit et al., 1993;

50   Anastasio et al., 1997).

51   Most previous studies on aqSOA formation via photosensitized non-carbonyl phenol oxidation have examined 3,4-

52   dimethoxybenzaldehyde (DMB), a non-phenolic methoxybenzaldehyde, as the photosensitizer (Smith et al., 2014, 2015; Yu

53   et al., 2014, 2016; Chen et al., 2020; Jiang et al., 2021; Misovich et al., 2021). By contrast, phenolic carbonyls have been

54   mainly studied as aqSOA precursors via $^{\bullet}$OH-, nitrate-, nitrite-, and ^{3}DMB*-mediated oxidation (Li et al., 2014; Huang et al.,

55   2018; Pang et al., 2019; Jiang et al., 2021; Misovich et al., 2021). However, strongly light-absorbing phenolic carbonyls

56   (e.g., molar absorptivity above 300 nm $\geq$7 $\times$ 10^3 M^{-1} cm^{-1}) can also serve as photosensitizers to promote aqSOA formation

57   (Smith et al., 2016; Mabato et al., 2022). For instance, the direct photosensitized oxidation of phenolic carbonyls (i.e.,

58   oxidation of phenolic carbonyls by their ^{3}C* or ^{3}C*-derived oxidants) such as vanillin (VL; another methoxybenzaldehyde)

59   efficiently form low-volatility products, with aqSOA mass yields of up to 140% (Smith et al., 2016). Moreover, the aqSOA

60   mass yields from the oxidation of syringol by ^{3}DMB* and ^{3}VL* are similar (111% and 114%, respectively; Smith et al.,

61   2014, 2016). In addition, we recently reported that the direct photosensitized oxidation of VL and guaiacol oxidation by

62   ^{3}VL* yield similar products (oligomers, functionalized monomers, and oxygenated ring-opening products) as observed with

63   ^{3}DMB* (Yu et al., 2014; Mabato et al., 2022). Guaiacol is a non-carbonyl BB methoxyphenol with an emission rate from

64 fireplace wood combustion in the range of 172 to 279 mg/kg (Schauer et al., 2001; Simoneit, 2002). The atmospheric

65 reactivity of methoxyphenols has recently been reviewed (Liu et al., 2022). However, our previous experiments (Mabato et

66 al., 2022) were performed at a concentration (0.1 mM VL) higher than what was typically used for DMB (0.005 to 0.01 mM;

67 Smith et al., 2014, 2015; Yu et al., 2014, 2016). Therefore, direct comparisons between photosensitization by ^{3}DMB* and

68 ^{3}VL* cannot be made. Despite the above findings, much is still unknown about how aqSOA formation proceeds in systems

69 using phenolic carbonyls as photosensitizers.

70   BB aerosols are typically internally mixed with other aerosol components, such as ammonium nitrate (AN;

71 Zielinski et al., 2020). Hence, aromatic carbonyls and phenols may coexist with AN in BB aerosols. Nitrate and ammonium

72 facilitate the formation of aqSOA and brown carbon (BrC) via a number of pathways. Nitrate photolysis can produce $^•$OH

73 and nitrating agents (e.g., $^•$NO$_2$; Minero et al., 2007; Huang et al., 2018; Mabato et al., 2022; Wang et al., 2022; Yang et al.,

74 2022), and ammonium reacts with carbonyls to yield N-containing heterocycles (e.g., imidazoles) and oligomers capable of

75 UV-Vis light absorption (De Haan et al., 2009, 2011; Nozière et al., 2009, 2010, 2018; Shapiro et al., 2009; Yu et al., 2011;

76 Lee et al., 2013; Powelson et al., 2014; Gen et al., 2018; Grace et al., 2019; Mabato et al., 2019). Furthermore, nitrate

77 photolysis may be an important process for SO$_2$ oxidation and SOA formation in the particle phase (Gen et al., 2019a,

78 2019b, 2022; Zhang et al., 2020, 2021, 2022), and it can potentially modify the morphology of atmospheric viscous particles

79 (Liang et al., 2021). Yet, understanding of the effects of inorganic nitrate on aqSOA formation remains limited. In addition,

80 aqSOA formation studies involving aromatic carbonyls and phenols have probed either photosensitization or nitrate-

81 mediated photo-oxidation, but these reactions can occur simultaneously. For instance, we previously reported nitrated

82 compounds, including a potential imidazole derivative from the direct photosensitized oxidation of VL in the presence of AN

83 (Mabato et al., 2022). Accordingly, investigations on reaction systems including both photosensitizers and AN may provide

84 further insights into the aqueous-phase processing of BB aerosols.

85   In this work, we compared aqSOA formation from photosensitized guaiacol (GUA) oxidation by ^{3}C* of non-

86 phenolic and phenolic methoxybenzaldehydes under identical conditions (simulated sunlight and concentration) relevant to

87 cloud and fog waters. The effects of AN on photosensitized aqSOA formation were also examined. In this study, the

88 dominant aqSOA precursor is GUA (Henry's law constant of 9.2×10^2 M atm^{-1}; Sagebiel et al., 1992), and DMB and VL

89 were used as photosensitizers to oxidize GUA. DMB and VL (Henry's law constants of $\sim$5.4$7.3 \times 10^{\cancel{13}}$ M atm^{-1} and 4.7×10^5

90 M atm^{-1}, respectively; Yaws, 1994; EPI Suite version 4.1, 2012; Felber et al., 2021), which are also abundant in BB

91 emissions (Schauer et al., 2001; Li et al., 2014; Chen et al., 2017; Pang et al., 2019; Mabato et al., 2022) and whose

92 structures differ only by one functional group (–OCH$_3$ for the former and –OH for the latter, Fig. 1), represented non-

93 phenolic and phenolic methoxybenzaldehydes, respectively. The structures of GUA, DMB, and VL are provided in Figure 1.

94 Based on their quantum yield of ^{3}C* formation, DMB and VL have been classified as moderate and poor photosensitizers,

95 respectively (Felber et al., 2021). The photosensitized oxidation of GUA by ^{3}DMB* or ^{3}VL* in the absence (and presence)

96 of AN are referred to as GUA+DMB(+AN) and GUA+VL(+AN), respectively. GUA photo-oxidation by AN alone

97 (GUA+AN) was also explored for comparison with GUA+DMB+AN and GUA+VL+AN. The molar absorptivities of GUA,

3

98 DMB, VL, and nitrate are shown in Figure 1. The precursor and photosensitizer decay kinetics, detected products, and
99 absorbance enhancement were used to characterize the reactions. However, it should be noted that we mainly focused on the
100 analyses of the reaction products and product distribution.

101   While several studies on photo-oxidation of BB emissions are available, this work focuses on the comparison
102 between non-phenolic and phenolic methoxybenzaldehydes as photosensitizers in the absence and presence of AN for
103 aqSOA formation. We found that GUA oxidation by ^{3}DMB* was faster and exhibited greater light absorption relative to
104 GUA+VL. These are likely attributed to the stronger photosensitizing ability of DMB and the –OH group of VL, making it
105 more prone to oxidation and more reactive towards electrophilic aromatic substitution. Oligomerization and functionalization
106 dominated in GUA+DMB and GUA+VL, but functionalization appeared to be more significant in GUA+VL due to VL
107 transformation products. Although AN did not significantly influence the oxidation kinetics due to the predominant role of
108 photosensitizer chemistry compared to nitrate, AN promoted the formation of N-containing products. These include N-
109 heterocycles (e.g., imidazoles), suggesting the participation of ammonium in the reactions. Moreover, the product
110 distributions indicate distinct interactions between photosensitization by ^{3}DMB* and ^{3}VL* and AN photolysis. In particular,
111 AN generated more N-containing products in GUA+DMB+AN than in GUA+VL+AN, and increased the oligomers in
112 GUA+VL+AN. Furthermore, increased nitrated compounds in GUA+DMB+AN and GUA+VL+AN compared to GUA+AN
113 suggest that photosensitized reactions may promote reactions by nitrate photolysis.

114 **2 Methods**

115 **2.1 Aqueous phase photo-oxidation experiments**

116 Procedures for the photo-oxidation experiments are presented in detail in our previous study (Mabato et al., 2022).
117 Experimental solutions were prepared using 0.1 mM guaiacol (GUA, Sigma Aldrich, ≥98.0%) and 0.01 mM 3,4-
118 dimethoxybenzaldehyde (DMB, Acros Organics, 99+%) or 0.01 mM vanillin (VL, Acros Organics, 99%, pure), in the
119 absence and presence of ammonium nitrate (1 mM; AN, Acros Organics, 99+%, for analysis). These GUA and
120 methoxybenzaldehydes concentrations are within the values expected in cloud or fog drops in areas with significant wood
121 combustion (Anastasio et al., 1997; Rogge et al., 1998; Nolte et al., 2001). The AN concentration represents values usually
122 observed in cloud and fog waters (Munger et al., 1983; Collett et al., 1998; Zhang and Anastasio, 2003; Li et al., 2011;
123 Giulianelli et al., 2014; Bianco et al., 2020). It must be noted that this study did not intend to identify the AN concentrations
124 that would affect the kinetics but attempted to analyze the effects of AN on photosensitized aqSOA formation. A solution
125 composed of 0.1 mM GUA and 1 mM AN (GUA+AN) was also examined for comparison with GUA+DMB+AN and
126 GUA+VL+AN. Sulfuric acid (H$_2$SO$_4$; Acros Organics, ACS reagent, 95% solution in water) was used to adjust the pH of the
127 solutions to 4, which is within typical cloud pH values (2–7; Pye et al., 2020) and pH values observed in wood burning-
128 impacted cloud and fog waters (Collett et al., 1998; Raja et al., 2008). The solutions (initial volume of 500 mL) were
129 bubbled with synthetic air (0.5 dm^3/min) for 30 min before irradiation and throughout the reactions to achieve air-saturated

130   conditions (Du et al., 2011; Chen et al., 2020) and were continuously magnetically stirred. In this study, the reactions can

131   generate ^{3}DMB*/^{3}VL* and secondary oxidants ($^1O_2$, $O_2^{•-}/^•HO_2$, $^•OH$) but not ozone. Solutions contained in a quartz

132   photoreactor were irradiated using a xenon lamp (model 6258, Ozone free xenon lamp, 300 W, Newport) equipped with a

133   longpass filter (20CGA-305 nm cut-on filter, Newport) to eliminate light below 300 nm. The reaction temperatures were

134   maintained at 27 ± 2 °C using cooling fans positioned around the photoreactor and lamp housing. The averaged initial

135   photon flux in the reactor measured from 300 to 380 nm was ~3 × 10^{15} photons cm^{-2} s^{-1} nm^{-1} (Fig. 1), similar to our previous

136   work (Mabato et al., 2022). Samples were collected every 30 mins for 180 mins for offline analyses of (1) GUA, DMB, and

137   VL concentrations using ultra-high-performance liquid chromatography with photodiode array detector (UHPLC-PDA), and

138   (2) absorbance measurements using UV-Vis spectrophotometry. Moreover, the samples collected before and after irradiation

139   (180 min) were analyzed for (32) reaction products using UHPLC coupled with heated electrospray ionization Orbitrap mass

140   spectrometry (UHPLC-HESI-Orbitrap-MS) operated in positive and negative ion modes and; (43) concentrations of small

141   organic acids using ion chromatography (IC).; and (4) absorbance measurements using UV-Vis spectrophotometry. Each

142   experiment was repeated independently at least three times. The reported decay rate constants, small organic acids

143   concentration, and absorbance enhancement were averaged from triplicate experiments, and the corresponding errors

144   represent one standard deviation. The pseudo-first-order rate constant (k') for GUA decay was determined using the

145   following equation (Huang et al., 2018):

146   $$ln\,([GUA]_t/[GUA]_0) = -k't \qquad \text{(Eq. 1)}$$

147   where [GUA]$_t$ and [GUA]$_0$ are GUA concentrations at time t and 0, respectively. DMB or VL decay rate constants were

148   calculated by replacing GUA with DMB or VL in Eq. 1. The decay rate constants were normalized to the photon flux

149   measured for each experiment through dividing k' by the measured 2-nitrobenzaldehyde (2NB; a chemical actinometer)

150   decay rate constant, j(2NB) (Mabato et al., 2022). In addition, the decay rate constants were corrected for the internal light

151   screening due to DMB, VL, and AN (Leifer, 1988; Zhang and Anastasio, 2003; Smith et al., 2014, 2016). The values of the

152   internal light screening factor (S_λ) determined around the peak in the light absorption action spectrum (DMB: 310-335 nm,

153   VL: 304-364 nm, nitrate: 300-331 nm) (Smith et al., 2014, 2016) for an 8.5 cm cell were 0.95 for GUA+AN, 0.51 for

154   GUA+DMB, 0.54 for GUA+DMB+AN, 0.57 for GUA+VL, and 0.59 for GUA+VL+AN. Moreover, two independently

155   prepared samples for each reaction condition were analyzed using UHPLC-HESI-Orbitrap-MS. Only peaks that were

156   reproducibly detected in both sets of samples were considered. For clarity, the formulas discussed in this work correspond to

157   neutral analytes (e.g., with H$^+$ or NH$_4^+$ removed from the ion formula). The details of the analytical procedures are provided

158   in the Supplement (Sects. S1 to S4).

159   **2.2 Calculation of the normalized abundance of products**

160   Several recent studies have used comparisons of relative abundance of products based on peak areas from mass spectrometry

161   (MS) results (e.g., Lee et al., 2014; Romonosky et al., 2017; Wang et al., 2017; Fleming et al., 2018; Song et al., 2018; Klodt

162   et al., 2019; Ning et al., 2019) to show the relative importance of different types of compounds (K. Wang et al., 2021).

163 However, comparisons of relative abundance among different compounds can be subject to uncertainties as ionization

164 efficiencies in soft ionization, such as ESI, may significantly vary between different compounds (Kebarle, 2000; Schmidt et

165 al., 2006; Leito et al., 2008; Perry et al., 2008; Kruve et al., 2014). ~~The normalized abundance of products ([P], unitless) was~~

166 ~~introduced in our previous work (Mabato et al., 2022).~~ In our previous work (Mabato et al., 2022), we introduced the

167 normalized abundance of products ([P], unitless) (Eq. 2) as a semi-quantitative analysis that gives an overview of how the

168 signal intensities changed under different experimental conditions but not the quantification of the absolute product

169 concentration. ~~Briefly,~~ The calculation assumes equal ionization efficiencies of different compounds, which is commonly

170 used to estimate O:C ratios of SOA (Bateman et al., 2012; Lin et al., 2012; Laskin et al., 2014; De Haan et al., 2019) ~~was~~

171 ~~assumed for the calculation~~:

172

$$[P] = \frac{A_{P,t}}{A_{GUA,t}} \cdot \frac{[GUA]_t}{[GUA]_0} \qquad \text{(Eq. 2)}$$

174 where $A_{P,t}$ and $A_{GUA,t}$ are the extracted ion chromatogram (EIC) peak areas of the product P and GUA from UHPLC-HESI-

175 Orbitrap-MS analyses at time t, respectively; $[GUA]_t$ and $[GUA]_0$ are the GUA concentrations (μM) determined using

176 UHPLC-PDA at time t and 0, respectively. Note that the normalized abundance of products has intrinsic uncertainties due to

177 the variability in ionization efficiencies for various compounds. ~~Nevertheless, it is a semi-quantitative analysis that gives an~~

178 ~~overview of how the signal intensities changed under different experimental conditions but not the quantification of the~~

179 ~~absolute product concentration.~~ Moreover, it should be noted that the normalized abundance of products was calculated

180 using only the positive ion mode data as the GUA signal from the negative ion mode was weak and thus may present large

181 uncertainties during normalization. Therefore, products that may not give signals or may have weak signals in the positive

182 ion mode were possibly underestimated in the normalized product abundance. Nevertheless, it enables the comparison of MS

183 results among different experiments. As demonstrated in our previous work (Mabato et al., 2022) and the current study, a

184 higher normalized abundance of products generally correlates with higher efficiency of oxidation. The reported uncertainties

185 were propagated from the changes in [GUA] measured using UHPLC-PDA and the MS signal intensities.

186

187 **3 Results and Discussion**

188 Using kinetics data, MS analyses, and absorbance enhancement data, we first examined the differences between GUA+DMB

189 and GUA+VL (Sect. 3.1). Then, we analyzed GUA+DMB+AN, GUA+VL+AN, and GUA+AN (Sect. 3.2) to explore the

190 effects of nitrate photolysis and ammonium on photosensitized aqSOA formation.

3.1 Comparison of photosensitized GUA oxidation by non-phenolic (^{3}DMB*) and phenolic (^{3}VL*) methoxybenzaldehydes

Prior studies have reported that photosensitized non-carbonyl phenol oxidation in the presence of 3,4-dimethoxybenzaldehyde (DMB) and vanillin (VL) (separately) was mainly driven by ^{3}DMB* and ^{3}VL*, respectively (Smith et al., 2014; Mabato et al., 2022), while contributions from secondary oxidants such as $^1O_2$ and ·OH were likely minor. However, both ^{3}DMB* and ^{3}VL* are efficiently quenched by O_2, suggesting that energy transfer should be considered in evaluating photosensitized processes involving these methoxybenzaldehydes (Felber et al., 2021). Moreover, it was found that ^{3}DMB*, $^1O_2$, and $O_2^{·-}$ were the major contributors to the photosensitized oxidation of 4-ethylguaiacol (Chen et al., 2020). Recently, the oxidation of guaiacyl acetone (a non-conjugated phenolic carbonyl) in the presence of DMB has been reported to be initiated by ^{3}DMB*, $^1O_2$, ·OH, or methoxy radical (·OCH$_3$) (Misovich et al., 2021). Further studies are thus required to identify the specific oxidants in these reaction systems. In this study, reactions initiated in the presence of DMB or VL are collectively referred to as photosensitized reactions. The reaction conditions, initial guaiacol (GUA) and DMB or VL decay rate constants, normalized product abundance, and the chemical characteristics of aqSOA formed in this work are summarized in Table 1.

3.1.1 Kinetic analysis of photosensitization by ^{3}DMB* and ^{3}VL*

No significant loss of GUA or photosensitizers was observed for dark experiments ($p > 0.05$). Figure S1 shows the decay of GUA, DMB, and VL under different experimental conditions. Upon irradiation, the GUA decay rate constant in GUA+DMB was ~4 times higher than in GUA+VL. In GUA+DMB, the decay rate constant of GUA was ~8 times higher than that of DMB, consistent with a previous study (Smith et al., 2014). Contrastingly, the decay rate constant of VL was 2.4 times higher than that of GUA in GUA+VL. This VL consumption was also observed in our earlier work using 0.1 mM GUA + 0.1 mM VL (Mabato et al., 2022). These trends could be explained by the following reasons. First, DMB has a stronger photosensitizing ability than VL based on its higher quantum yield of ^{3}C* formation and longer lifetime of ^{3}DMB* compared to ^{3}VL* (Felber et al., 2021). Second, VL is also a phenolic compound similar to GUA, and is therefore highly reactive towards oxidation. For instance, its –OH group can be oxidized by ^{3}VL* via H-atom abstraction to form phenoxy radicals which can undergo coupling to form oligomers (Kobayashi and Higashimura, 2003; Sun et al., 2010; Mabato et al., 2022). The faster consumption of VL than GUA suggests a competition between ground-state VL and GUA for reaction with ^{3}VL*. Moreover, compared to a –OCH$_3$ group (in DMB), an –OH group (in VL) has a stronger electron-donating ability and is thus more activating towards. Relative to DMB, VL is more reactive towards electrophilic addition of ·OH and electrophilic aromatic substitution. It should be noted that the differences in the GUA decay rate constants among different reaction systems are not quantitatively equivalent to photosensitizing efficiencies, and a detailed quantitative analysis of which is beyond the scope of this study. Nonetheless, these results suggested that GUA oxidation in GUA+DMB was overall more efficient than in GUA+VL. Our kinetic analysis focused on the decay rate constants of the aqSOA precursor (GUA) and the photosensitizers (DMB and VL) during photosensitization under the same experimental conditions (same aqSOA

7

224 precarsor and concentration, same photosensitizer concentration, and same lamp photon flux). The effects of other factors
225 (e.g., intersystem crossing efficiency) on the rate constants were not examined. Explicit kinetic studies (e.g., Smith et al.,
226 2014, 2015) that measure second-order rate constants should be conducted in the future to extend the applicability of the
227 kinetic parameters to other conditions.

3.1.2 Product distributions and chemical characteristics of aqSOA from photosensitization by ^{3}DMB* and ^{3}VL*

229 The products detected using UHPLC-HESI-Orbitrap-MS were used to characterizerepresent the aqSOA formed in this work.
230 The signal-weighted distributions of aqSOA calculated from combined positive (POS) and negative (NEG) ion modes MS
231 results are summarized in Figure 2. The signal-weighted distributions calculated separately from POS and NEG ion modes
232 MS results are available in Figures S12 and S32. It should be noted that in this work, the product distributions for all
233 experiments were based on the same irradiation time of 180 min. An irradiation time of 180 min was chosen as it was
234 sufficient to show the differences in the extent of reaction of GUA among the reaction systems studied. For reaction systems
235 with precursors of different reactivities, chemical analysis at a fixed reaction time may be looking at different generations of
236 products of each precursor, as Yu et al. (2014) reported. Measuring the product distribution at a fixed time might have
237 missed the information on what/how many products are formed at the similar amounts of precursors reacted. The situation
238 could be even more complicated if different precursors had major differences in pathways and dominant intermediates.
239 However, comparing the product distributions after a certain time of light exposure, as is the case for this study, is useful to
240 evaluate what products would form after a certain time of photosensitization. Oligomers and derivatives of GUA dominated
241 both GUA+DMB and GUA+VL, in agreement with pronounced oligomerization from triplet-mediated oxidation of
242 relatively high phenol concentration (e.g., 0.1 to 3 mM; Li et al., 2014; Yu et al., 2014, 2016; Slikboer et al., 2015; Ye et al.,
243 2019; Mabato et al., 2022). GUA+DMB had a higher oligomer contribution than GUA+VL, attributable to faster GUA
244 oxidation by ^{3}DMB*. Figure 3 schematically depicts the main differences between photosensitized GUA oxidation by
245 ^{3}DMB* and ^{3}VL* in the absence and presence of AN. As shown in Fig. 3, ^{3}DMB* and ^{3}VL* can oxidize GUA via H-atom
246 abstraction to form phenoxy radicals which undergo coupling to form oligomers (Kobayashi and Higashimura, 2003; Sun et
247 al., 2010; Mabato et al., 2022). The higher oligomer contribution in GUA+DMB is likely due to the better photosensitizing
248 ability of DMB than VL and partly the lower abundance of ^{3}VL* due to fast VL consumption. VL was consumed faster than
249 DMB during GUA oxidation ascribable to the –OH group of VL, making it more susceptible to oxidation and more reactive
250 towards electrophilic aromatic substitution. In addition, the normalized product abundance for GUA+DMB was ~4 times
251 higher than that for GUA+VL (Table 1), further suggesting more efficient photosensitized GUA oxidation by ^{3}DMB* than
252 by ^{3}VL*. The oxidation of GUA or transient organic intermediates by secondary oxidants (e.g., ^{1}O$_2$ and $^•$OH) from ^{3}DMB* or
253 ^{3}VL* and the fragmentation of larger compounds generate highly oxidized ring-opening products (Yu et al., 2014; Huang et
254 al., 2018; Chen et al., 2020). GUA+DMB had a higher contribution of ring-opening products than GUA+VL, likely due to
255 the greater availability of secondary oxidants in the former and fast VL consumption lowering the production of these
256 species in GUA+VL. The IC analyses also indicate the formation of small organic acids (e.g., formic acid), which appeared

257 to have higher concentrations in the presence of DMB than in VL (Fig. S43). Although no data is available for the
258 concentration changes (every 30 min) of small organic acids during the reaction, it is likely that an increasing trend would be
259 observed as fragmentation, which leads to the decomposition of initially formed oligomers and the generation of smaller
260 oxygenated products, becomes important at longer irradiation times (Huang et al., 2018). This trend has also been observed
261 in our previous work on the direct photosensitized oxidation of VL (Mabato et al., 2022), as well as other studies on
262 photosensitized oxidation of non-carbonyl phenols and phenolic carbonyls (e.g., Yu et al., 2016; Jiang et al., 2021). The
263 reactions of secondary oxidants or ring-opening products with GUA can form functionalized products. Notably, the
264 contribution of monomers in GUA+VL was almost twice as high as in GUA+DMB, ascribable to VL transformation
265 products. We previously showed that for the direct photosensitized oxidation of VL, functionalization prevails over
266 oligomerization at 0.01 mM VL, the [VL] used in this work, while oligomerization dominates at higher [VL] (0.1 mM;
267 Mabato et al., 2022).

268 It has been reported that oligomerization could occur during the electrospray ionization process (Yasmeen et al.,
269 2010). In this work, it was confirmed that the oligomers observed were generated in the solutions via aqueous reactions
270 instead of being artefacts of HESI-MS. This is based on the absence of dimers and higher oligomers in the HESI mass
271 spectra of dark control solutions acquired by direct infusion (Yu et al., 2016).

272 The major GUA+DMB and GUA+VL products (Tables S1-S2) are mostly oligomers which can be formed through
273 the coupling of phenoxy radicals (Kobayashi and Higashimura, 2003; Sun et al., 2010; Mabato et al., 2022). GUA+DMB
274 products matched those reported in previous works on ^{3}DMB*- and/or ˙OH-mediated phenol oxidation (Yu et al., 2014,
275 2016). These include GUA dimers and trimers (e.g., $C_{14}H_{14}O_4$ and $C_{21}H_{18}O_8$, #1 and 19; Table S1), aldehydes ($C_7H_6O_4$, #13;
276 Table S1), and esters ($C_{16}H_{18}O_6$, #14; Table S1). Functionalized products include $C_{11}H_{12}O_5$ and $C_{10}H_{12}O_3$ (#8 and 12; Table
277 S1). More than half of the major GUA+VL products are the same oligomers detected from GUA+DMB (e.g., $C_{13}H_{10}O_4$ and
278 $C_{20}H_{18}O_6$, #4 and 21; Table S1). The rest are mainly functionalized species such as $C_7H_8O_4$ and $C_8H_8O_5$ (#28 and 35; Table
279 S2), corresponding to a hydroxylated GUA and hydroxylated VL, respectively.

280 The average elemental ratios and elemental distribution of the products (Fig. S54a–d) were consistent with those in
281 previous studies on similar reaction systems (Yu et al., 2014, 2016; Mabato et al., 2022). The majority of the GUA+DMB
282 and GUA+VL products had H:C ≤1.0 and O:C ≤0.5, typical for aromatic species (Mazzoleni et al., 2012; Kourtchev et al.,
283 2014; Jiang et al., 2021). GUA+DMB had more compounds with higher O:C (≥0.6), in agreement with higher contributions
284 of ring-opening products than in GUA+VL (Fig. 2). The higher ⟨OS$_C$⟩ for GUA+VL than in GUA+DMB (Table 1) was
285 probably due to the significant functionalization in the former. Moreover, the distributions of OS$_C$ and carbon number (Fig.
286 S65a–d) show that these aqSOA products have similar elemental composition to those of low-volatility oxygenated organic
287 aerosols (LV-OOA), semi-volatile oxygenated organic aerosols (SV-OOA), and slightly with biomass burning organic
288 aerosols (BBOA) (Kroll et al., 2011). Further discussions on van Krevelen diagrams (Fig. S54a–d) and OS$_C$ vs. carbon
289 number plots (Fig. S65a–d) for GUA+DMB and GUA+VL aqSOA are available in the Supplement (Sect. S5). In brief,
290 ^{3}DMB*-initiated GUA oxidation was faster and yielded higher normalized product abundance than oxidation by ^{3}VL*. This

9

291 is likely due to the stronger photosensitizing ability of DMB than VL and the –OH group of VL facilitating its rapid

292 consumption. In addition, oligomerization and functionalization dominated in both GUA+DMB and GUA+VL, as reported

293 in similar studies (Yu et al., 2014, 2016; Chen et al., 2020; Jiang et al., 2021; Misovich et al., 2021; Mabato et al., 2022).

294 However, functionalization was more prominent in the latter, attributable to the transformation of VL. Nonetheless, it must

295 be noted that for phenolic aqSOA, fragmentation will ultimately be more predominant at longer irradiation times (Huang et

296 al., 2018; Yu et al., 2016; Mabato et al., 2022).

3.1.3 Light absorption of aqSOA from photosensitization by ^{3}DMB* and ^{3}VL*

298 The absorbance enhancement of phenolic aqSOA generated via reactions with ^{3}DMB*/^{3}VL* has been linked to the

299 formation of conjugated structures due to oligomerization and functionalization (e.g., additions of hydroxyl and carbonyl

300 groups; Yu et al., 2014, 2016; Smith et al., 2016; Chen et al., 2020; Jiang et al., 2021; Misovich et al., 2021; Mabato et al.,

301 2022). Moreover, the aqueous-phase photo-oxidation of BB emissions can enhance BrC absorbance via the formation of

302 aromatic dimers and functionalized products (Hems et al., 2020). The increase in light absorption throughout 180 min of

303 irradiation and the change in the rate of sunlight absorption (ΔR_{abs}) (Jiang et al., 2021) from 350 to 550 nm at 180 min during

304 typical clear and haze days in Beijing, China for all the reaction systems studied are provided in Figure 4. Figure S7 shows

305 the absorption spectra after 180 min of irradiation for each reaction system studied. In this work, the absorbance

306 enhancement of GUA+DMB and GUA+VL (Fig. 4a) could be due tocorrelates with oligomers and functionalized

307 monomers, which are the highest contributors to the product signals. Identifying the chromophores responsible for the

308 absorbance enhancement may be beneficial in understanding the impact of aqSOA on the Earth's radiative balance and

309 determining the reactions that affect light absorption by aqSOA (Mabato et al., 2022). However, the detected products did

310 not exhibit distinct peaks in the UHPLC-PDA chromatograms, likely due to the concentration of the chromophores being

311 below the detection limit of PDA. Nevertheless, the higher absorbance enhancement and ΔR_{abs} for GUA+DMB than

312 GUA+VL was most likely associated with probably due to the higher contribution and normalized abundance (by ~6 times)

313 of oligomers in the former.

314 Additional information about aqSOA light-absorption can be deduced from the plots of the double bond equivalent

315 (DBE) values vs. carbon number (n_C) (Lin et al., 2018). Figure S68 shows these plots along with the DBE reference values

316 of fullerene-like hydrocarbons (Lobodin et al., 2012), cata-condensed polycyclic aromatic hydrocarbons (PAHs; Siegmann

317 and Sattler, 2000), and linear conjugated polyenes with a general formula C_xH_{x+2}. The shaded area indicates a sufficient level

318 of conjugation for visible light absorption, and species within this region are potential BrC chromophores. GUA+DMB and

319 GUA+VL aqSOA exhibited a significant overlap in the DBE vs. n_C space; nearly all products from both systems, including

320 the high-relative-abundance species, are potential BrC chromophores. GUA+DMB had more oligomeric products with high

321 relative abundance ($n_C \geq 12$ and DBE ≥ 8). For GUA+VL, high-relative-abundance products also include monomeric species

322 (n_C = 7-8 and 4-5 DBE) corresponding to hydroxylated products (e.g., $C_7H_8O_4$ and $C_8H_8O_5$; 28 and 35; Table S2). These

323 observations further indicate the importance of oligomerization and functionalization for the absorbance enhancement of

10

aqSOA generated via photosensitization by ^{3}DMB* and ^{3}VL*. In summary, ^{3}DMB* and ^{3}VL* can oxidize GUA resulting in aqSOA and BrC formation, but GUA+DMB products exhibited stronger light absorption. In GUA+VL, the extent of GUA oxidation was limited by significant VL consumption.

3.2 Comparison of photosensitized GUA oxidation by non-phenolic (^{3}DMB*) and phenolic (^{3}VL*) methoxybenzaldehydes in the presence of AN

3.2.1 Kinetic analysis of photosensitization by ^{3}DMB* and ^{3}VL* in the presence of AN

Ammonium nitrate (AN) did not significantly affect ($p > 0.05$) the decay rate constants of GUA, DMB, and VL for both GUA+DMB+AN and GUA+VL+AN (Table 1), likely due to the higher molar absorptivities of the photosensitizers compared to that of nitrate. This implies that the chemistry of ^{3}DMB* and ^{3}VL* dominated that of nitrate. In this work, the GUA decay rate constants decreased in the order of GUA+DMB/GUA+DMB+AN > GUA+VL/GUA+VL+AN > GUA+AN (Table 1). Note that as the molar absorptivities of the photosensitizers are higher than that of nitrate, the kinetics data were also analyzed on a per-photon-absorbed basis for a more appropriate comparison of reaction efficiency (Sect. S6). The apparent quantum efficiency of GUA photodegradation (φ_{GUA}) in the presence of nitrate (GUA+AN: 0.17~~1.3 × 10^{-2}~~ ± ~~3~~2.~~8~~9 × 10^{-3}~~3~~) was ~2 and ~7 times higher than that in the presence of DMB (0.10~~7.2 × 10^{-3}~~ ± ~~2~~1.9 × 10^{-4}~~3~~) or VL (0.026~~1.8 × 10^{-3}~~ ± ~~7~~4.2~~9~~ × 10^{-4}~~3~~), respectively. This suggests that nitrate-mediated GUA photo-oxidation is more efficient than photosensitization by ^{3}DMB* or ^{3}VL* on a per-photon-absorbed basis.

3.2.2 Product distributions and chemical characteristics of aqSOA from photosensitization by ^{3}DMB* and ^{3}VL* in the presence of AN

For both GUA+DMB+AN and GUA+VL+AN, AN had no significant effect on the normalized product abundance (Table 1), but it induced the formation of N-containing products composed of N-heterocycles (e.g., imidazoles and pyridines) and oligomers, as well as nitrated species. Similarly, we previously reported a potential imidazole derivative from the direct photosensitized oxidation of VL in the presence of AN, which was attributed to the reaction of ring-opening products with dissolved ammonia (Mabato et al., 2022). Oligomers remained the highest signal contributors in the presence of AN (Fig. 2), but interactions between photosensitization by ^{3}DMB* and ^{3}VL* and AN photolysis were distinct. First, nitrated species had similar contributions in both cases, but the contribution and normalized abundance of all N-containing products in GUA+DMB+AN were 2 and ~14 times higher, respectively, than in GUA+VL+AN. This difference can be attributed to the higher contribution of N-heterocycles and N-containing oligomers in GUA+DMB+AN. Compared to GUA+VL, GUA+DMB had a higher contribution of ring-opening products which can react with ammonia, as discussed earlier (Figs. 2 and 3). Second, the decrease in oligomers in GUA+DMB+AN may be due to their fragmentation induced by •OH from nitrate photolysis, then conversion to N-containing products. Correspondingly, the contribution of possibly ring-retaining N-containing products in GUA+DMB+AN (18.6%) was ~3 times higher than that in GUA+VL+AN (6.5%). While fragmentation of oligomers likely occurred in GUA+VL+AN as well, the increase in oligomers suggests that other reactions

356 have taken place. For GUA+VL+AN, $^{\bullet}$OH or $^{\bullet}$NO$_2$ from nitrate photolysis may have initiated H-atom abstraction from the –

357 OH group of VL, generating phenoxy radicals which can undergo coupling to form more oligomers (Kobayashi and

358 Higashimura, 2003; Sun et al., 2010; Mabato et al., 2022). This may also explain the more significant decrease of monomers

359 in GUA+VL+AN (~3 times) compared to GUA+DMB+AN (~2 times). Similarly, we previously observed an increase in

360 oligomers during the direct photosensitized oxidation of ~~upon adding 1 mM AN to~~ 0.01 mM VL (Mabato et al., 2022), the

361 [VL] used in this work, upon adding 1 mM AN. These findings indicate that photosensitization by non-phenolic and

362 phenolic methoxybenzaldehydes may interact differently with AN photolysis.

363 GUA+AN mainly formed oligomers analogous to $^{\bullet}$OH-mediated phenol oxidation (Yu et al., 2014, 2016), followed

364 by N-containing products. The normalized product abundance of GUA+AN was the lowest among all experiments, likely

365 due to the lower GUA decay constant relative to photosensitized oxidation. Moreover, the normalized abundance of N-

366 containing products in GUA+AN was ~12 times lower than that in GUA+DMB+AN but comparable to that in

367 GUA+VL+AN. This discrepancy for GUA+VL+AN might be due to the weaker signals of its N-containing products in the

368 positive compared to the negative ion mode. As previously mentioned, the normalized product abundance was calculated

369 using only the positive ion mode data as the GUA signal from the negative ion mode was weak and thus may present large

370 uncertainties during normalization. Interestingly, the contributions from nitrated species in GUA+DMB+AN and

371 GUA+VL+AN were higher than in GUA+AN, suggesting possible enhancement of nitration reactions. This is likely due to

372 the increased formation of $^{\bullet}$NO$_2$, for instance, via the reactions of $^{\bullet}$OH and O$_2^{\bullet-}$ (from ^{3}DMB* or ^{3}VL*) with NO$_2^-$ (Pang et

373 al., 2019; Mabato et al., 2022). Similarly, we previously reported enhanced nitration via the direct photosensitized oxidation

374 of VL in the presence of AN under air-saturated conditions (O$_2$ is present) relative to nitrogen-saturated conditions (Mabato

375 et al., 2022). These~~is~~ imply~~ies~~ that photosensitiz~~ed reactions~~ation may promote reactions induced by nitrate photolysis.

376 The major products from GUA+DMB+AN, GUA+VL+AN, and GUA+AN (Tables S3–S5) include oligomers and

377 functionalized monomers detected in GUA+DMB and GUA+VL (Tables S1–S2). The N-heterocycles from

378 GUA+DMB+AN include C$_6$H$_6$N$_4$ (#41; Table S3), which may be 2,2'-biimidazole (BI), a reaction product from glyoxal +

379 reduced nitrogenous compounds (e.g., ammonium salts) (De Haan et al., 2009; Galloway et al., 2009; Nozière et al., 2009;

380 Shapiro et al., 2009; Yu et al., 2011; Kampf et al., 2012; Gen et al., 2018; Mabato et al., 2019). The nitrated products include

381 C$_{12}$H$_{11}$N$_3$O$_3$ and C$_{15}$H$_{10}$N$_4$O$_3$ (#42 and 49; Table S3), which possibly have a nitrated imidazole moiety and a nitrophenol

382 moiety, respectively. For GUA+VL+AN, oligomers (C$_{14}$H$_{12}$O$_6$ and C$_{20}$H$_{16}$O$_7$; #55 and 59, Table S4) which were not among

383 the major products in GUA+VL were noted. C$_{10}$H$_8$O$_2$ likely has a furanone group (#50; Table S4); furanones are the primary

384 products of the reaction of $^{\bullet}$OH with toluene and other aromatic hydrocarbons (Smith et al., 1999). Moreover, C$_{11}$H$_9$N$_3$O$_3$

385 (#57; Table S4) has a nitrated imidazole moiety. Among the N-containing compounds in GUA+AN is C$_4$H$_3$N$_3$O$_3$ (#69; Table

386 S5), which may be a nitrated imidazole-2-carboxaldehyde. Imidazole-2-carboxaldehyde is also a reaction product from

387 glyoxal + reduced nitrogenous compounds (e.g., ammonium salts) (De Haan et al., 2009; Galloway et al., 2009; Nozière et

388 al., 2009; Shapiro et al., 2009; Yu et al., 2011; Kampf et al., 2012; Gen et al., 2018; Mabato et al., 2019).

389   The ⟨O:C⟩ for GUA+DMB+AN and GUA+VL+AN were lower than those in the absence of AN (Table 1), ~~likely~~
390 ~~due to the rapid formation of highly oxidized species followed by their decomposition (Huang et al., 2018)~~ possibly due to
391 the formation of N-heterocycles, altering the elemental ratios. The ⟨O:C⟩ and ⟨H:C⟩ were comparable in GUA+DMB+AN
392 and GUA+VL+AN, but the ⟨N:C⟩ for the former was higher, implying a greater extent of reactions involving AN. Relative
393 to GUA+DMB+AN and GUA+VL+AN, GUA+AN had a higher ⟨N:C⟩, as can be expected given that AN was the only
394 oxidant source. The lower ⟨OS$_C$⟩ of GUA+DMB+AN and GUA+VL+AN compared to GUA+AN may be attributed to
395 triplet-initiated oxidation generating higher-molecular-weight products with less fragmentation compared to ˙OH-mediated
396 oxidation (Yu et al., 2014; Chen et al., 2020). Nonetheless, AN generally increased the ⟨OS$_C$⟩ for both GUA+DMB and
397 GUA+VL, with a more noticeable increase for the former, suggesting more oxidized products. Similarly, in a previous work,
398 the more oxygenated and oxidized aqSOA from the photo-oxidation of phenolic carbonyls in AN solutions than in
399 ammonium sulfate solutions has been ascribed to nitrate photolytic products promoting the reactions (Huang et al., 2018).
400 Furthermore, GUA+DMB+AN and GUA+VL+AN aqSOA had mainly similar features in the OS$_C$ vs. n$_C$ plots as those
401 observed in the absence of AN (Fig. S6~~5~~). More information on van Krevelen diagrams (Figs. S5~~4~~e–h and S9~~7~~) and OS$_C$ vs.
402 n$_C$ plots (Figs. S6~~5~~e–h and S10~~8~~) for GUA+DMB+AN, GUA+VL+AN, and GUA+AN aqSOA are provided in the
403 Supplement (Sect. S7). In essence, AN had no significant effect on the decay kinetics ascribable to photosensitizer chemistry
404 prevailing over nitrate, but it induced the formation of N-containing products. Moreover, AN modified the product
405 distributions, albeit in different ways (Figs. 2 and 3). In particular, N-containing products were more abundant in
406 GUA+DMB+AN, probably due to more extensive fragmentation in GUA+DMB than in GUA+VL. In GUA+VL+AN, AN
407 promoted oligomer formation likely via the -OH group of VL. Furthermore, GUA+DMB+AN and GUA+VL+AN had more
408 nitrated products than GUA+AN, suggesting that photosensitized reactions may promote nitrate photolysis-initiated
409 reactions.

410 **3.2.3 Light absorption of aqSOA from photosensitization by ³DMB* and ³VL* in the presence of AN**

411 The presence of AN also did not appreciably affect the absorbance enhancement and ΔR_{abs} for both GUA+DMB+AN and
412 GUA+VL+AN (Fig. 4). For GUA+DMB+AN, the N-containing products may have offset the decrease in oligomers to
413 maintain the absorbance enhancement observed from GUA+DMB. Wang et al. (2022) reported that nitration might
414 contribute significantly to absorbance enhancement for methoxyphenols in sodium nitrate ~~(Wang et al., 2022)~~. In
415 GUA+VL+AN, the decrease in monomers may have counteracted the increased oligomers and the generated N-containing
416 products. Compared to GUA+DMB+AN, the N-containing products from GUA+VL+AN probably had less impact on the
417 absorbance enhancement based on their smaller signal contribution.
418   Similar to experiments without AN, CHO species from GUA+DMB+AN and GUA+VL+AN were mainly
419 overlapped in the DBE vs. n$_C$ space (Fig. S8~~6~~c,d) and were mostly potential BrC chromophores. In both systems, GUA
420 dimers were the products with the highest relative abundance. For GUA+DMB+AN, products with high relative abundance
421 also include a CHN species, while two CHON species had high n$_C$ (18,20) and DBE (16,14) values. In GUA+VL+AN,

13

422 products with high relative abundance include a CHON species (n_C = 11 and 9 DBE). Approximately 30% and 43% of the
423 N-containing products for GUA+DMB+AN and GUA+VL+AN, respectively, were among the potential BrC chromophores.
424 This suggests the possible significance of N-containing products for light absorption of aqSOA from photosensitization by
425 methoxybenzaldehydes and AN photolysis. Correspondingly, nitroaromatic compounds and N-heterocycles are frequently
426 noted in BBOA (Iinuma et al., 2010; Kitanovski et al., 2012; Kourtchev et al., 2016) and have been proposed to be potential
427 contributors to BrC light absorption (Laskin et al., 2015). Relative to GUA+DMB+AN and GUA+VL+AN, only 19% of the
428 N-containing products in GUA+AN were potential BrC chromophores (Fig. S86e,f), and these did not include CHN species.
429 These indicate that the N-containing products formed in the presence of both photosensitizers and AN may be more
430 significant contributors to the light absorption of phenolic aqSOA than those formed in AN only.

431 **4 Conclusions and atmospheric implications**

432 The photosensitized oxidation of guaiacol (GUA) by triplet excited states of 3,4-dimethoxybenzaldehyde ([3]DMB*) and
433 vanillin ([3]VL*) (separately) in the absence and presence of ammonium nitrate (AN) were compared under identical
434 conditions (simulated sunlight and concentration) relevant to atmospheric cloud and fog waters. Compared to GUA+VL,
435 faster GUA oxidation and stronger light absorption by the products were observed in GUA+DMB. Moreover, VL was
436 consumed faster relative to DMB, limiting the extent of GUA oxidation in GUA+VL. These differences are rooted in DMB
437 having a better photosensitizing ability than VL and the –OH group of VL, making it more susceptible to oxidation and more
438 reactive towards electrophilic aromatic substitution. Both GUA+DMB and GUA+VL generated aqSOA (, including potential
439 BrC chromophores) composed of oligomers, functionalized monomers, oxygenated ring-opening products, and N-containing
440 products in the presence of AN. The major aqSOA formation processes for GUA+DMB and GUA+VL were oligomerization
441 and functionalization, but functionalization appeared to be more significant in GUA+VL due to VL transformation products.
442 The photochemical evolution of aqSOA from GUA+DMB has been reported by Yu et al. (2016). Similar experiments for
443 aqSOA from GUA+VL should be conducted in the future to better understand photosensitized reactions involving phenolic
444 carbonyl photosensitizers.
445 AN did not significantly affect the decay kinetics due to the predominant effect of [3]DMB* and [3]VL* chemistry
446 compared to nitrate, but it promoted the formation of N-containing products; these are composed of N-heterocycles (e.g.,
447 imidazoles) and oligomers and nitrated species. The observation of N-heterocycles agrees with our previous findings that
448 ammonium participates in photosensitized oxidation of phenolic compounds in the presence of AN (Mabato et al., 2022).
449 These results also suggest that photosensitized oxidation of phenolic compounds in the presence of AN might be an
450 important source of N-heterocycles and nitrated products. Identifying the sources of N-heterocycles and nitrated compounds
451 is important due to their environmental and health impacts (Laskin et al., 2009). Moreover, photosensitized reactions by non-
452 phenolic and phenolic methoxybenzaldehydes may be differently influenced by AN photolysis. For instance, the more
453 extensive fragmentation in GUA+DMB than in GUA+VL possibly resulted in more N-containing products in

14

GUA+DMB+AN. Furthermore, the increased oligomers in GUA+VL+AN may be due to VL-derived phenoxy radicals induced by $^{\bullet}$OH or $^{\bullet}$NO$_2$ from nitrate photolysis. In addition, more nitrated compounds observed in GUA+DMB+AN and GUA+VL+AN than in GUA+AN imply that photosensitized reactions may promote nitrate-mediated photolytic reactions. On a related note, the significance of photosensitization by BrC (via formation of solvated electrons; Y. Wang et al., 2021) and marine dissolved organic matter (via O$_2^{\bullet-}$ formation; Garcia et al., 2021) in enhanced nitrite production from nitrate photolysis have been reported. A recent study from our group has shown that glyoxal photo-oxidation mediated by both nitrate photolysis and photosensitization can significantly enhance the atmospheric sink of glyoxal (Zhang et al., 2022). Further studies are needed to improve our understanding of the interplay between photosensitized reactions and nitrate photolysis.

This study demonstrates that the structural features of photosensitizers affect aqSOA formation via non-carbonyl phenol oxidation. The VL results are broadly relevant to other phenolic carbonyls, but the effects of different functional groups should still be considered. For instance, the aldehyde/ketone pair of syringaldehyde and acetosyringone, both phenolic carbonyls, have been reported to have equal reactivity towards direct photosensitized oxidation. This is due to the greater light absorption by the aldehyde form but higher quantum efficiency for loss for the ketone form (Smith et al. 2016). However, more aqSOA was observed from syringaldehyde than acetosyringone (in either AN or ammonium sulfate; Huang et al., 2018). Our findings also imply that while the contributions of photosensitization by ^{3}VL* (and other phenolic carbonyls) to aqSOA formation would be relatively less compared to that of ^{3}DMB* (and other non-phenolic carbonyls), these are not negligible. As both non-phenolic and phenolic carbonyls such as the methoxybenzaldehydes examined in this work are emitted in large amounts from biomass burning, future experiments should probe the aqSOA contribution of a wider variety of photosensitizers. Moreover, further experiments on photosensitized reactions in authentic particulate matter (PM) samples should be conducted in the future. Multicomponent reactions such as GUA+DMB+AN and GUA+VL+AN should also be explored for a more accurate simulation of ambient conditions. These would be useful in assessing the overall impact of photosensitized reactions and AN photolysis on aqSOA formation in areas impacted by biomass burning and high AN concentrations, and for their better representation in aqSOA models.

References

Anastasio, C., Faust, B. C., and Rao, C. J.: Aromatic carbonyl compounds as aqueous-phase photochemical sources of hydrogen peroxide in acidic sulfate aerosols, fogs, and clouds. 1. Non-phenolic methoxybenzaldehydes and methoxyacetophenones with reductants (phenols), Environ. Sci. Technol., 31, 218−232, https://doi.org/10.1021/es960359g, 1997.

Bateman, A. P., Laskin, J., Laskin, A., and Nizkorodov, S. A.: Applications of high-resolution electrospray ionization mass spectrometry to measurements of average oxygen to carbon ratios in secondary organic aerosols, Environ. Sci. Technol., 46, 8315–832, https://doi.org/10.1021/es3017254, 2012.

Bianco, A., Passananti, M., Brigante, M., and Mailhot, G.: Photochemistry of the cloud aqueous phase: a review, Molecules, 25, 423, https://doi.org/10.3390/molecules25020423, 2020.

Calvert, J. G. and Madronich, S.: Theoretical study of the initial products of the atmospheric oxidation of hydrocarbons, J. Geophys. Res., 92, 2211−2220, https://doi.org/10.1029/JD092iD02p02211, 1987.

Chen, Y., Li, N., Li, X., Tao, Y., Luo, S., Zhao, Z., Ma, S., Huang, H., Chen, Y., Ye, Z., and Ge, X.: Secondary organic aerosol formation from $^3C^*$-initiated oxidation of 4-ethylguaiacol in atmospheric aqueous-phase, Sci. Total Environ., 723, 137953, https://doi.org/10.1016/j.scitotenv.2020.137953, 2020.

Chen, Z. and Anastasio, C.: Concentrations of a triplet excited state are enhanced in illuminated ice, Environ. Sci.: Processes Impacts, 19, 12−21, https://doi.org/10.1039/C6EM00534A, 2017.

Collett, J. L. Jr., Hoag, K. J., Sherman, D. E., Bator, A., and Richards, L. W.: Spatial and temporal variations in San Joaquin Valley fog chemistry, Atmos. Environ., 33, 129−140, https://doi.org/10.1016/S1352-2310(98)00136-8, 1998.

De Haan, D. O., Tolbert, M. A., and Jimenez, J. L.: Atmospheric condensed-phase reactions of glyoxal with methylamine, Geophys. Res. Lett., 36, No. L11819, https://doi.org/10.1029/2009GL037441, 2009.

De Haan, D. O., Hawkins, L. N., Kononenko, J. A., Turley, J. J., Corrigan, A. L., Tolbert, M. A., and Jimenez, J. L.: Formation of nitrogen-containing oligomers by methylglyoxal and amines in simulated evaporating cloud droplets, Environ. Sci. Technol., 45, 984−991, https://doi.org/10.1021/es102933x, 2011.

De Haan, D. O., Pajunoja, A., Hawkins, L. N., Welsh, H. G., Jimenez, N. G., De Loera, A., Zauscher, M., Andretta, A. D., Joyce, B. W., De Haan, A. C., Riva, M., Cui, T., Surratt, J. D., Cazaunau, M., Formenti, P., Gratien, A., Pangui, E., and Doussin, J-F.: Methylamine's effects on methylglyoxal-containing aerosol: chemical, physical, and optical changes, ACS Earth Space Chem., 3, 1706–1716, https://doi.org/10.1021/acsearthspacechem.9b00103, 2019.

531

532 De Haan, D. O., Tolbert, M. A., and Jimenez, J. L.: Atmospheric condensed phase reactions of glyoxal with methylamine,
533 Geophys. Res. Lett., 36, No. L11819, https://doi.org/10.1029/2009GL037441, 2009.

534

535 Du, Y., Fu, Q. S., Li, Y., and Su, Y.: Photodecomposition of 4-chlorophenol by reactive oxygen species in UV/air system, J.
536 Hazard. Mater., 186, 491–496, https://doi.org/10.1016/j.jhazmat.2010.11.023, 2011.

537

538 Edye, L. A. and Richards, G. N.: Analysis of condensates from wood smoke. components derived from polysaccharides and
539 lignins, Environ. Sci. Technol., 25, 1133−1137, https://doi.org/10.1021/es00018a018, 1991.

540

541 Felber, T., Schaefer, T., He, L., and Herrmann, H.: Aromatic carbonyl and nitro compounds as photosensitizers and their
542 photophysical properties in the tropospheric aqueous phase, J. Phys. Chem. A, 125, 5078−5095,
543 https://doi.org/10.1021/acs.jpca.1c03503, 2021.

544

545 Fleming, L. T., Lin, P., Laskin, A., Laskin, J., Weltman, R., Edwards, R. D., Arora, N. K., Yadav, A., Meinardi, S., Blake, D.
546 R., Pillarisetti, A., Smith, K. R., and Nizkorodov, S. A.: Molecular composition of particulate matter emissions from dung
547 and brushwood burning household cookstoves in Haryana, India, Atmos. Chem. Phys., 18, 2461–2480,
548 https://doi.org/10.5194/acp-18-2461-2018, 2018.

549

550 Galloway, M. M., Chhabra, P. S., Chan, A. W. H., Surratt, J. D., Flagan, R. C., Seinfeld, J. H., and Keutsch, F. N.: Glyoxal
551 uptake on ammonium sulphate seed aerosol: reaction products and reversibility of uptake under dark and irradiated
552 conditions, Atmos. Chem. Phys., 9, 3331–3345, https://doi.org/10.5194/acp-9-3331-2009, 2009.

553

554 Garcia, S. L. M., Pandit, S., Navea, J. G., and Grassian, V. H.: Nitrous acid (HONO) formation from the irradiation of
555 aqueous nitrate solutions in the presence of marine chromophoric dissolved organic matter: comparison to other organic
556 photosensitizers, ACS Earth Space Chem., 5, 3056−3064, https://doi.org/10.1021/acsearthspacechem.1c00292, 2021.

557

558 Gen, M., Huang, D. D., and Chan, C. K.: Reactive uptake of glyoxal by ammonium-containing salt particles as a function of
559 relative humidity, Environ. Sci. Technol., 52, 6903−6911, https://doi.org/10.1021/acs.est.8b00606, 2018.

560

561 Gen, M., Zhang, R., Huang, D. D., Li, Y. J., and Chan, C. K.: Heterogeneous SO_2 oxidation in sulfate formation by
562 photolysis of particulate nitrate, Environ. Sci. Technol. Lett., 6, 86–91, https://doi.org/10.1021/acs.estlett.8b00681, 2019a.

563

564 Gen, M., Zhang, R., Huang, D. D., Li, Y. J., and Chan, C. K.: Heterogeneous oxidation of SO_2 in sulfate production during
565 nitrate photolysis at 300 nm: effect of pH, relative humidity, irradiation intensity, and the presence of organic compounds,
566 Environ. Sci. Technol., 53, 8757–8766, https://doi.org/10.1021/acs.est.9b01623, 2019b.

567

568 Gen, M., Liang, Z., Zhang, R., Mabato, B. R. G., and Chan, C. K.: Particulate nitrate photolysis in the atmosphere, Environ.
569 Sci.: Atmos., 2, 111–127, https://doi.org/10.1039/d1ea00087j, 2022.

570

571 George, C., Brüggemann, M., Hayeck, N., Tinel, L., and Donaldson, J.: Interfacial photochemistry: physical chemistry of
572 gas-liquid interfaces, in: Developments in Physical & Theoretical Chemistry, edited by: Faust, J. A. and House, J. E.,
573 Elsevier, 435–457, https://doi.org/10.1016/B978-0-12-813641-6.00014-5, 2018.

574

575 Giulianelli, L., Gilardoni, S., Tarozzi, L., Rinaldi, M., Decesari, S., Carbone, C., Facchini, M. C., and Fuzzi, S.: Fog
576 occurrence and chemical composition in the Po valley over the last twenty years, Atmos. Environ., 98, 394–401,
577 https://doi.org/10.1016/j.atmosenv.2014.08.080, 2014.

578

Grace, D. N., Sharp, J. R., Holappa, R. E., Lugos, E. N., Sebold, M. B., Griffith, D. R., Hendrickson, H. P., and, Galloway, M. M.: Heterocyclic product formation in aqueous brown carbon systems, ACS Earth Space Chem., 3, 2472−2481, https://doi.org/10.1021/acsearthspacechem.9b00235, 2019.

Hawthorne, S. B., Miller, D. J., Langenfeld, J. J., and Krieger, M. S.: PM-10 High-volume collection and quantitation of semi- and nonvolatile phenols, methoxylated phenols, alkanes, and polycyclic aromatic hydrocarbons from winter urban air and their relationship to wood smoke emissions, Environ. Sci. Technol., 26, 2251−2262, https://doi.org/10.1021/es00035a026, 1992.

Hems, R. F., Schnitzler, E. G., Bastawrous, M., Soong, R., Simpson, A. J., and Abbatt, J. P. D.: Aqueous photoreactions of wood smoke brown carbon, ACS Earth Space Chem., 4, 1149−1160, https://doi.org/10.1021/acsearthspacechem.0c0011, 2020.

Hoshino, M., Akimoto, H., and Okuda, M.: Photochemical oxidation of benzene, toluene, and ethylbenzene initiated by OH radicals in the gas phase, Bull. Chem. Soc. Jpn., 51, 718−724, https://doi.org/10.1246/bcsj.51.718, 1978.

Huang, D. D., Zhang, Q., Cheung, H. H. Y., Yu, L., Zhou, S., Anastasio, C., Smith, J. D., and Chan, C. K.: Formation and evolution of aqSOA from aqueous-phase reactions of phenolic carbonyls: comparison between ammonium sulfate and ammonium nitrate solutions, Environ. Sci. Technol., 52, 9215–9224, https://doi.org/10.1021/acs.est.8b03441, 2018.

Iinuma, Y., Böge, O., Gräfe, R., and Herrmann, H.: Methyl-nitrocatechols: atmospheric tracer compounds for biomass burning secondary organic aerosols, Environ. Sci. Technol., 44, 8453–8459, https://doi.org/10.1021/es102938a, 2010.

Jiang, W., Misovich, M. V., Hettiyadura, A. P. S., Laskin, A., McFall, A. S., Anastasio, C., and Zhang, Q.: Photosensitized reactions of a phenolic carbonyl from wood combustion in the aqueous phase—chemical evolution and light absorption properties of aqSOA, Environ. Sci. Technol., 55, 5199−5211, https://doi.org/10.1021/acs.est.0c07581, 2021.

Kampf, C. J., Jakob, R., and Hoffmann, T.: Identification and characterization of aging products in the glyoxal/ammonium sulfate system – implications for light-absorbing material in atmospheric aerosols, Atmos. Chem. Phys., 12, 6323–6333, https://doi.org/10.5194/acp-12-6323-2012, 2012.

Kebarle, P. A.: A brief overview of the mechanisms involved in electrospray mass spectrometry, J. Mass Spectrom., 35, 804−817, https://doi.org/10.1002/9783527628728.ch1, 2000.

Kitanovski, Z., Grgić, I., Vermeylen, R., Claeys, M., and Maenhaut, W.: Liquid chromatography tandem mass spectrometry method for characterization of monoaromatic nitro-compounds in atmospheric particulate matter, J. Chromatogr. A, 1268, 35–43, https://doi.org/10.1016/j.chroma.2012.10.021, 2012.

Klodt, A.L., Romonosky, D.E., Lin, P., Laskin, J., Laskin, A., and Nizkorodov, S.A.: Aqueous photochemistry of secondary organic aerosol of α-pinene and α-humulene in the presence of hydrogen peroxide or inorganic salts, ACS Earth Space Chem., 3, 12, 2736–2746, https://doi.org/10.1021/acsearthspacechem.9b00222, 2019.

Kobayashi, S. and Higashimura, H.: Oxidative polymerization of phenols revisited, Prog. Polym. Sci., 28, 1015–1048, https://doi.org/10.1016/S0079-6700(03)00014-5, 2003.

Kourtchev, I., Fuller, S. J., Giorio, C., Healy, R. M., Wilson, E., O'Connor, I., Wenger, J. C., McLeod, M., Aalto, J., Ruuskanen, T. M., Maenhaut, W., Jones, R., Venables, D. S., Sodeau, J. R., Kulmala, M., and Kalberer, M.: Molecular composition of biogenic secondary organic aerosols using ultrahigh-resolution mass spectrometry: comparing laboratory and field studies, Atmos. Chem. Phys., 14, 2155−2167, https://doi.org/10.5194/acp-14-2155-2014, 2014.

629

630 Kourtchev, I., Godoi, R. H. M., Connors, S., Levine, J. G., Archibald, A. T., Godoi, A. F. L., Paralovo, S. L., Barbosa, C. G.
631 G., Souza, R. A. F., Manzi, A. O., Seco, R., Sjostedt, S., Park, J., Guenther, A., Kim, S., Smith, J., Martin, S. T., and
632 Kalberer, M.: Molecular composition of organic aerosols in central Amazonia: an ultra-high-resolution mass spectrometry
633 study, Atmos. Chem. Phys., 16, 11899–11913, https://doi.org/10.5194/acp-16-11899-2016, 2016.

634

635 Kroll, J. H., Donahue, N. M., Jimenez, J. L., Kessler, S. H., Canagaratna, M. R., Wilson, K. R., Altieri, K. E., Mazzoleni, L.
636 R., Wozniak, A. S., Bluhm, H., Mysak, E. R., Smith, J. D., Kolb, C. E., and Worsnop, D. R.: Carbon oxidation state as a
637 metric for describing the chemistry of atmospheric organic aerosol, Nat. Chem., 3, 133–139,
638 https://doi.org/10.1038/nchem.948, 2011.

639

640 Kruve, A., Kaupmees, K., Liigand, J., and Leito, I.: Negative electrospray ionization via deprotonation: predicting the
641 ionization efficiency, Anal. Chem., 86, 4822–4830, https://doi.org/10.1021/ac404066v, 2014.

642

643 Laskin, A., Smith, J. S., and Laskin, J.: Molecular characterization of nitrogen-containing organic compounds in biomass
644 burning aerosols using high-resolution mass spectrometry, Environ. Sci. Technol., 43, 3764–3771,
645 https://doi.org/10.1021/es803456n, 2009.

646

647 Laskin, A., Laskin, J., and Nizkorodov, S. A.: Chemistry of atmospheric brown carbon, Chem. Rev., 115, 4335–4382,
648 https://doi.org/10.1021/cr5006167, 2015.

649

650 Laskin, J., Laskin, A., Nizkorodov, S. A., Roach, P., Eckert, P., Gilles, M. K., Wang, B., Lee, H. J., and Hu, Q.: Molecular
651 selectivity of brown carbon chromophores, Environ. Sci. Technol., 48, 12047–12055, https://doi.org/10.1021/es503432r,
652 2014.

653

654 Lee, A. K. Y., Zhao, R., Li, R., Liggio, J., Li, S., and Abbatt, J. P. D.: Formation of light absorbing organo-nitrogen species
655 from evaporation of droplets containing glyoxal and ammonium sulfate, Environ. Sci. Technol., 47, 12819−12826,
656 https://doi.org/10.1021/es402687w, 2013.
657 Lee, H. J., Aiona, P. K., Laskin, A., Laskin, J., and Nizkorodov, S. A.: Effect of solar radiation on the optical properties and
658 molecular composition of laboratory proxies of atmospheric brown carbon, Environ. Sci. Technol., 48, 10217–10226,
659 https://doi.org/10.1021/es502515r, 2014.

660

661 Leifer, A.: The Kinetics of environmental aquatic photochemistry: Theory and practice, American Chemical Society,
662 Washington, DC, 1988.

663

664 Leito, I., Herodes, K., Huopolainen, M., Virro, K., Künnapas, A., Kruve, A., and Tanner, R.: Towards the electrospray
665 ionization mass spectrometry ionization efficiency scale of organic compounds, Rapid Commun. Mass Sp., 22, 379–384,
666 https://doi.org/10.1002/rcm.3371, 2008.

667

668 Li, P., Li, X., Yang, C., Wang, X., Chen, J., and Collett, J. L. Jr.: Fog water chemistry in Shanghai, Atmos. Environ., 45,
669 4034−4041, https://doi.org/10.1016/j.atmosenv.2011.04.036, 2011.

670

671 Li, Y. J., Huang, D. D., Cheung, H. Y., Lee, A. K. Y., and Chan, C. K.: Aqueous-phase photochemical oxidation and direct
672 photolysis of vanillin - a model compound of methoxy phenols from biomass burning, Atmos. Chem. Phys., 14, 2871−2885,
673 https://doi.org/10.5194/acp-14-2871-2014, 2014.

674

675 Liang, Z., Zhang, R., Gen, M., Chu, Y., and Chan, C. K.: Nitrate photolysis in mixed sucrose–nitrate–sulfate particles at
676 different relative humidities, J. Phys. Chem. A, 125, 3739–3747, https://doi.org/10.1021/acs.jpca.1c00669, 2021.

677

678 Lin, P., Yu, J. Z., Engling, G., and Kalberer, M.: Organosulfates in humic-like substance fraction isolated from aerosols at
679 seven locations in East Asia: a study by ultra-high-resolution mass spectrometry, Environ. Sci. Technol., 46, 13118–13127,
680 https://doi.org/10.1021/es303570v, 2012.

682 Lin, P., Fleming, L. T., Nizkorodov, S. A., Laskin, J., and Laskin, A.: Comprehensive molecular characterization of
683 atmospheric brown carbon by high resolution mass spectrometry with electrospray and atmospheric pressure
684 photoionization, Anal. Chem., 90, 12493–12502, https://doi.org/10.1021/acs.analchem.8b02177, 2018.

686 Lipari, F., Dasch, J. M., and Scruggs, W. F.: Aldehyde emissions from wood-burning fireplaces, Environ. Sci. Technol., 18,
687 326−330, https://doi.org/10.1021/es00123a007, 1984.

689 Liu, C., Chen, D., and Chen, X.: Atmospheric reactivity of methoxyphenols: a review, Environ. Sci. Technol., 56, 2897–
690 2916, https://doi.org/10.1021/acs.est.1c06535, 2022.

692 Lobodin, V. V., Marshall, A. G., and Hsu, C. S.: Compositional space boundaries for organic compounds, Anal. Chem., 84,
693 3410–3416, https://doi.org/10.1021/ac300244f, 2012.

695 Mabato, B. R. G., Gen, M., Chu, Y., and Chan, C. K.: Reactive uptake of glyoxal by methylaminium-containing salts as a
696 function of relative humidity, ACS Earth Space Chem., 3, 150–157, https://doi.org/10.1021/acsearthspacechem.8b00154,
697 2019.

699 Mabato, B. R. G., Lyu, Y., Ji, Y., Li, Y. J., Huang, D. D., Li, X., Nah, T., Lam, C. H., and Chan, C. K.: Aqueous secondary
700 organic aerosol formation from the direct photosensitized oxidation of vanillin in the absence and presence of ammonium
701 nitrate, Atmos. Chem. Phys., 22, 273−293, https://doi.org/10.5194/acp-22-273-2022, 2022.

703 Mazzoleni, L. R., Saranjampour, P., Dalbec, M. M., Samburova, V., Hallar, A. G., Zielinska, B., Lowenthal, D. H., and
704 Kohl, S.: Identification of water-soluble organic carbon in non-urban aerosols using ultrahigh-resolution FT-ICR mass
705 spectrometry: organic anions, Environ. Chem., 9, 285−297, https://doi.org/10.1071/EN11167, 2012.

707 Minero, C., Bono, F., Rubertelli, F., Pavino, D., Maurino, V., Pelizzetti, E., and Vione, D.: On the effect of pH in aromatic
708 photonitration upon nitrate photolysis, Chemosphere, 66, 650−656, https://doi.org/10.1016/j.chemosphere.2006.07.082, 2007.

710 Misovich, M. V., Hettiyadura, A. P. S., Jiang, W., Zhang, Q., and Laskin, A.: Molecular-level study of the photo-oxidation
711 of aqueous-phase guaiacyl acetone in the presence of $^3C^*$: formation of brown carbon products, ACS Earth Space Chem., 5,
712 1983−1996, https://doi.org/10.1021/acsearthspacechem.1c00103, 2021.

714 Munger, J. W., Jacob, D. J., Waldman, J. M., and Hoffmann, M. R.: Fogwater chemistry in an urban atmosphere, J.
715 Geophys. Res. [Oceans], 88, 5109–5121, https://doi.org/10.1029/JC088iC09p05109, 1983.

717 Ning, C., Gao, Y., Zhang, H., Yu, H., Wang, L., Geng, N., Cao, R., and Chen, J.: Molecular characterization of dissolved
718 organic matters in winter atmospheric fine particulate matters (PM2.5) from a coastal city of northeast China, Sci. Total
719 Environ., 689, 312–321, https://doi.org/10.1016/j.scitotenv.2019.06.418, 2019.

721 Nolte, C. G., Schauer, J. J., Cass, G. R., and Simoneit, B. R. T.: Highly polar organic compounds present in wood smoke and
722 in the ambient atmosphere, Environ. Sci. Technol., 35, 1912−1919, https://doi.org/10.1021/es001420r, 2001.

724 Nozière, B., Dziedzic, P., and Córdova, A.: Products and kinetics of the liquid-phase reaction of glyoxal catalyzed by
725 ammonium ions (NH_4^+), J. Phys. Chem. A, 113, 231−237, https://doi.org/10.1021/jp8078293, 2009.

Nozière, B., Dziedzic, P., and Córdova, A.: Inorganic ammonium salts and carbonate salts are efficient catalysts for aldol condensation in atmospheric aerosols, Phys. Chem. Chem. Phys., 12, 3864−3872, https://doi.org/10.1039/B924443C, 2010.

Nozière, B., Fache, F., Maxut, A., Fenet, B., Baudouin, A., Fine, L., and Ferronato, C.: The hydrolysis of epoxides catalyzed by inorganic ammonium salts in water: kinetic evidence for hydrogen bond catalysis, Phys. Chem. Chem. Phys., 20, 1583−1590, https://doi.org/10.1039/C7CP06790A, 2018.

Pang, H., Zhang, Q., Lu, X., Li, K., Chen, H., Chen, J., Yang, X., Ma, Y., Ma, J., and Huang, C.: Nitrite-mediated photooxidation of vanillin in the atmospheric aqueous phase, Environ. Sci. Technol., 53, 14253−14263, https://doi.org/10.1021/acs.est.9b03649, 2019.

Perry, R. H., Cooks, R. G., and Noll, R. J.: Orbitrap mass spectrometry: instrumentation, ion motion and applications, Mass Spectrom. Rev., 27, 661–699, https://doi.org/10.1002/mas.20186, 2008.

Powelson, M. H., Espelien, B. M., Hawkins, L. N., Galloway, M. M., and De Haan, D. O.: Brown carbon formation by aqueous-phase carbonyl compound reactions with amines and ammonium sulfate, Environ. Sci. Technol., 48, 985−993, https://doi.org/10.1021/es4038325, 2014.

Pye, H. O. T., Nenes, A., Alexander, B., Ault, A. P., Barth, M. C., Clegg, S. L., Collett, J. L. Jr., Fahey, K. M., Hennigan, C. J., Herrmann, H., Kanakidou, M., Kelly, J. T., Ku, I., McNeill, V. F., Riemer, N., Schaefer, T., Shi, G., Tilgner, A., Walker, J. T., Wang, T., Weber, R., Xing, J., Zaveri, R. A., and Zuend, A.: The acidity of atmospheric particles and clouds, Atmos. Chem. Phys., 20, 4809–4888, https://doi.org/10.5194/acp-20-4809-2020, 2020.

Raja, S., Raghunathan, R., Yu, X., Lee, T., Chen, J., Kommalapati, R. R., Murugesan, K., Shen, X., Qingzhong, Y., Valsaraj, K. T., and Collett, J. L. Jr.: Fog chemistry in the Texas-Louisiana Gulf Coast corridor, Atmos. Environ., 42, 2048−2061, https://doi.org/10.1016/j.atmosenv.2007.12.004, 2008.

Rogge, W. F., Hildemann, L. M., Mazurek, M. A., and Cass, G. R.: Sources of fine organic aerosol. 9. Pine, oak, and synthetic log combustion in residential fireplaces, Environ. Sci. Technol., 32, 13−22, https://doi.org/10.1021/es960930b, 1998.

Romonosky, D. E., Li, Y., Shiraiwa, M., Laskin, A., Laskin, J., and Nizkorodov, S. A.: Aqueous photochemistry of secondary organic aerosol of α-Pinene and α-Humulene oxidized with ozone, hydroxyl radical, and nitrate radical, J. Phys. Chem. A, 121, 1298–1309, https://doi.org/10.1021/acs.jpca.6b10900, 2017.

Sagebiel, J. C., Seiber, J. N., and Woodrow, J. E.: Comparison of headspace and gas-stripping methods for determining the Henry's law constant (H) for organic compounds of low to intermediate H, Chemosphere, 25, 1763–1768, https://doi.org/10.1016/0045-6535(92)90017-L, 1992.

Schauer, J. J., Kleeman, M. J., Cass, G. R., and Simoneit, B. R. T.: Measurement of emissions from air pollution sources. 3. C_1-C_{29} organic compounds from fireplace combustion of wood, Environ. Sci. Technol., 35, 1716−1728, https://doi.org/10.1021/es001331e, 2001.

Schmidt, A-C., Herzschuh, R., Matysik, F-M., and Engewald, W.: Investigation of the ionisation and fragmentation behaviour of different nitroaromatic compounds occurring as polar metabolites of explosives using electrospray ionisation tandem mass spectrometry, Rapid Commun. Mass Sp., 20, 2293–2302, https://doi.org/10.1002/rcm.2591, 2006.

Shapiro, E. L., Szprengiel, J., Sareen, N., Jen, C. N., Giordano, M. R., and McNeill, V. F.: Light-absorbing secondary organic material formed by glyoxal in aqueous aerosol mimics, Atmos. Chem. Phys., 9, 2289−2300, https://doi.org/10.5194/acp-9-2289-2009, 2009.

777

778 Siegmann, K. and Sattler, K.: Formation mechanism for polycyclic aromatic hydrocarbons in methane flames, J. Chem.
779 Phys., 112, 698–709, https://doi.org/10.1063/1.480648, 2000.

780

781 Simoneit, B. R. T.: Biomass burning — a review of organic tracers for smoke from incomplete combustion, Appl.
782 Geochem., 17, 129–162, https://doi.org/10.1016/S0883-2927(01)00061-0, 2002.

783

784 Simoneit, B. R. T., Rogge, W. F., Mazurek, M. A., Standley, L. J., Hildemann, L. M., and Cass, G. R.: Lignin pyrolysis
785 products, lignans, and resin acids as specific tracers of plant classes in emissions from biomass combustion, Environ. Sci.
786 Technol., 27, 2533−2541, https://doi.org/10.1021/es00048a034, 1993.

787

788 Simoneit, B. R. T., Schauer, J. J., Nolte, C. G., Oros, D. R., Elias, V. O., Fraser, M. P., Rogge, W. F., and Cass, G. R.:
789 Levoglucosan, a tracer for cellulose in biomass burning and atmospheric particles, Atmos. Environ., 33, 173−182,
790 https://doi.org/10.1016/S1352-2310(98)00145-9, 1999.

791

792 Simpson, C. D., Paulsen, M., Dills, R. L., Liu, L.-J. S., and Kalman, D. A.: Determination of methoxyphenols in ambient
793 atmospheric particulate matter: tracers for wood combustion, Environ. Sci. Technol., 39, 631−637,
794 https://doi.org/10.1021/es0486871, 2005.

795

796 Slikboer, S., Grandy, L., Blair, S. L., Nizkorodov, S. A., Smith, R. W., and Al-Abadleh, H. A.: Formation of light absorbing
797 soluble secondary organics and insoluble polymeric particles from the dark reaction of catechol and guaiacol with Fe(III),
798 Environ. Sci. Technol., 49, 7793–7801, https://doi.org/10.1021/acs.est.5b01032, 2015.

799

800 Smith, D. F., Kleindienst, T. E., and McIver, C. D.: Primary product distributions from the reaction of OH with m-, p-xylene,
801 1,2,4-and 1,3,5-trimethylbenzene, J. Atmos. Chem., 34, 339–364, https://doi.org/10.1023/A:1006277328628, 1999.

802

803 Smith, J. D., Sio, V., Yu, L., Zhang, Q., and Anastasio, C.: Secondary organic aerosol production from aqueous reactions of
804 atmospheric phenols with an organic triplet excited state, Environ. Sci. Technol., 48, 1049–1057,
805 https://doi.org/10.1021/es4045715, 2014.

806

807 Smith, J. D., Kinney, H., and Anastasio, C.: Aqueous benzene-diols react with an organic triplet excited state and hydroxyl
808 radical to form secondary organic aerosol, Phys. Chem. Chem. Phys., 17, 10227−10237,
809 https://doi.org/10.1039/C4CP06095D, 2015.

810

811 Smith, J. D., Kinney, H., and Anastasio, C.: Phenolic carbonyls undergo rapid aqueous photodegradation to form low-
812 volatility, light-absorbing products, Atmos. Environ., 126, 36−44, https://doi.org/10.1016/j.atmosenv.2015.11.035, 2016.

813

814 Song, J., Li, M., Jiang, B., Wei, S., Fan, X., and Peng, P.: Molecular characterization of water-soluble humic like substances
815 in smoke particles emitted from combustion of biomass materials and coal using ultrahigh-resolution electrospray ionization
816 Fourier transform ion cyclotron resonance mass spectrometry, Environ. Sci. Technol., 52, 2575–2585,
817 https://doi.org/10.1021/acs.est.7b06126, 2018.

818

819 Sun, Y. L., Zhang, Q., Anastasio, C., and Sun, J.: Insights into secondary organic aerosol formed via aqueous-phase
820 reactions of phenolic compounds based on high resolution mass spectrometry, Atmos. Chem. Phys., 10, 4809−4822,
821 https://doi.org/10.5194/acp-10-4809-2010, 2010.

822

823 US EPA: Estimation Programs Interface Suite™ for Microsoft® Windows, v 4.1, United States Environmental Protection
824 Agency, Washington, DC, USA, 2012.

825

Wang, K., Huang, R-J., Brüggemann, M., Zhang, Y., Yang, L., Ni, H., Guo, J., Wang, M., Han, J., Bilde, M., Glasius, M., and Hoffmann, T.: Urban organic aerosol composition in eastern China differs from north to south: molecular insight from a liquid chromatography–mass spectrometry (Orbitrap) study, Atmos. Chem. Phys., 21, 9089–9104, https://doi.org/10.5194/acp-21-9089-2021, 2021.

Wang, X., Hayeck, N., Brüggemann, M., Yao, L., Chen, H., Zhang, C., Emmelin, C., Chen, J., George, C., and Wang, L.: Chemical characterization of organic aerosols in Shanghai: A study by ultrahigh-performance liquid chromatography coupled with orbitrap mass spectrometry, J. Geophys. Res. Atmos., 122, 11703–11722, https://doi.org/10.1002/2017JD026930, 2017.

Wang, Y., Huang, D. D., Huang, W., Liu, B., Chen, Q., Huang, R., Gen, M., Mabato, B. R. G., Chan, C. K., Li, X., Hao, T., Tan, Y., Hoi, K. I., Mok, K. M., and Li, Y. J.: Enhanced nitrite production from the aqueous photolysis of nitrate in the presence of vanillic acid and implications for the roles of light-absorbing organics, Environ. Sci. Technol., 55, 15694−15704, https://doi.org/10.1021/acs.est.1c04642, 2021.

Wang, Y., Huang, W., Tian, L., Wang, Y., Li, F., Huang, D. D., Zhang, R., Mabato, B. R. G., Huang, R., Chen, Q., Ge, X., Du, L., Ma, Y. G., Gen, M., Hoi, K. I., Mok, K. M., Yu, J. Z., Chan, C. K., Li, X., and Li, Y. J.: Decay kinetics and absorption changes of methoxyphenols and nitrophenols during nitrate-mediated aqueous photochemical oxidation at 254 and 313 nm, ACS Earth Space Chem., 6, 1115−1125, https://doi.org/10.1021/acsearthspacechem.2c00021, 2022.

Yang, J., Au, W. C., Law, H., Leung, C. H., Lam, C. H, and Nah, T.: pH affects the aqueous-phase nitrate-mediated photooxidation of phenolic compounds: implications for brown carbon formation and evolution, Environ. Sci.: Processes Impacts, https://doi.org/10.1039/D2EM00004K, 2022.

Yasmeen, F., Vermeylen, R., Szmigielski, R., Iinuma, Y., Böge, O., Herrmann, H., Maenhaut, W., and Claeys, M.: Terpenylic acid and related compounds: precursors for dimers in secondary organic aerosol from the ozonolysis of α and β-pinene, Atmos. Chem. Phys., 10, 9383–9392, https://doi.org/10.5194/acp-10-9383-2010, 2010.

Yaws, C. L.: Handbook of vapor pressure, volume 3: Organic compounds C8 to C28, Gulf Professional Publishing, 1994.

Ye, Z., Qu, Z., Ma, S., Luo, S., Chen, Y., Chen, H., Chen, Y., Zhao, Z., Chen, M., and Ge, X.: A comprehensive investigation of aqueous-phase photochemical oxidation of 4-ethylphenol, Sci. Total Environ., 685, 976–985, https://doi.org/10.1016/j.scitotenv.2019.06.276, 2019.

Yu, G., Bayer, A. R., Galloway, M. M., Korshavn, K. J., Fry, C. G., and Keutsch, F. N.: Glyoxal in aqueous ammonium sulfate solutions: products, kinetics and hydration effects, Environ. Sci. Technol., 45, 6336−6342, https://doi.org/10.1021/es200989n, 2011.

Yu, L., Smith, J., Laskin, A., Anastasio, C., Laskin, J., and Zhang, Q.: Chemical characterization of SOA formed from aqueous-phase reactions of phenols with the triplet excited state of carbonyl and hydroxyl radical, Atmos. Chem. Phys., 14, 13801−13816, https://doi.org/10.5194/acp-14-13801-2014, 2014.

Yu, L., Smith, J., Laskin, A., George, K. M., Anastasio, C., Laskin, J., Dillner, A. M., and Zhang, Q.: Molecular transformations of phenolic SOA during photochemical aging in the aqueous phase: competition among oligomerization, functionalization, and fragmentation, Atmos. Chem. Phys., 16, 4511−4527, https://doi.org/10.5194/acp-16-4511-2016.

Zhang, Q. and Anastasio, C.: Conversion of fogwater and aerosol organic nitrogen to ammonium, nitrate, and NO_x during exposure to simulated sunlight and ozone, Environ. Sci. Technol., 37, 3522–3530, https://doi.org/10.1021/es034114x, 2003.

875 Zhang, R., Gen, M., Huang, D. D., Li, Y. J., and Chan, C. K.: Enhanced sulfate production by nitrate photolysis in the
876 presence of halide ions in atmospheric particles, Environ. Sci. Technol., 54, 3831–3839,
877 https://doi.org/10.1021/acs.est.9b06445, 2020.

879 Zhang, R., Gen, M., Fu, T-M., and Chan, C. K.: Production of formate via oxidation of glyoxal promoted by particulate
880 nitrate photolysis, Environ. Sci. Technol., 55, 5711–5720, https://doi.org/10.1021/acs.est.0c0819, 2021.

882 Zhang, R., Gen, M., Liang, Z., Li, Y. J., and Chan, C. K.: Photochemical reactions of glyoxal during particulate ammonium
883 nitrate photolysis: Brown carbon formation, enhanced glyoxal decay, and organic phase formation, Environ. Sci. Technol.,
884 56, 1605–1614, https://doi.org/10.1021/acs.est.1c07211, 2022.

886 Zielinski, T., Bolzacchini, E., Cataldi, M., Ferrero, L., Graßl, S., Hansen, G., Mateos, D., Mazzola, M., Neuber, R., Pakszys,
887 P., Posyniak, M., Ritter, C., Severi, M., Sobolewski, P., Traversi, R., and Velasco-Merino, C.: Study of chemical and optical
888 properties of biomass burning aerosols during long-range transport events toward the Arctic in summer 2017, Atmosphere,
889 11, 84, https://doi.org/10.3390/atmos11010084, 2020.

Table 1. Reaction conditions, initial GUA (and DMB or VL) decay rate constants, normalized abundance of products, average elemental ratios, and average carbon oxidation state ($\langle OS_C \rangle$) in each experiment. The reaction systems consisted of GUA (0.1 mM), DMB (0.01 mM), VL (0.01 mM), and AN (1 mM) under air-saturated conditions after 180 min of simulated sunlight irradiation. The UHPLC-HESI-Orbitrap-MS data were obtained in both positive (POS) and negative (NEG) ion modes.

Exp no.	Reaction conditions	Initial GUA (and DMB or VL) decay rate constants (min^{-1}/~~s^{-1}~~)[a]	Normalized abundance of products[b]	Normalized abundance of N-containing compounds[b]	$\langle O{:}C \rangle$[c]	$\langle H{:}C \rangle$[c]	$\langle N{:}C \rangle$[c]	$\langle OS_C \rangle$[c]
1	GUA+DMB	GUA: ~~5.4 × 10^{-2}~~6.3 ± 0.25~~3.0 × 10^{-4}~~ DMB: ~~0.~~6.7 × 10^{-3}~~78~~ ± ~~0~~1.~~10~~2 × 10^{-4}	376 ± 22	NA	POS: 0.34 / NEG: 0.40	0.91 / 0.94	NA / NA	-0.22 / -0.15
2	GUA+ DMB+AN	GUA: ~~4.8 × 10^{-2}~~5.3 ± 0~~6~~.5~~04 × 10^{-4}~~ DMB: ~~6.2 × 10^{-3}~~0.69 ± -0.05~~6.25 × 10^{-5}~~	310 ± 4	114	POS: 0.28 / NEG: 0.37	0.94 / 0.91	0.12 / 0.04	-0.03 / -0.05
3	GUA+VL	GUA: ~~1.4 × 10^{-2}~~1.5 ± 0~~1~~.1~~48 × 10^{-4}~~ VL: ~~3.3 × 10^{-2}~~3.6 ± 0.55~~7.0 × 10^{-4}~~	94 ± 5	NA	POS: 0.41 / NEG: 0.40	0.91 / 0.94	NA / NA	-0.10 / -0.14
~~3~~4	GUA+ VL+AN	GUA: ~~1.5 × 10^{-2}~~1.6 ± 0.1~~26 × 10^{-4}~~ VL: ~~2.8 × 10^{-2}~~2.9 ± 0.03~~24.9 × 10^{-5}~~	100 ± 2	8	POS: 0.31 / NEG: 0.39	1.02 / 0.91	0.02 / 0.03	-0.34 / -0.02
5	GUA+AN	~~8.1 × 10^{-3}~~0.57 ± 0.03~~7.62 × 10^{-5}~~	23 ± 1	9	POS: 0.35 / NEG: 0.38	0.99 / 1.01	0.16 / 0.05	0.19 / -0.08

[a]The data fitting was performed in the initial linear region. Each value is the average of results from triplicate experiments, corrected for internal light screening due to DMB, VL, and AN, and normalized to the experimental photon flux. Errors represent one standard deviation. [b]The normalized product abundance was calculated using the data from UHPLC-HESI-Orbitrap-MS in the positive (POS) ion mode as the GUA signal from the negative (NEG) ion mode was weak, which may introduce significant uncertainties during normalization. The uncertainties were propagated from the changes in [GUA] measured using UHPLC-PDA and the MS signal intensities. The samples for experiments without AN (marked with NA) were not analyzed for N-containing compounds. [c]The average elemental ratios ($\langle O{:}C \rangle$, $\langle H{:}C \rangle$, and $\langle N{:}C \rangle$) and $\langle OS_C \rangle$ were

929 based on the UHPLC-HESI-Orbitrap-MS results and estimated using the signal-weighted method (Bateman et al., 2012).

930 The {OS_C} of GUA, DMB, and VL are -0.57, -0.44, and -0.25, respectively.

931

932

933

934

935

936

937

938

939

940
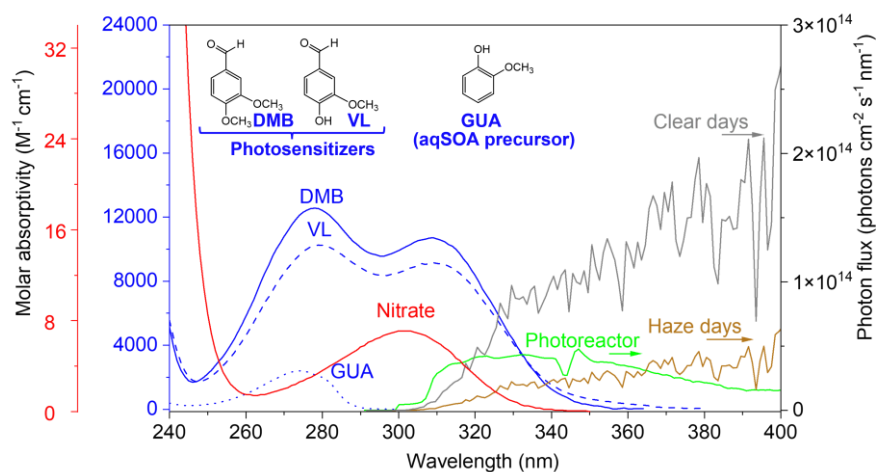
949 **Figure 1.** The base-10 molar absorptivities (M^{-1} cm^{-1}) of 3,4-dimethoxybenzaldehyde (DMB, blue solid line), vanillin (VL, blue dashed line), guaiacol (GUA, blue dotted line), and nitrate (red solid line). The green line is the photon flux in the aqueous photoreactor. The gray and brown lines are the photon fluxes on typical clear andor haze days, respectively, in Beijing, China (Mabato et al., 2022). The top of the figure also shows the structures of DMB, VL, and GUA.
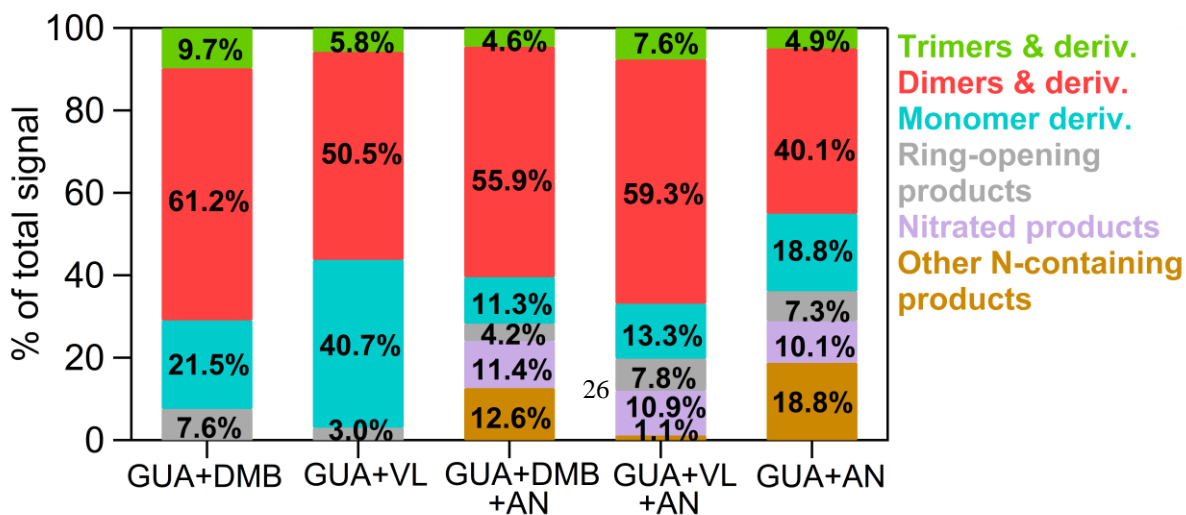
953 **Figure 2.** Signal-weighted distributions of aqSOA from GUA+DMB, GUA+VL, GUA+DMB+AN, GUA+VL+AN, and

954 GUA+AN. These product distributions were calculated from combined UHPLC-HESI-Orbitrap-MS data obtained in positive

955 (POS) and negative (NEG) ion modes. The values indicate the contribution of different product classifications to the total

956 signals for each reaction condition.

957
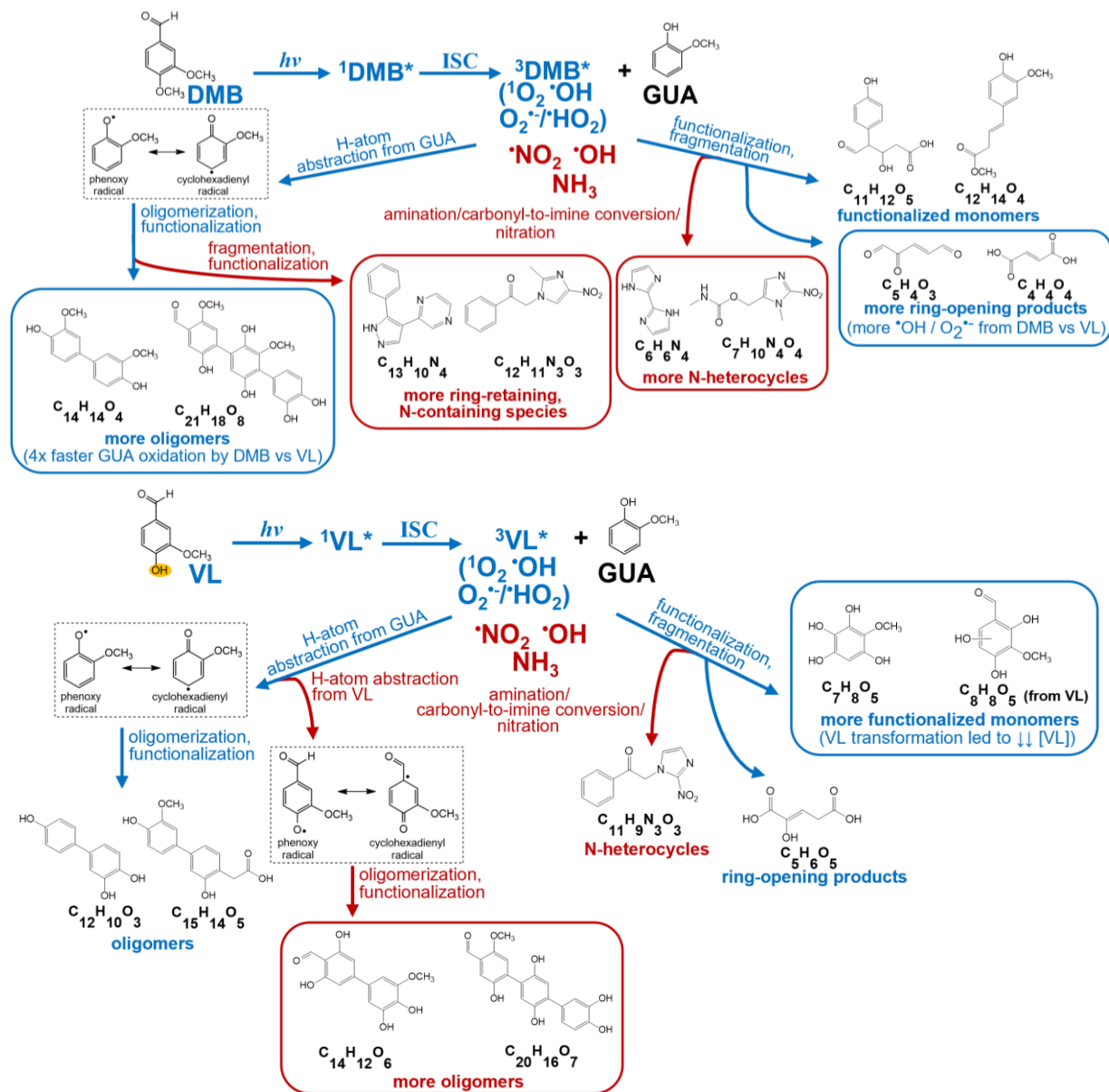
Figure 3. Summary of the main differences between photosensitized GUA oxidation by ^{3}DMB* (top) and ^{3}VL* (bottom) in the absence (blue labels and boxes) and presence (red labels and boxes) of ammonium nitrate at pH 4 under air-saturated conditions. Boxed structures indicate product classifications with notable differences. DMB and VL absorb light and are promoted to their singlet excited states (^{1}DMB* and ^{1}VL*), which then undergo intersystem crossing (ISC) to form ^{3}DMB* and ^{3}VL*. Secondary oxidants (^{1}O$_2$, O$_2^{\bullet-}$/$^{\bullet}$HO$_2$, $^{\bullet}$OH) can be formed from ^{3}DMB* and ^{3}VL* upon reactions with O$_2$ and GUA (George et al., 2018; Chen et al., 2020; Misovich et al., 2021; Mabato et al., 2022). The structures shown are examples of the major products (Tables S1 to S4) for different product classifications.

28

965
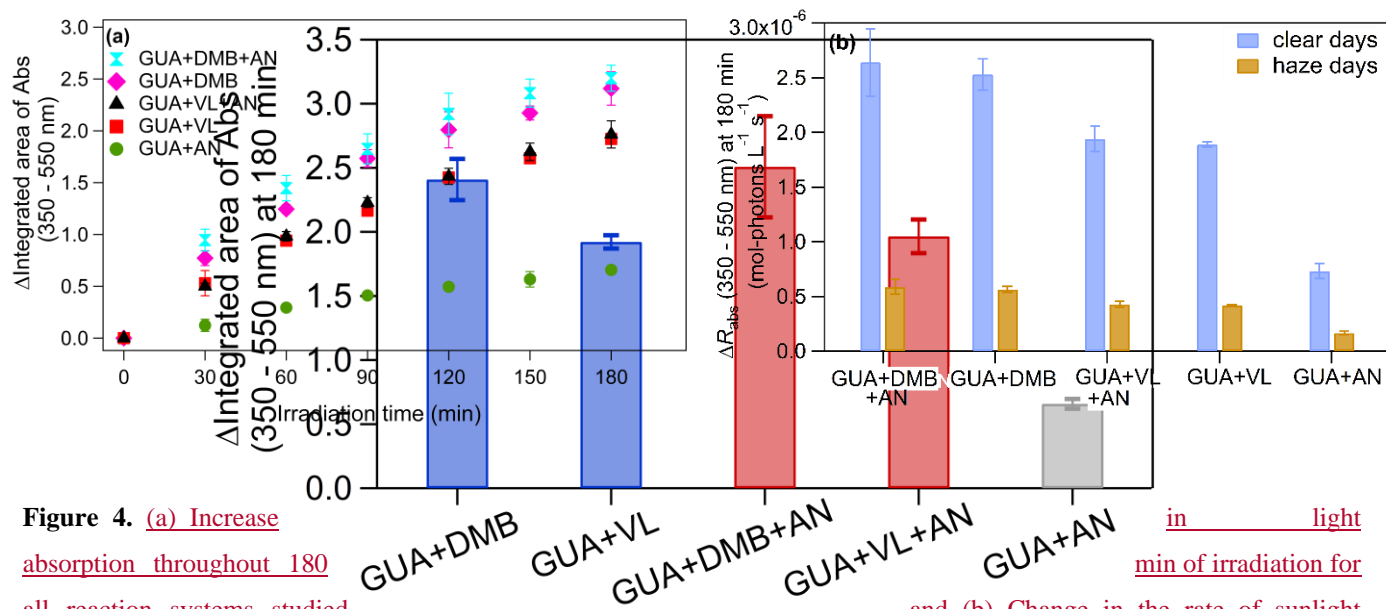
966
967
968

969 **Figure 4.** (a) Increase
970 absorption throughout 180
971 all reaction systems studied
972 absorption (ΔR_{abs}) from 350-550 nm at 180 min during typical clear and haze days in Beijing, China for aqSOA from
973 GUA+DMB+AN, GUA+DMB, GUA+VL+AN, GUA+VL, and GUA+AN. ~~Increase in visible light absorption for~~
974 ~~aqSOA from GUA+DMB, GUA+VL, GUA+DMB+AN, and GUA+VL+AN.~~ Error bars represent one
975 standard deviation of triplicate experiments.

976

in   light
min of irradiation for
and (b) Change in the rate of sunlight

Supplementary material

Comparison of ~~aA~~queous SOA product distributions ~~formation~~ from ~~photosensitized~~ guaiacol oxidation by: ~~Comparison between~~ non-phenolic and phenolic methoxybenzaldehydes as photosensitizers in the absence and presence of ammonium nitrate

Beatrix Rosette Go Mabato[1,2], Yong Jie Li[3], Dan Dan Huang[4], Yalin Wang[3], and Chak K. Chan[1,2]*

[1]School of Energy and Environment, City University of Hong Kong, Hong Kong, China

[2]City University of Hong Kong Shenzhen Research Institute, Shenzhen, China

[3]Department of Civil and Environmental Engineering, and Centre for Regional Ocean,

Faculty of Science and Technology, University of Macau, Macau, China

[4]Shanghai Academy of Environmental Sciences, Shanghai 200233, China

Correspondence to: Chak K. Chan (Chak.K.Chan@cityu.edu.hk)

32

Section S1. UHPLC-PDA analyses

An ultra-high performance liquid chromatography system (UHPLC, Waters Acquity H-Class, Waters, Milford, USA) coupled to a photodiode array (PDA) detector (Waters, Milford, USA) was used for the quantification of GUA, DMB, and VL concentrations. The samples were first filtered through a 0.2 μm Chromafil® Xtra PTFE filter (Macherey-Nagel GmbH & Co. KG, Germany). The separation of products was conducted using an Acquity HSS T3 column (1.8 μm, 2.1 mm × 100 mm; Waters Corp.). The column oven was held at 30 °C, and the autosampler was cooled at 4 °C. The injection volume was set to 5 μL. The binary mobile phase was composed of water (A) and acetonitrile (B). The gradient elution was performed at a flow rate of 0.2 mL/min: 0–1 min, 10% eluent B; 1–25 min, linear increase to 90% eluent B; 25–29.9 min, hold 90% eluent B; 29.9–30 min, decrease to 10% eluent B; 30–35 min, re-equilibrate at 10% eluent B for 5 min. GUA, DMB, and VL were analyzed using the channels with UV absorption at 274, 274, and 300 nm, respectively.

Section S2. UHPLC-HESI-Orbitrap-MS analyses

A Thermo Orbitrap Fusion Lumos Mass Spectrometry (Thermo Fisher Scientific, Waltham, MA, USA) connected to a Thermo Scientific UltiMate 3000 UHPLC system (Thermo Fisher Scientific, Waltham, MA, USA) via heated electrospray ionization (HESI) as the interface (UHPLC-HESI-Orbitrap-MS) was used to characterize the reaction products. The mobile phases used were 0.1% (v/v) formic acid (in milli-Q water) (A) and acetonitrile (B). The same settings (e.g., column, gradient, oven temperature) used in the UHPLC-PDA (Sect. S1) were applied in the UHPLC-HESI-Orbitrap-MS system. The HESI-MS spectra were acquired in both positive and negative ion modes. The HESI parameters were as follows: Spray voltage, 2500 V for both positive and negative HESI; sheath gas, 35 arbitrary units; nebulizer auxiliary gas, 10 arbitrary units; sweep gas, 3 arbitrary units. General instrumental parameters were set as follows: ion transfer tube temperature, 320 °C; vaporizer temperature, 350 °C. The mass

range for full scan MS was set at 50-1000 m/z with a mass resolution of 60,000 at 200 m/z. The automatic gain control (AGC) target was 4.0×10^5 with a maximum injection time of 50 ms. The UHPLC-HESI-Orbitrap-MS data obtained in positive and negative ion modes were pretreated using Progenesis QI (version 2.4; Nonlinear Dynamics) for peak picking and alignment. Most peaks detected in the blank (~99% for all experiments) were excluded from the samples except for peaks with a minimum of 2.5 times greater intensity in the sample spectrum than in the blank (Laskin et al., 2014). In addition, a peak was considered a product if the difference in the peak area between the samples before and after irradiation is ≥10 times. In this work, two independently prepared samples for each reaction condition were analyzed using the UHPLC-HESI-Orbitrap-MS. Only peaks that were reproducibly detected in both sets of samples were retained. The formula assignments were carried out using the MIDAS molecular formula calculator (http://magnet.fsu.edu/~midas/) with the following constraints: C ≤100, H ≤150, O ≤30, and N ≤10, and mass error of 10 ppm. The nitrogen atom was excluded in the constraints for experiments without AN. The ChemSpider database (Royal Society of Chemistry) was also queried to return valid molecules that may be useful for proposing product structures. Overall, the proposed structures in this work are based on the molecular formulas, DBE values, and structural and mechanistic information provided in earlier similar works on methoxyphenols (Yee et al., 2013; Li et al., 2014; Yu et al., 2014, 2016; He et al., 2019; Chen et al., 2020; Jiang et al., 2021; Misovich et al., 2021; Mabato et al., 2022). For clarity, the formulas discussed in this work correspond to neutral analytes (e.g., with H^+ or NH_4^+ removed from the ion formula).

The double bond equivalent (DBE) values (Koch and Dittmar, 2006) and carbon oxidation state (OS_C; Kroll et al., 2011, 2015; Lv et al., 2016) of the neutral formulas were calculated using the following equations:

83    $DBE = C - H/2 + N/2 + 1$ (Eq. S1)

84    $OS_C = 2 \times O/C + 3 \times N/C - H/C$ (Eq. S2)

85   where C, H, O, and N correspond to the number of carbon, hydrogen, oxygen, and nitrogen

86   atoms in the neutral formula. Moreover, the average oxygen to carbon (O:C) ratios, $\langle O:C \rangle$:

87    $(\langle O:C \rangle = \sum_i (\text{abundance}_i) O_i / \sum_i (\text{abundance}_i) C_i)$, average nitrogen to carbon (N:C) ratios,

88    $\langle N:C \rangle$: $(\langle N:C \rangle = \sum_i (\text{abundance}_i) N_i / \sum_i (\text{abundance}_i) C_i)$, and average hydrogen to carbon

89   (H:C) ratios, $\langle H:C \rangle$: $(\langle H:C \rangle = \sum_i (\text{abundance}_i) H_i / \sum_i (\text{abundance}_i) C_i)$ after the reactions

90   were further estimated using the signal-weighted method (Bateman et al., 2012). The average

91   OS_C, $\langle OS_C \rangle$ was also calculated as follows:

92    $\langle OS_C \rangle = 2 \times \langle O:C \rangle + 3 \times \langle N:C \rangle - \langle H:C \rangle$ (Eq. S3)

93   **Section S3. IC analyses of small organic acids**

94   An ion chromatography system (IC, Dionex ICS-1100, Sunnyvale, CA) equipped with a

95   Dionex AS-DV autosampler (Sunnyvale, CA) enabled the analyses of small organic acids. The

96   separation was achieved using an IonPac^{TM} AS11 column (4 $\times$ 250 mm) with an IonPac^{TM}

97   AG11 guard column (4 $\times$ 50 mm). The isocratic elution was applied at a 1.0 mL/min flow rate

98   with 12 mM sodium hydroxide (NaOH) as the eluent. The total run time was set at 10 min. The

99   standard solutions (1–50 μM) of formic, succinic, and oxalic acid were analyzed three times

100   along with the samples and water blank. Formic, succinic, and oxalic acid had retention times

101   of 1.9 min, 3.7 min, and 5.9 min, respectively.

102   **Section S4. UV-Vis spectrophotometric analyses**

103   A UV-Vis spectrophotometer (UV-3600, Shimadzu Corp., Japan) was used to measure the

104   absorbance changes for the samples. The absorbance values from 200 to 700 nm were measured

105   instantly after sample collection, and measurements were done in triplicate. The change in the

106   integrated area of absorbance from 350 to 550 nm was used to represent the absorbance

107   enhancements. The increase of light absorption at this wavelength range, where GUA, DMB,

108   and VL did not initially absorb light, suggests the formation of light-absorbing products (Smith

109   et al., 2016).

110   **Section S5. Further discussions on van Krevelen diagrams and OS_c vs. n_C plots for**

111   **GUA+DMB and GUA+VL aqSOA**

112   Consistent with the higher contribution of ring-opening species, GUA+DMB had more

113   products with H:C ≥1.5 and O:C ≤0.5 (Fig. S54a–b), possibly due to more oxygenated aliphatic

114   species. GUA+VL (Fig. S54c–d) also had high-relative-abundance products with H:C of ~1

115   and O:C ≥0.5. Similar to our previous work (0.1 mM GUA + 0.1 mM VL; Mabato et al., 2022),

116   the two high-relative-abundance species with O:C ≥0.5 were associated with hydroxylated

117   products ($C_7H_8O_4$ and $C_8H_8O_5$, #28 and 35; Table S2) that were also observed in earlier works

118   on $^3DMB^*$ and $^•OH$-mediated oxidation (Yu et al., 2014, 2016). These hydroxylated products

119   were also present in GUA+DMB but with lower relative abundance. Triplet-mediated phenol

120   oxidation can generate H_2O_2 (Anastasio et al., 1997), a photolytic source of $^•OH$. Indeed,

121   hydroxylation is significant in aqueous-phase phenol oxidation (Li et al., 2014; Yu et al., 2014,

122   2016; Chen et al., 2020; Jiang et al., 2021; Misovich et al., 2021; Mabato et al., 2022).

123   The OS_C vs. n_C plots for both GUA+DMB and GUA+VL display high-relative-

124   abundance species clustered at n_C of 12 to 15 and OS_C >-1, which can be ascribed to dimers

125   and derivatives (Fig. S65a–d). The species with n_C >15 had the highest DBE values and can be

126   attributed to trimers. These compounds were more abundant in GUA+DMB, likely due to the

127   greater extent of photosensitized reactions by $^3DMB^*$ compared to $^3VL^*$. Indeed,

128   oligomerization is an important process in aqSOA formation via triplet-mediated oxidation (Yu

129   et al., 2014, 2016; Chen et al., 2020; Jiang et al., 2021; Misovich et al., 2021; Mabato et al.,

130   2022). As indicated by the higher quantity of low DBE species, ring-opening and fragmentation

131   pathways were more extensive in GUA+DMB. In GUA+VL, there were also high-relative-

132   abundance products with n_C <10, OS_C ≥0, and DBE <5, corresponding to the hydroxylated

133   products mentioned earlier.

134   **Section S6. Estimation of the apparent quantum efficiency of guaiacol photodegradation**

135   The apparent quantum efficiency of GUA photodegradation (φ_{GUA}) in the presence of DMB,

136   VL, or nitrate during simulated sunlight illumination can be defined as (Anastasio et al., 1997;

137   Smith et al., 2014, 2016):

138    $$\Phi_{GUA} = \frac{\text{mol GUA destroyed}}{\text{mol photons absorbed}}$$ (Eq. S4)

139   Φ_{GUA} was calculated using the measured rate of GUA decay and rate of light absorption by

140   DMB, VL, or nitrate through the following equation:

141    $$\Phi_{GUA} = \frac{\text{rate of GUA decay}}{\text{rate of light absorption by DMB or VL or nitrate}} = \frac{k\prime_{GUA} \times [GUA]}{\sum[(1-10^{-\varepsilon_\lambda[C]l}) \times I'_\lambda]}$$ (Eq. S5)

142   where $k\prime_{GUA}$ is the pseudo-first-order rate constant for GUA decay, [GUA] is the concentration

143   of GUA (M), ε_λ is the base-10 molar absorptivity (M^{-1} cm^{-1}) of DMB, VL, or nitrate at

144   wavelength λ, [C] is the concentration of DMB, VL, or nitrate (M), l is the pathlength of the

145   illumination cell (cm), and I'_λ is the volume-averaged photon flux (mol-photons L^{-1} s^{-1} nm^{-1})

146   determined from 2NB actinometry:

147    $$j(2NB) = 2.303 \times \Phi_{2NB} \times l \times \Sigma_{300\ nm}^{350\ nm}(\varepsilon_{2NB,\lambda} \times I'_\lambda \times \Delta\lambda)$$ (Eq. S6)

148   where j(2NB) is the decay rate constant of 2-nitrobenzaldehyde (2NB), the chemical

149   actinometer used to determine the photon flux in the aqueous photoreactor, $\Phi_{2NB,\lambda}$ and $\varepsilon_{2NB,\lambda}$

150   are the quantum yield (molecule $photon^{-1}$) and base-10 molar absorptivity (M^{-1} cm^{-1}) for 2NB,

151   respectively, and Δλ is the wavelength interval between actinic flux data points (nm).

152   **Section S7. Further discussions on van Krevelen diagrams and OS_c vs. n_C plots for**

153   **GUA+DMB+AN, GUA+VL+AN, and GUA+AN aqSOA**

154   The position of the CHO, CHON, and CHN species in the van Krevelen diagrams for

155   GUA+DMB+AN and GUA+VL+AN broadly resembled those of CHO species in the absence

156 of AN (Fig. S5~4~). The CHON species for GUA+DMB+AN and GUA+VL+AN mostly had

157 O:C ratios <0.7, consistent with previous studies on BBOA e.g., wheat straw burning in K-

158 Puszta in the Great Hungarian Plain of Hungary, biomass burning at Canadian rural sites such

159 as Saint Anicet, and BBOA from Amazonia (Schmitt-Kopplin et al., 2010; Claeys et al., 2012;

160 Kourtchev et al., 2017).

161   The CHN species in GUA+DMB+AN and GUA+VL+AN appeared to have analogous

162 H:C ratios. GUA+DMB+AN had ~2 times more CHON and CHN species than GUA+VL+AN,

163 and there were more of these species with higher abundance in the former, indicating a greater

164 extent of reactions with AN. The high-relative-abundance products for GUA+DMB+AN and

165 GUA+VL+AN were similar to those in the absence of AN, except the hydroxylated products

166 (e.g., $C_7H_8O_4$; #28; Table S2) previously mentioned for GUA+VL. Among the high-relative-

167 abundance products for GUA+DMB+AN was a CHN species with H:C of ~0.8. For

168 GUA+VL+AN, the high-relative-abundance products include two CHON species with O:C

169 and H:C ratios of 0.3-0.6 and 0.6-0.8. The major difference between GUA+AN and

170 GUA+DMB+AN/GUA+VL+AN was the presence of more high-relative-abundance CHON

171 and CHN species (Fig. S9~7~) in GUA+AN which can be expected given that AN was the only

172 source of oxidants in this case. Compared to GUA+AN, more species (CHO, CHON, and

173 CHN) were observed for GUA+DMB+AN and GUA+VL+AN, attributable to contributions

174 from both photosensitization and (ammonium) nitrate photolysis.

175   Moreover, GUA+DMB+AN and GUA+VL+AN aqSOA had mainly similar features in

176 the OS_C vs~.~ n_C plots as those observed in the absence of AN (Fig. S6~5~). GUA+DMB+AN and

177 GUA+VL+AN aqSOA also had more CHON and CHN species with higher OS_C, n_C, and DBE

178 (Fig. S6~5~e–h) relative to GUA+AN (Fig. S10~8~), indicating more conjugated N-containing

179 compounds. For GUA+DMB+AN and GUA+VL+AN, the CHON and CHN species had a

180 wider range of OS_C compared to CHO species (Fig. S6~5~e–h). The high-relative-abundance

181   species (n_C of 12 to 15 and OS_C >-1) corresponded to dimers and trimers similar to those noted

182   in the absence of AN, along with some N-containing species. These include a CHN species

183   with n_C of 13, OS_C ~0, and 11 DBE for GUA+DMB+AN, and 2 CHON species with n_C of 5

184   and 11, OS_C of 2.5 and 1, and 6 and 9 DBE for GUA+VL+AN.

185

186

187
188
189
190
191
192
193
194
195
196
197
198
199
200
201
202
203
204
205
206
207
208
209
210
211
212
213
214
215
216
217
218
219
220
221
222
223
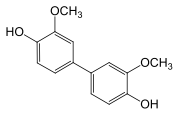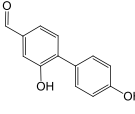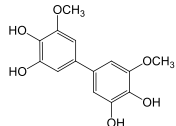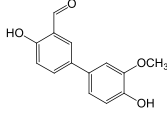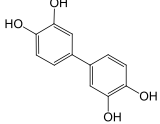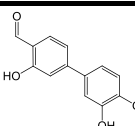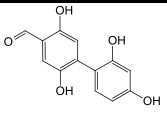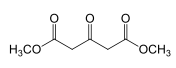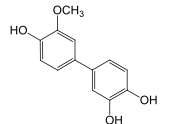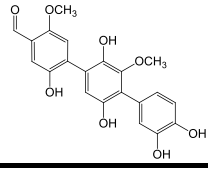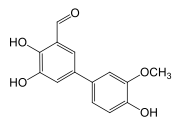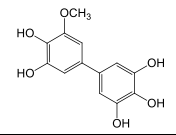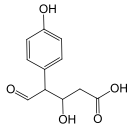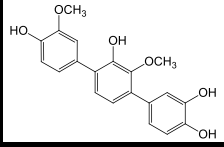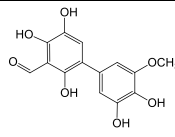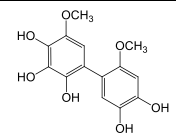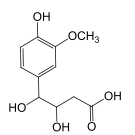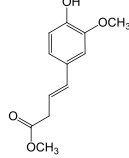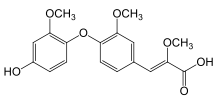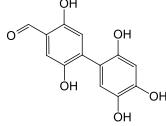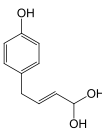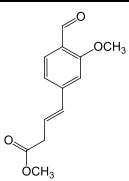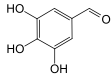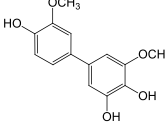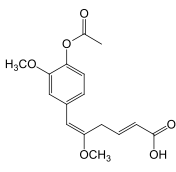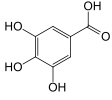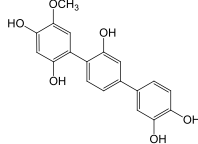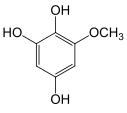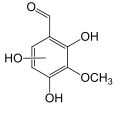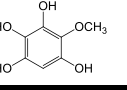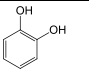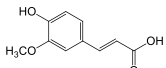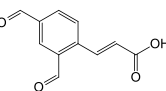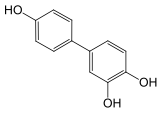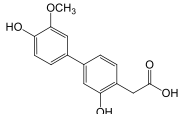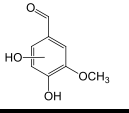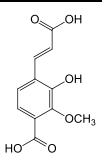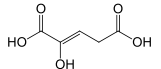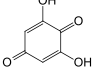
Table S1. Possible structures of the major products detected from GUA+DMB using UHPLC-
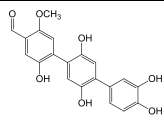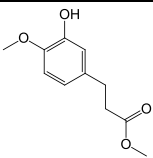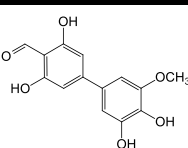HESI-Orbitrap-MS operated in positive (POS) and negative (NEG) ion modes.
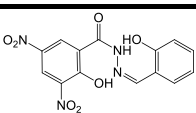
No.	GUA+DMB POS Molecular formula and exact mass	DBE	Possible structure	No.	GUA+DMB NEG Molecular formula and exact mass	DBE	Possible structure
1	$C_{14}H_{14}O_4$ (246.0892)	8			$C_{14}H_{14}O_4$ (246.0892) (No. 1; GUA+DMB POS)		
2	$C_{13}H_{10}O_3$ (214.0630)	9		16	$C_{14}H_{14}O_6$ (278.0790)	8	
3	$C_{14}H_{12}O_4$ (244.0736)	9		17	$C_{12}H_{10}O_4$ (218.0579)	8	
4	$C_{13}H_{10}O_4$ (230.0579)	9			$C_{13}H_{12}O_4$ (232.0736) (No. 6; GUA+DMB POS)		
5	$C_{13}H_{10}O_5$ (246.0528)	9		18	$C_7H_{10}O_5$ (174.0528)	3	
6	$C_{13}H_{12}O_4$ (232.0736)	8		19	$C_{21}H_{18}O_8$ (398.1002)	13	
7	$C_{14}H_{12}O_5$ (260.0685)	9		20	$C_{13}H_{12}O_6$ (264.0634)	8	
8	$C_{11}H_{12}O_5$ (224.0685)	6		21	$C_{20}H_{18}O_6$ (354.1103)	12	
9	$C_{14}H_{12}O_7$ (292.0583)	9		22	$C_{14}H_{14}O_7$ (294.0740)	8	
10	$C_{11}H_{14}O_6$ (242.0790)	5		23	$C_{12}H_{14}O_4$ (222.0892)	6	

11	$C_{18}H_{18}O_7$ (346.1053)	10		24	$C_{13}H_{10}O_6$ (262.0477)	9	
12	$C_{10}H_{12}O_3$ (180.0786)	5		25	$C_{13}H_{14}O_4$ (234.0892)	7	
13	$C_7H_6O_4$ (154.0266)	5		26	$C_{14}H_{14}O_5$ (262.0841)	8	
14	$C_{16}H_{18}O_6$ (306.1103)	8		$C_{13}H_{10}O_5$ (246.0528) (No. 5; GUA+DMB POS)			
15	$C_7H_6O_5$ (170.0215)	5		27	$C_{19}H_{16}O_6$ (340.0947)	12	
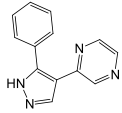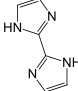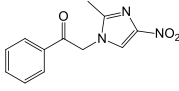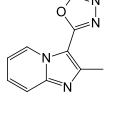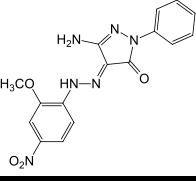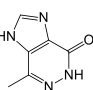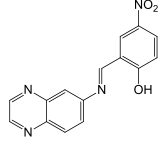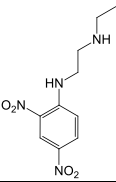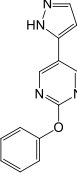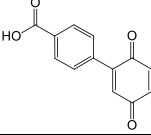
227
228
229
230
231
232
233
234
235
236
237
238
239
240
241
242
243
244
245
246
247
248
249
250
251
252

253 **Table S2**. Possible structures of the major products detected from GUA+VL using UHPLC-
254 HESI- Orbitrap-MS operated in positive (POS) and negative (NEG) ion modes.
255
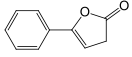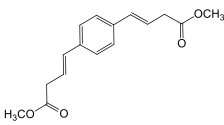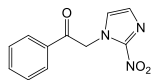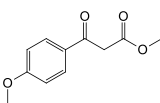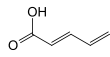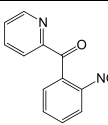
No.	GUA+VL POS Molecular formula and exact mass	DBE	Possible structure	No.	GUA+VL NEG Molecular formula and exact mass	DBE	Possible structure
28	$C_7H_8O_4$ (156.0423)	4		35	$C_8H_8O_5$ (184.0372)	5	
$C_{13}H_{10}O_4$ (230.0579) (No. 4; GUA+DMB, Table S1)				$C_{13}H_{12}O_4$ (232.0736) (No. 6; GUA+DMB, Table S1)			
$C_{13}H_{12}O_4$ (232.0736) (No. 6; GUA+DMB, Table S1)				$C_{14}H_{14}O_4$ (246.0892) (No. 1; GUA+DMB, Table S1)			
$C_{13}H_{10}O_5$ (246.0528) (No. 5; GUA+DMB, Table S1)				$C_{14}H_{14}O_6$ (278.0790) (No. 16; GUA+DMB, Table S1)			
29	$C_7H_8O_5$ (172.0372)	4		$C_{20}H_{18}O_6$ (354.1103) (No. 21; GUA+DMB, Table S1)			
30	$C_6H_6O_2$ (110.0368)	4		$C_{12}H_{10}O_4$ (218.0579) (No. 17; GUA+DMB, Table S1)			
31	$C_{10}H_{10}O_4$ (194.0579)	6		$C_6H_6O_2$ (110.0368) (No. 30; GUA+VL POS)			
32	$C_{11}H_8O_4$ (204.0423)	8		$C_7H_{10}O_5$ (174.0528) (No. 18; GUA+DMB, Table S1)			
33	$C_{12}H_{10}O_3$ (202.0630)	8		36	$C_{15}H_{14}O_5$ (274.0841)	9	
$C_{14}H_{12}O_5$ (260.0685) (No. 7; GUA+DMB, Table S1)				$C_{13}H_{12}O_6$ (264.0634) (No. 20; GUA+DMB, Table S1)			
$C_{13}H_{14}O_4$ (234.0892) (No. 25; GUA+DMB, Table S1)				37	$C_8H_8O_4$ (168.0423)	5	
34	$C_{11}H_{10}O_6$ (238.0477)	7		$C_{19}H_{16}O_6$ (340.0947) (No. 27; GUA+DMB, Table S1)			
$C_{13}H_{10}O_6$ (262.0477) (No. 24; GUA+DMB, Table S1)				$C_{11}H_{10}O_6$ (238.0477) (No. 34; GUA+VL POS)			
$C_{13}H_{12}O_6$ (264.0634) (No. 20; GUA+DMB, Table S1)				38	$C_5H_6O_5$ (146.0215)	3	
$C_7H_6O_4$ (154.0266) (No. 13; GUA+DMB, Table S1)				39	$C_6H_4O_4$ (140.0110)	5	

256

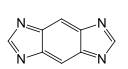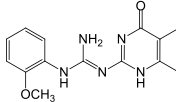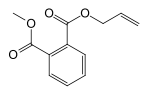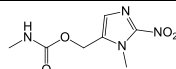| No.	GUA+DMB+AN POS Molecular formula and exact mass	DBE	Possible structure	No.	GUA+DMB +AN NEG Molecular formula and exact mass	DBE	Possible structure
C$_{14}$H$_{14}$O$_4$ (246.0892) (No. 1; GUA+DMB, Table S1)				C$_{13}$H$_{12}$O$_4$ (232.0736) (No. 6; GUA+DMB, Table S1)			
40	C$_{13}$H$_{10}$N$_4$ (222.0905)	11			C$_{14}$H$_{14}$O$_6$ (278.0790) (No. 16; GUA+DMB, Table S1)		
C$_{13}$H$_{10}$O$_5$ (246.0528) (No. 5; GUA+DMB, Table S1)				C$_{14}$H$_{14}$O$_4$ (246.0892) (No. 1; GUA+DMB, Table S1)			
C$_{13}$H$_{10}$O$_4$ (230.0579) (No. 4; GUA+DMB, Table S1)				C$_{12}$H$_{10}$O$_4$ (218.0579) (No. 17; GUA+DMB, Table S1)			
41	C$_6$H$_6$N$_4$ (134.0592)	6			C$_{21}$H$_{18}$O$_8$ (398.1002) (No. 19; GUA+DMB, Table S1)		
C$_{13}$H$_{12}$O$_4$ (232.0736) (No. 6; GUA+DMB, Table S1)				C$_7$H$_{10}$O$_5$ (174.0528) (No. 18; GUA+DMB, Table S1)			
42	C$_{12}$H$_{11}$N$_3$O$_3$ (245.0800)	9			C$_{13}$H$_{12}$O$_6$ (264.0634) (No. 20; GUA+DMB, Table S1)		
43	C$_{10}$H$_8$N$_4$O (200.0698)	9		48	C$_{16}$H$_{14}$N$_6$O$_4$ (354.1076)	13	
44	C$_6$H$_6$N$_4$O (150.0542)	6		49	C$_{15}$H$_{10}$N$_4$O$_3$ (294.0753)	13	
45	C$_{10}$H$_{14}$N$_4$O$_4$ (245.1015)	6			C$_{13}$H$_{10}$O$_6$ (262.0477) (No. 24; GUA+DMB, Table S1)		
46	C$_{13}$H$_{10}$N$_4$O (238.0855)	11			C$_{10}$H$_{10}$O$_4$ (194.0579) (No. 31; GUA+VL, Table S2)		
C$_{13}$H$_{12}$O$_6$ (264.0634) (No. 20; GUA+DMB, Table S1)				C$_7$H$_8$O$_4$ (156.0423) (No. 28; GUA+VL, Table S2)			
C$_7$H$_6$O$_4$ (154.0266) (No. 13; GUA+DMB, Table S1)				C$_{13}$H$_{14}$O$_4$ (234.0892) (No. 25; GUA+DMB, Table S1)			
C$_{12}$H$_{10}$O$_3$ (202.0630) (No. 33; GUA+VL, Table S2)				C$_{13}$H$_{10}$O$_5$ (246.0528) (No. 5; GUA+DMB, Table S1)			
47	C$_{13}$H$_8$O$_4$ (228.0423)	10			C$_{14}$H$_{14}$O$_5$ (262.0841) (No. 26; GUA+DMB, Table S1)		

S12
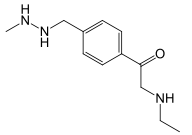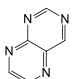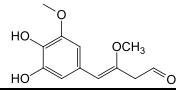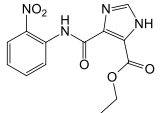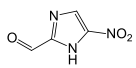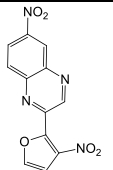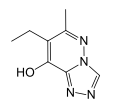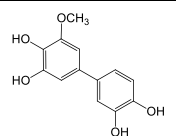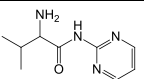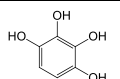
259 **Table S4**. Possible structures of the major products detected from GUA+VL+AN using
260 UHPLC-HESI-Orbitrap-MS operated in positive (POS) and negative (NEG) ion modes.
261

No.	GUA+VL+AN POS Molecular formula and exact mass	DBE	Possible structure	No.	GUA+VL+AN NEG Molecular formula and exact mass	DBE	Possible structure
	$C_{14}H_{14}O_4$ (246.0892) (No. 1; GUA+DMB, Table S1)				$C_{13}H_{12}O_4$ (232.0736) (No. 6; GUA+DMB, Table S1)		
50	$C_{10}H_8O_2$ (160.0524)	7			$C_{14}H_{14}O_6$ (278.0790) (No.16; GUA+DMB, Table S1)		
51	$C_{16}H_{18}O_4$ (274.1205)	8			$C_{12}H_{10}O_4$ (218.0579) (No.17; GUA+DMB, Table S1)		
	$C_{11}H_{12}O_5$ (224.0685) (No. 8; GUA+DMB, Table S1)			57	$C_{11}H_9N_3O_3$ (231.0644)	9	
	$C_{14}H_{12}O_5$ (260.068) (No. 7; GUA+DMB, Table S1)				$C_7H_{10}O_5$ (174.0528) (No.18; GUA+DMB, Table S1)		
	$C_{12}H_{14}O_4$ (222.0892) (No. 23; GUA+DMB, Table S1)				$C_{15}H_{14}O_5$ (274.0841) (No. 36; GUA+VL, Table S2)		
52	$C_{11}H_{12}O_4$ (208.0736)	6			$C_{13}H_{12}O_6$ (264.0634) (No. 20; GUA+DMB, Table S1)		
	$C_6H_6N_4O$ (150.0542) (No. 44; GUA+DMB+AN, Table S3)			58	$C_5H_6O_2$ (98.0368)	3	
	$C_{13}H_{12}O_4$ (232.0736) (No. 6; GUA+DMB, Table S1)				$C_{19}H_{16}O_6$ (340.0947) (No. 27; GUA+DMB, Table S1)		
53	$C_{12}H_8N_2O_3$ (228.0535)	10		59	$C_{20}H_{16}O_7$ (368.0896)	13	
54	$C_{11}H_{14}O_4$ (210.0892)	5			$C_{21}H_{18}O_8$ (398.1002) (No. 19; GUA+DMB, Table S1)		
	$C_7H_6O_4$ (154.0266) (No. 13; GUA+DMB, Table S1)				$C_7H_6O_4$ (154.0266) (No. 13; GUA+DMB, Table S1)		
55	$C_{14}H_{12}O_6$ (276.0634)	9			$C_{15}H_{10}N_4O_3$ (294.0753) (No. 49; GUA+DMB+AN, Table S3)		
56	$C_{14}H_{10}N_4O_7$ (346.0550)	12			$C_{13}H_{10}O_6$ (262.0477) (No. 24; GUA+DMB, Table S1)		
	$C_{13}H_{12}O_6$ (264.0634) (No. 20; GUA+DMB, Table S1)				$C_5H_6O_5$ (146.0215) (No. 38; GUA+VL, Table S2)		

262

263 **Table S5**. Possible structures of the major products detected from GUA+AN using UHPLC-
264 HESI-Orbitrap-MS operated in positive (POS) and negative (NEG) ion modes.
265

No.	GUA+AN POS Molecular formula and exact mass	DBE	Possible structure	No.	GUA+AN NEG Molecular formula and exact mass	DBE	Possible structure
	$C_{13}H_{10}O_4$ (230.0579) (No. 4; GUA+DMB, Table S1)				$C_{14}H_{14}O_6$ (278.0790) (No. 16; GUA+DMB, Table S1)		
	$C_6H_6N_4O$ (150.0542) (No. 44; GUA+DMB+AN, Table S3)			68	$C_{12}H_{19}N_3O$ (221.1528)	5	
	$C_{11}H_{12}O_5$ (224.0685) (No. 8; GUA+DMB, Table S1)				$C_{12}H_{10}O_4$ (218.0579) (No. 17; GUA+DMB, Table S1)		
	$C_7H_8O_4$ (156.0423) (No. 28; GUA+VL, Table S2)				$C_{14}H_{14}O_4$ (246.0892) (No. 1; GUA+DMB, Table S1)		
60	$C_6H_4N_4$ (132.0436)	7			$C_{20}H_{18}O_6$ (354.1103) (No. 21; GUA+DMB, Table S1)		
61	$C_{12}H_{14}O_5$ (238.0841)	6			$C_7H_{10}O_5$ (174.0528 (No. 18; GUA+DMB, Table S1)		
62	$C_{13}H_{12}N_4O_5$ (304.0808)	10		69	$C_4H_3N_3O_3$ (141.0174)	5	
	$C_{13}H_{12}O_6$ (264.0634) (No. 20; GUA+DMB, Table S1)				$C_{13}H_{12}O_6$ (264.0634) (No. 20; GUA+DMB, Table S1)		
	$C_{13}H_{12}O_4$ (232.0736) (No. 6; GUA+DMB, Table S1)			70	$C_{12}H_6N_4O_5$ (286.0338)	12	
63	$C_8H_{10}N_4O$ (178.0855)	6		71	$C_{13}H_{12}O_5$ (248.0685)	8	
64	$C_9H_{14}N_4O$ (194.1168)	5		72	$C_6H_6O_4$ (142.0266)	4	
65	$C_8H_4N_4$ (156.0436)	9			$C_{12}H_{10}O_3$ (202.0630) (No. 33; GUA+VL, Table S2)		
66	$C_{15}H_{19}N_5O_2$ (301.1539)	9		73	$C_{12}H_{12}O_4$ (220.0736)	7	
67	$C_7H_{10}N_4O_4$ (214.0702)	5			$C_7H_6O_5$ (170.0215) (No. 15; GUA+DMB, Table S1)		
	$C_7H_8O_5$ (172.0372) (No. 29; GUA+VL, Table S2)				$C_7H_8O_4$ (156.0423) (No. 28; GUA+VL, Table S2)		
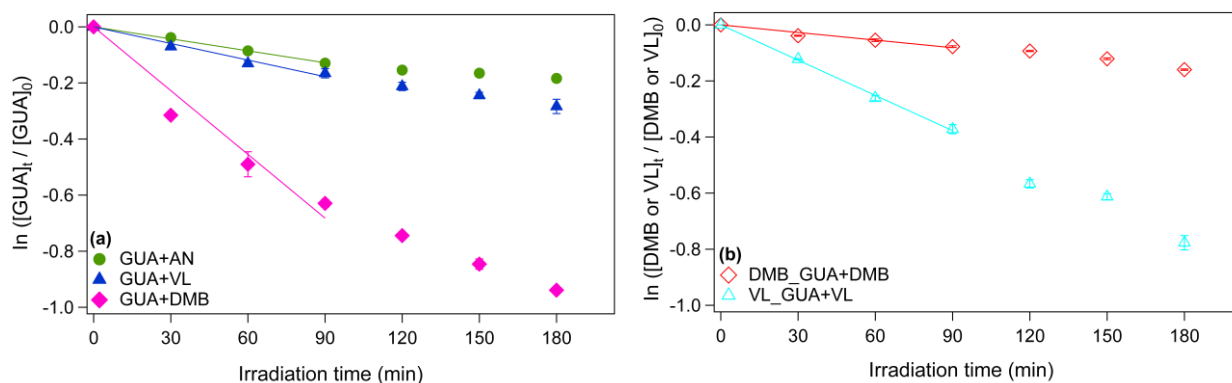
266

Figure S1. (a) The decay of GUA during (ammonium) nitrate-mediated photo-oxidation (GUA+AN) and photosensitized oxidation by $^3VL^*$ (GUA+VL) or $^3DMB^*$ (GUA+DMB). (b) The decay of DMB or VL during GUA photo-oxidation in GUA+DMB and GUA+VL, respectively. No statistically significant difference ($p > 0.05$) was noted between GUA+DMB and GUA+DMB+AN and between GUA+VL and GUA+VL+AN. Error bars represent 1 standard deviation; most error bars are smaller than the markers.

267
268
269
270
271
272
273
274
275
276
277
278
279
280
281
282
283
284
285
286
287
288
289
290
291
292
293
294
295
296
297
298
299
300
301
302
303
304
305

306
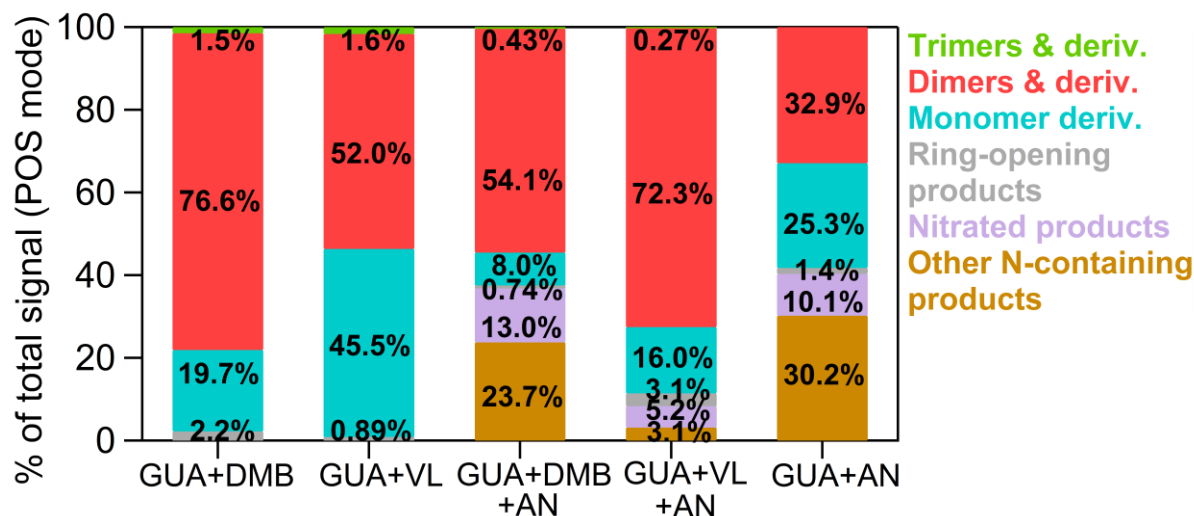
307

308 **Figure S2~~1~~.** Signal-weighted distributions of aqSOA from GUA+DMB, GUA+VL,
309 GUA+DMB+AN, GUA+VL+AN, and GUA+AN. These product distributions were calculated
310 from UHPLC-HESI-Orbitrap-MS data obtained in the positive (POS) ion mode. The values
311 indicate the contribution of different product classifications to the total signals for each reaction
312 condition.
313
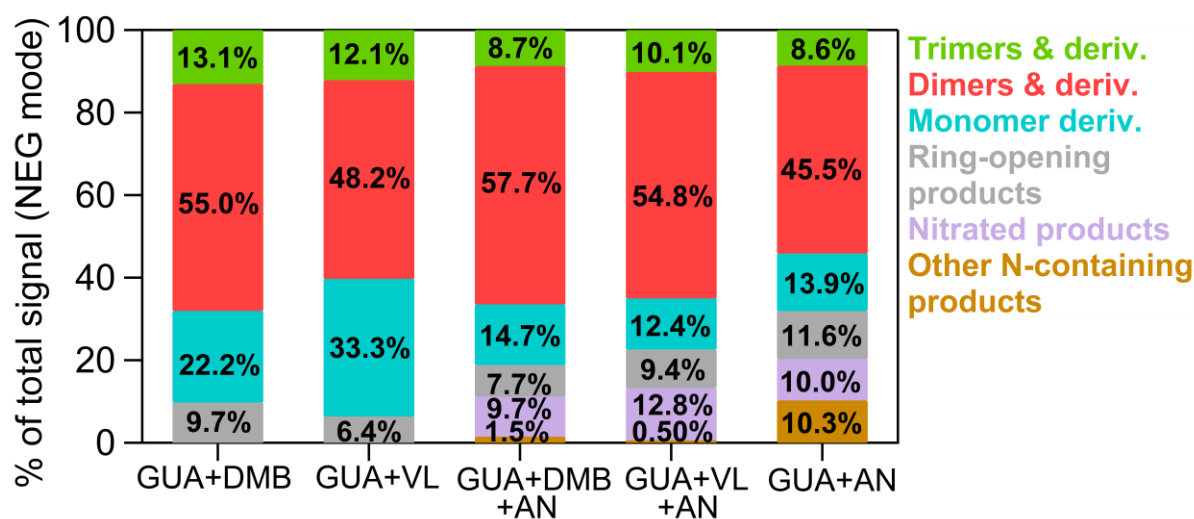
314 **Figure S3~~2~~.** Signal-weighted distributions of aqSOA from GUA+DMB, GUA+VL,
315 GUA+DMB+AN, GUA+VL+AN, and GUA+AN. These product distributions were calculated
316 from UPLC-HESI-Orbitrap-MS data obtained in the negative (NEG) ion mode. The values
317 indicate the contribution of different product classifications to the total signals for each reaction
318 condition.
319
320
321
322
323

324
325
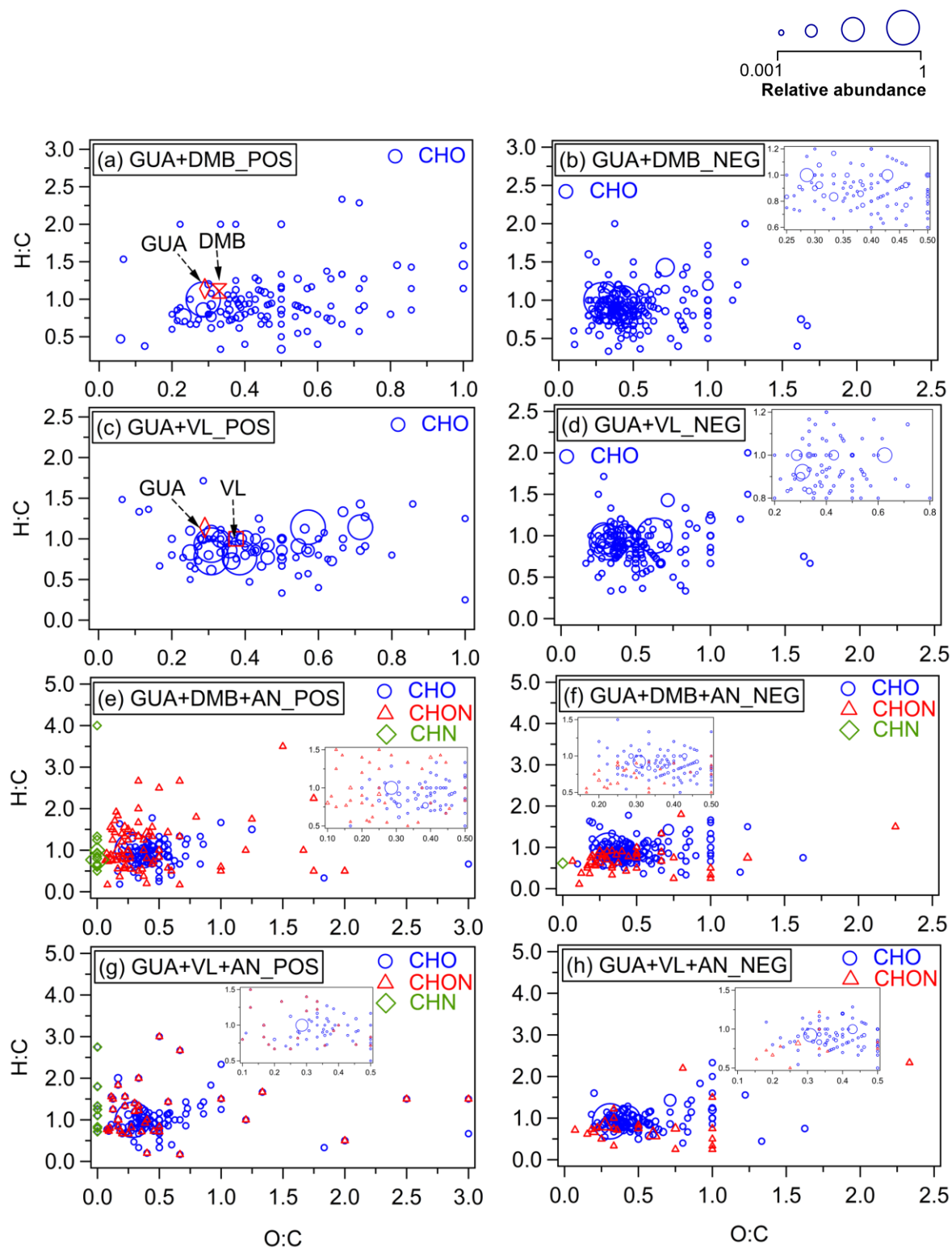326
327
328
329
330
331
332
333
334
335
336
337
338
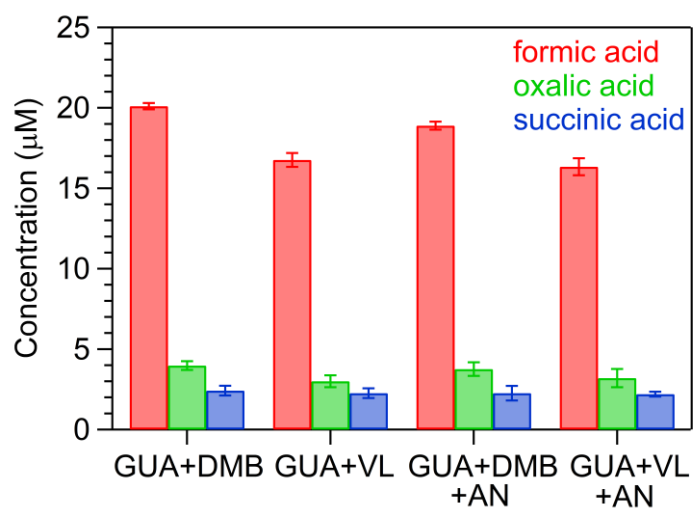
Figure S43. The concentration of formic, oxalic, and succinic acid for GUA+DMB, GUA+VL, GUA+DMB+AN, and GUA+VL+AN aqSOA. Error bars represent one standard deviation of triplicate experiments.

Figure S54. Van Krevelen diagrams of aqSOA from (a, b) GUA+DMB, (c, d) GUA+VL, (e, f) GUA+DMB+AN, and (g, h) GUA+VL+AN for positive (POS) and negative (NEG) ion modes. The blue circle markers indicate CHO classes, red triangle indicate CHON classes, and green diamond indicate CHN classes. The marker size reflects the relative abundance in the sample. The location of GUA, DMB, and VL in the plots are indicated only in panels a and c (red markers). The insets are expanded views of the crowded sections of the van Krevelen diagrams. Note the different scales on the axes.
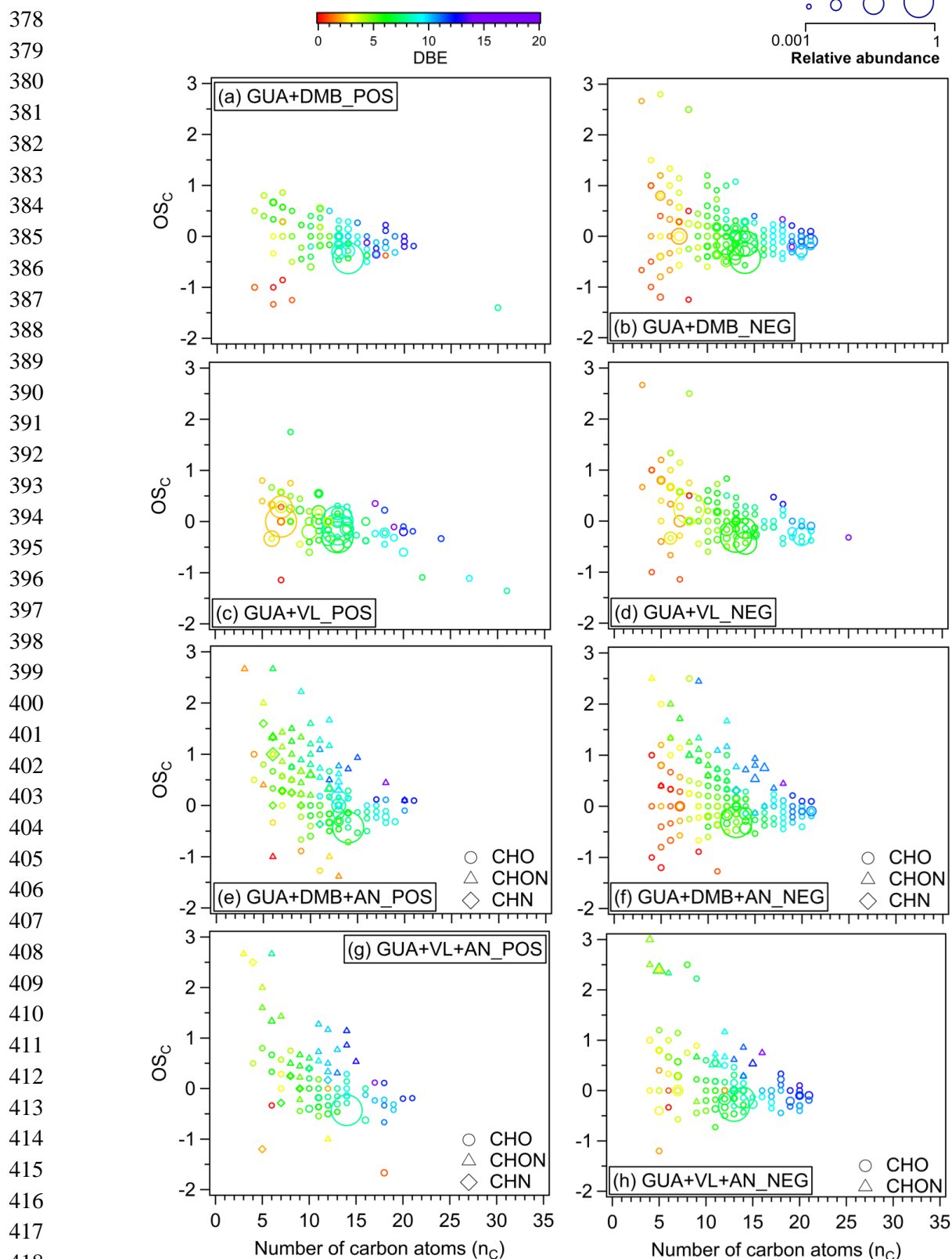
Figure S65. Plots of the carbon oxidation state (OS_C) vs. the number of carbon atoms (n_C) of aqSOA from (a, b) GUA+DMB, (c, d) GUA+VL, (e, f) GUA+DMB+AN, and (g, h) GUA+VL+AN for positive (POS) and negative (NEG) ion modes, colored by the double bond equivalent (DBE) values. The circle, triangle, and diamond markers indicate CHO, CHON and CHN classes, respectively. The marker size reflects the relative abundance in the sample.
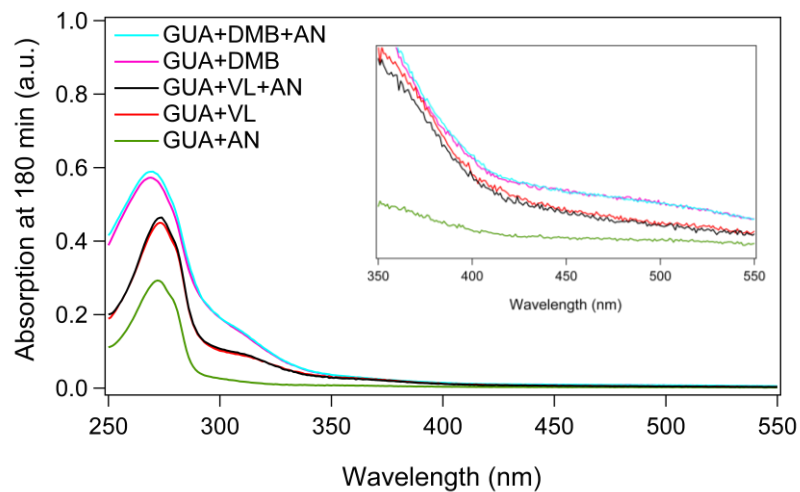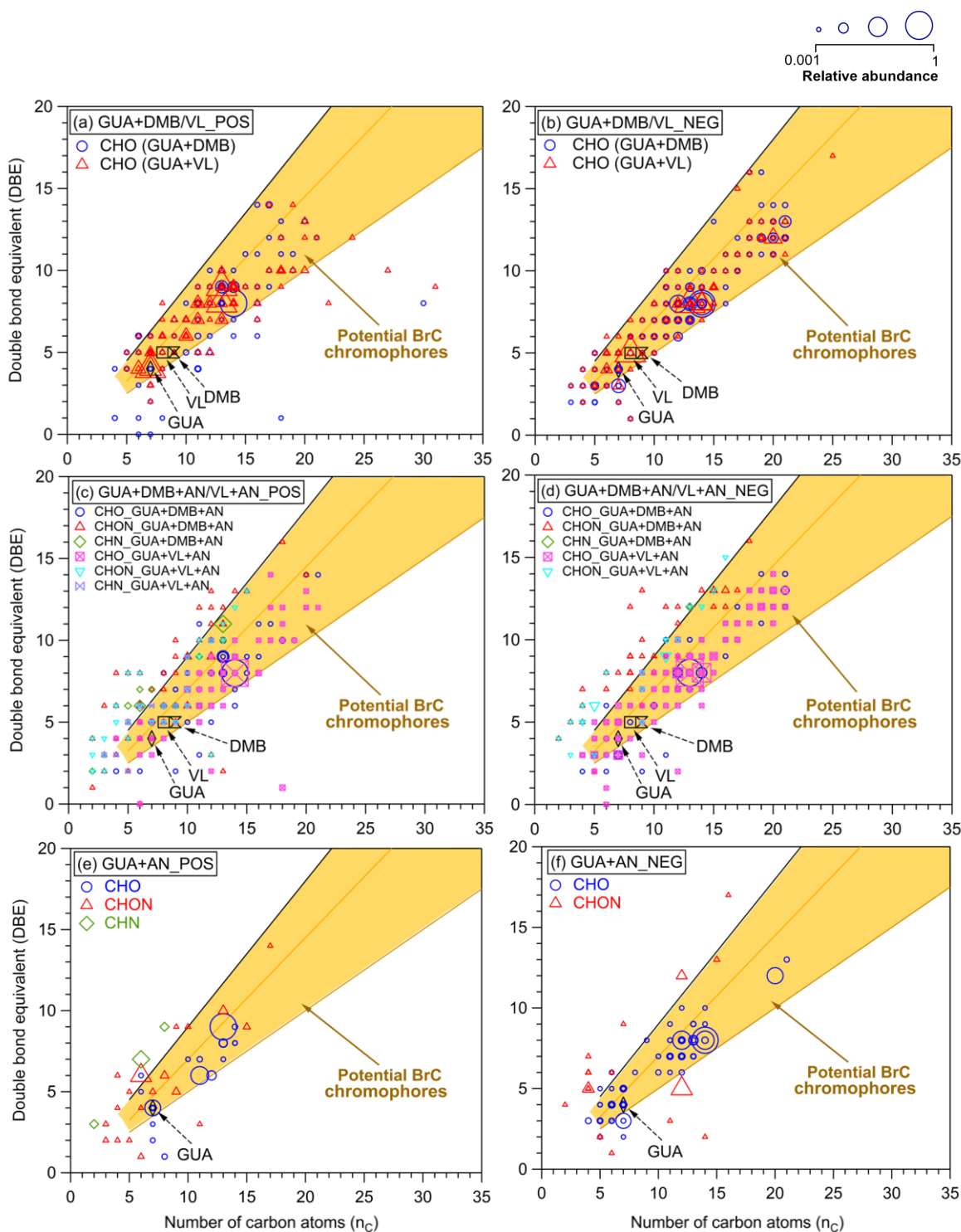
Figure S7. UV-Vis absorption spectra of GUA+DMB+AN, GUA+DMB, GUA+VL+AN, GUA+VL, and GUA+AN after 180 min of irradiation. The inset is the expanded view from 350 to 550 nm.
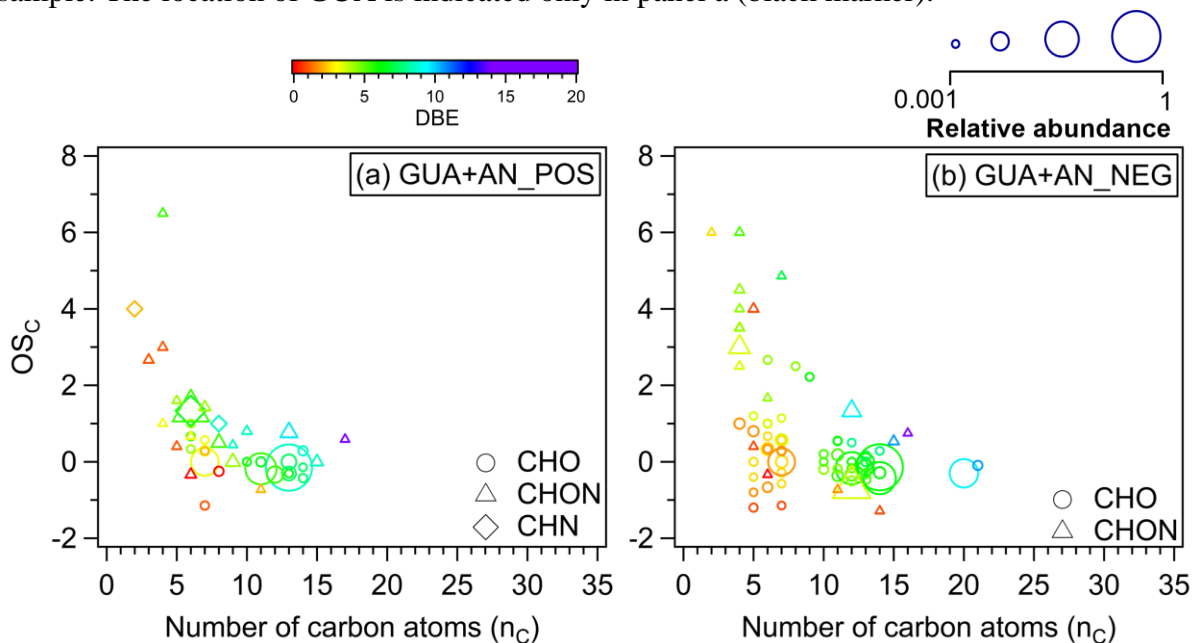
Figure S8. Plots of the double bond equivalent (DBE) values vs. the number of carbon atoms (nc) (Lin et al., 2018) of aqSOA from (a, b) GUA+DMB and GUA+VL, (c, d) GUA+DMB+AN and GUA+VL+AN, and (e, f) GUA+AN for positive (POS) and negative (NEG) ion modes. For a and b, the blue markers indicate CHO classes for GUA+DMB and red indicate CHO classes for GUA+VL. For c and d, the blue markers indicate CHO classes, red indicate CHON classes, and green indicate CHN classes for GUA+DMB+AN; the pink markers indicate CHO classes, cyan indicate CHON classes, and purple indicate CHN classes for GUA+VL+AN. For e and f, the blue markers indicate CHO classes, red indicate CHON classes, and green indicate

451　CHN classes for GUA+AN. The marker size reflects the relative abundance in the sample. The
452　three lines indicate DBE reference values of fullerene-like hydrocarbons (top, black solid line;
453　Lobodin et al, 2012), cata-condensed polycyclic aromatic hydrocarbons (PAHs; Siegmann and
454　Sattler, 2000) (middle, orange solid line), and linear conjugated polyenes (general formula
455　C_xH_{x+2}) (bottom, brown solid line). Species within the shaded area are potential BrC
456　chromophores.
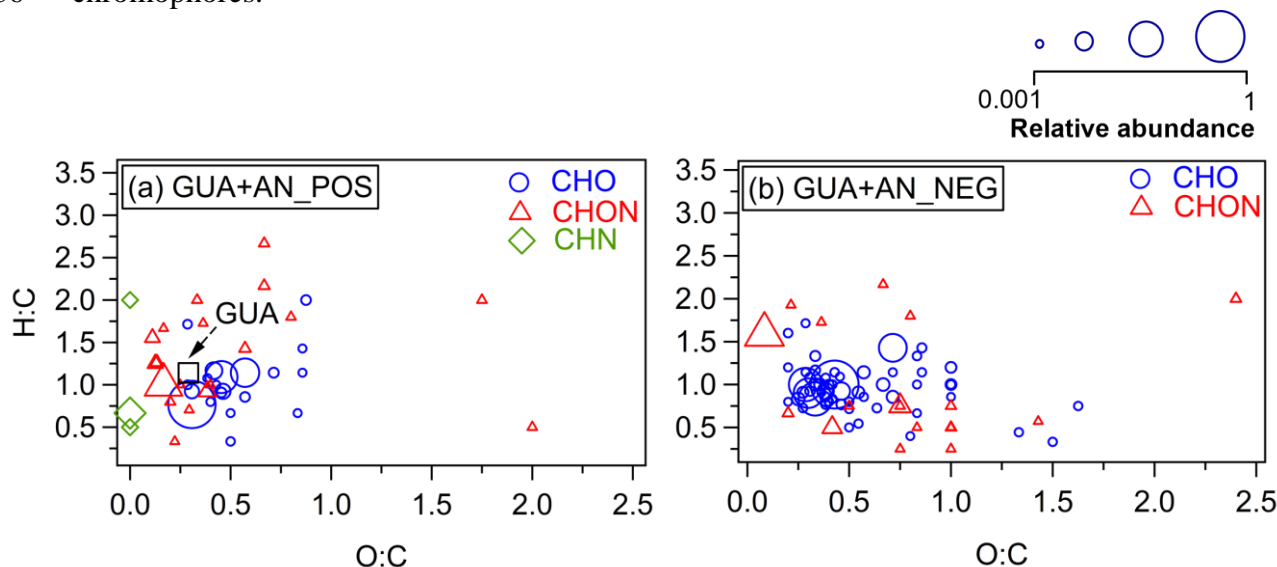
457　**Figure S97.** Van Krevelen diagrams of aqSOA from GUA+AN for (a) positive (POS) and (b)
458　negative (NEG) ion modes. The blue markers indicate CHO classes, red indicate CHON
459　classes, and green indicate CHN classes. The marker size reflects the relative abundance in the
460　sample. The location of GUA is indicated only in panel a (black marker).

461

462　**Figure S108.** Plots of the carbon oxidation state (OS_C) vs. the number of carbon atoms (n_C) of
463　aqSOA from GUA+AN for (a) positive (POS) and (b) negative (NEG) ion modes, colored by
464　the double bond equivalent (DBE) values. The circle, triangle, and diamond markers indicate
465　CHO, CHON and CHN classes, respectively. The marker size reflects the relative abundance
466　in the sample.

References

Anastasio, C., Faust, B. C., and Rao, C. J.: Aromatic carbonyl compounds as aqueous-phase photochemical sources of hydrogen peroxide in acidic sulfate aerosols, fogs, and clouds. 1. Non-phenolic methoxybenzaldehydes and methoxyacetophenones with reductants (phenols), Environ. Sci. Technol., 31, 218−232, https://doi.org/10.1021/es960359g, 1997.

Bateman, A. P., Laskin, J., Laskin, A., and Nizkorodov, S. A.: Applications of high-resolution electrospray ionization mass spectrometry to measurements of average oxygen to carbon ratios in secondary organic aerosols, Environ. Sci. Technol., 46, 8315–832, https://doi.org/10.1021/es3017254, 2012.

Chen, Y., Li, N., Li, X., Tao, Y., Luo, S., Zhao, Z., Ma, S., Huang, H., Chen, Y., Ye, Z., and Ge, X.: Secondary organic aerosol formation from $^3C^*$-initiated oxidation of 4-ethylguaiacol in atmospheric aqueous-phase, Sci. Total Environ., 723, 137953, https://doi.org/10.1016/j.scitotenv.2020.137953, 2020.

Claeys, M., Vermeylen, R., Yasmeen, F., Gómez-González, Y., Chi, X., Maenhaut, W., Mészáros, T., and Salma, I.: Chemical characterization of humic-like substances from urban, rural and tropical biomass burning environments using liquid chromatography with UV/vis photodiode array detection and electrospray ionization mass spectrometry, Environ. Chem., 9, 273–284, https://doi.org/10.1071/EN11163, 2012.

He, L., Schaefer, T., Otto, T., Kroflič, A., and Herrmann, H.: Kinetic and theoretical study of the atmospheric aqueous-phase reactions of OH radicals with methoxyphenolic compounds, J. Phys. Chem. A, 123, 7828−7838, https://doi.org/10.1021/acs.jpca.9b05696, 2019.

Jiang, W., Misovich, M. V., Hettiyadura, A. P. S., Laskin, A., McFall, A. S., Anastasio, C., and Zhang, Q.: Photosensitized reactions of a phenolic carbonyl from wood combustion in the aqueous phase—chemical evolution and light absorption properties of aqSOA, Environ. Sci. Technol., 55, 5199−5211, https://doi.org/10.1021/acs.est.0c07581, 2021.

Koch, B. P. and Dittmar, T.: From mass to structure: an aromaticity index for high-resolution mass data of natural organic matter, Rapid Commun. Mass Spectrom., 20, 926–932, https://doi.org/10.1002/rcm.2386, 2006.

Kourtchev, I., Godoi, R. H. M., Connors, S., Levine, J. G., Archibald, A. T., Godoi, A. F. L., Paralovo, S. L., Barbosa, C. G. G., Souza, R. A. F., Manzi, A. O., Seco, R., Sjostedt, S., Park, J., Guenther, A., Kim, S., Smith, J., Martin, S. T., and Kalberer, M.: Molecular composition of organic aerosols in central Amazonia: an ultra-high-resolution mass spectrometry study, Atmos. Chem. Phys., 16, 11899–11913, https://doi.org/10.5194/acp-16-11899-2016, 2016.

Kroll, J. H., Donahue, N. M., Jimenez, J. L., Kessler, S. H., Canagaratna, M. R., Wilson, K. R., Altieri, K. E., Mazzoleni, L. R., Wozniak, A. S., Bluhm, H., Mysak, E. R., Smith, J. D., Kolb, C. E., and Worsnop, D. R.: Carbon oxidation state as a metric for describing the chemistry of atmospheric organic aerosol, Nat. Chem., 3, 133–139, https://doi.org/10.1038/nchem.948, 2011.

Kroll, J. H., Lim, C. Y., Kessler, S. H., and Wilson, K. R.: Heterogeneous oxidation of atmospheric organic aerosol: kinetics of changes to the amount and oxidation state of particle-

phase organic carbon, J. Phys. Chem. A, 119, 10767−10783, https://doi.org/10.1021/acs.jpca.5b06946, 2015.

Laskin, J., Laskin, A., Nizkorodov, S. A., Roach, P., Eckert, P., Gilles, M. K., Wang, B., Lee, H. J., and Hu, Q.: Molecular selectivity of brown carbon chromophores, Environ. Sci. Technol., 48, 12047–12055, https://doi.org/10.1021/es503432r, 2014.

Li, Y. J., Huang, D. D., Cheung, H. Y., Lee, A. K. Y., and Chan, C. K.: Aqueous-phase photochemical oxidation and direct photolysis of vanillin - a model compound of methoxy phenols from biomass burning, Atmos. Chem. Phys., 14, 2871−2885, https://doi.org/10.5194/acp-14-2871-2014, 2014.

Lin, P., Fleming, L. T., Nizkorodov, S. A., Laskin, J., and Laskin, A.: Comprehensive molecular characterization of atmospheric brown carbon by high resolution mass spectrometry with electrospray and atmospheric pressure photoionization, Anal. Chem., 90, 12493–12502, https://doi.org/10.1021/acs.analchem.8b02177, 2018.

Lobodin, V. V., Marshall, A. G., and Hsu, C. S.: Compositional space boundaries for organic compounds, Anal. Chem., 84, 3410–3416, https://doi.org/10.1021/ac300244f, 2012.

Lv, J., Zhang, S., Luo, L., and Cao, D.: Solid-phase extraction-stepwise elution (SPE-SE) procedure for isolation of dissolved organic matter prior to ESI-FT-ICR-MS analysis, Anal. Chim. Acta, 948, 55−61, https://doi.org/10.1016/j.aca.2016.10.038, 2016.

Mabato, B. R. G., Lyu, Y., Ji, Y., Li, Y. J., Huang, D. D., Li, X., Nah, T., Lam, C. H., and Chan, C. K.: Aqueous secondary organic aerosol formation from the direct photosensitized oxidation of vanillin in the absence and presence of ammonium nitrate, Atmos. Chem. Phys., 22, 273−293, https://doi.org/10.5194/acp-22-273-2022, 2022.

Misovich, M. V., Hettiyadura, A. P. S., Jiang, W., Zhang, Q., and Laskin, A.: Molecular-level study of the photo-oxidation of aqueous-phase guaiacyl acetone in the presence of $^3C*$: formation of brown carbon products, ACS Earth Space Chem., 5, 1983−1996, https://doi.org/10.1021/acsearthspacechem.1c00103, 2021.

Schmitt-Kopplin, P., Gelencsér, A., Dabek-Zlotorzynska, E., Kiss, G., Hertkorn, N., Harir, M., Hong, Y., and Gebefügi, I.: Analysis of the unresolved organic fraction in atmospheric aerosols with ultrahigh–resolution mass spectrometry and nuclear magnetic resonance spectroscopy: organosulfates as photochemical smog constituents, Anal. Chem., 82, 8017–8026, https://doi.org/10.1021/ac101444r, 2010.

Siegmann, K. and Sattler, K.: Formation mechanism for polycyclic aromatic hydrocarbons in methane flames, J. Chem. Phys., 112, 698–709, https://doi.org/10.1063/1.480648, 2000.

Smith, J. D., Sio, V., Yu, L., Zhang, Q., and Anastasio, C.: Secondary organic aerosol production from aqueous reactions of atmospheric phenols with an organic triplet excited state, Environ. Sci. Technol., 48, 1049–1057, https://doi.org/10.1021/es4045715, 2014.

Smith, J. D., Kinney, H., and Anastasio, C.: Phenolic carbonyls undergo rapid aqueous photodegradation to form low-volatility, light-absorbing products, Atmos. Environ., 126, 36−44, https://doi.org/10.1016/j.atmosenv.2015.11.035, 2016.

567　Yee, L. D., Kautzman, K. E., Loza, C. L., Schilling, K. A., Coggon, M. M., Chhabra, P. S.,
568　Chan, M. N., Chan, A. W. H., Hersey, S. P., Crounse, J. D., Wennberg, P. O., Flagan, R. C.,
569　and Seinfeld, J. H.: Secondary organic aerosol formation from biomass burning intermediates:
570　phenol　and　methoxyphenols,　Atmos.　Chem.　Phys.,　13,　8019–8043,
571　https://doi.org/10.5194/acp- 13-8019-2013, 2013.
572
573　Yu, L., Smith, J., Laskin, A., Anastasio, C., Laskin, J., and Zhang, Q.: Chemical
574　characterization of SOA formed from aqueous-phase reactions of phenols with the triplet
575　excited state of carbonyl and hydroxyl radical, Atmos. Chem. Phys., 14, 13801−13816,
576　https://doi.org/10.5194/acp-14-13801-2014, 2014.
577
578　Yu, L., Smith, J., Laskin, A., George, K. M., Anastasio, C., Laskin, J., Dillner, A. M., and
579　Zhang, Q.: Molecular transformations of phenolic SOA during photochemical aging in the
580　aqueous phase: competition among oligomerization, functionalization, and fragmentation,
581　Atmos. Chem. Phys., 16, 4511−4527, https://doi.org/10.5194/acp-16-4511-2016.